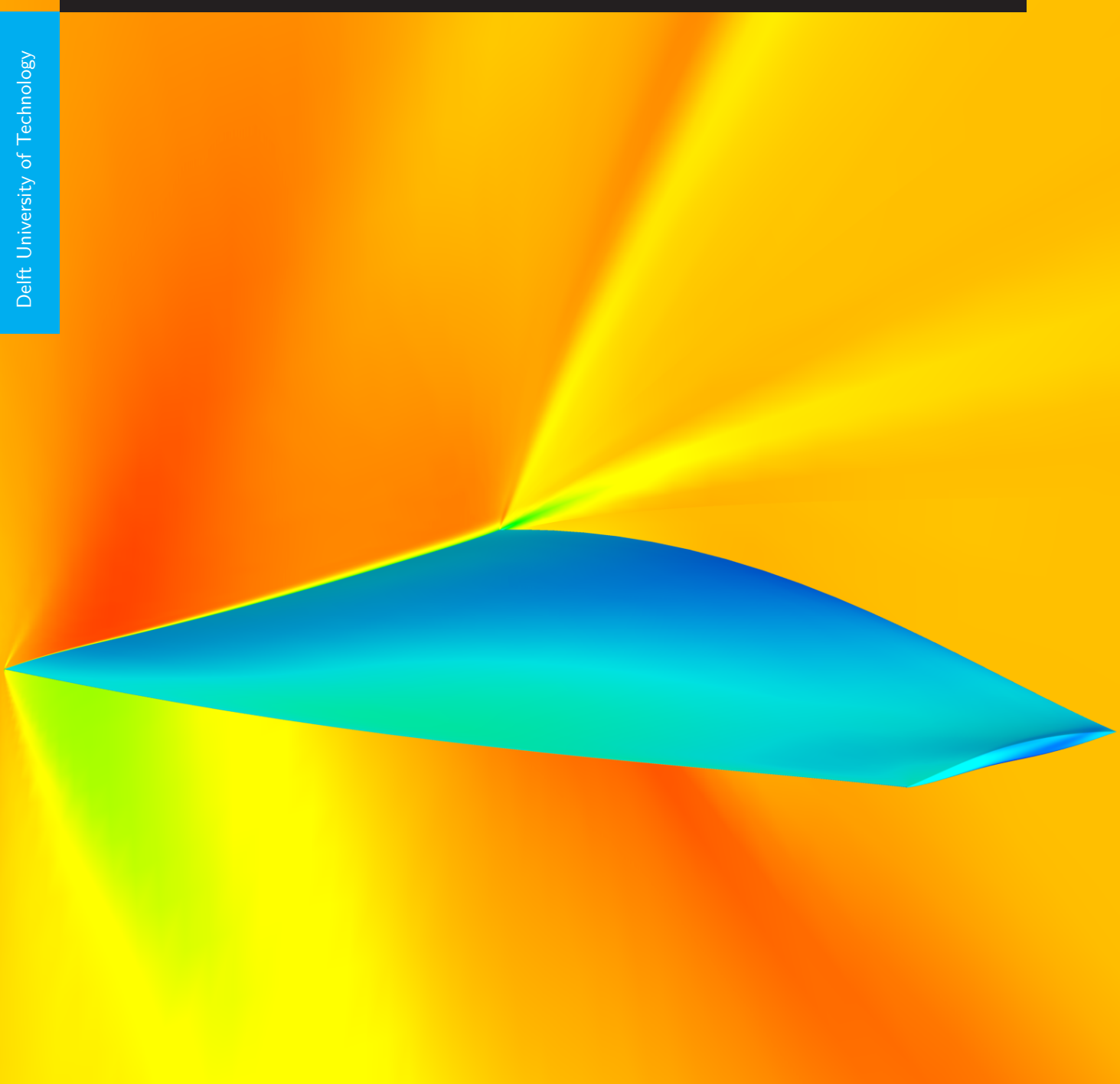


# Multi-point aerodynamic shape optimization for airfoils and wings at supersonic and subsonic regimes

Master Thesis Project

Marco Mangano      4516478

Delft University of Technology





# Multi-point aerodynamic shape optimization for airfoils and wings at supersonic and subsonic regimes

by

M. Mangano

to obtain the degree of Master of Science

at the Delft University of Technology,

to be defended publicly on Monday May 20<sup>th</sup>, 2019 at 2:30 PM.

Student number: 4516478  
Project duration: November 1, 2017 – December 21, 2018  
Thesis committee: Prof. dr. ir. L. L. M. Veldhuis, TU Delft, committee chair  
Dr. ir. G. La Rocca, TU Delft, supervisor  
Prof. dr. J. R. R. A. Martins, University of Michigan, supervisor  
Dr. R. P. Dwight, TU Delft

An electronic version of this thesis is available at <http://repository.tudelft.nl/>.



*Per Alberto*



# Contents

|  |           |
|--|-----------|
| <b>Abstract</b>  | <b>7</b>  |
| <b>Acknowledgements</b>  | <b>9</b>  |
| <b>List of Abbreviations</b>   | <b>13</b> |
| <b>List of Figures</b>   | <b>15</b> |
| <b>List of Tables</b>  | <b>20</b> |
| <b>1 Introduction</b>  | <b>23</b> |
| 1.0.1 Research aim   | 26        |
| 1.0.2 Report Overview  | 26        |
| 1.1 Brief review of compressible aerodynamics  | 27        |
| 1.2 Past, Present, and Future of Supersonic Transportation   | 31        |
| 1.2.1 Historical background on supersonic flight   | 33        |
| 1.2.2 Perspective on supersonic transportation in the XXI century                                      | 34        |
| 1.2.3 Current experimental research topics and industry concepts                                       | 35        |
| 1.2.4 Supersonic Mission Profile   | 36        |
| 1.3 Aerodynamic shape optimization: conceptual approach and applications to supersonic aircraft design | 37        |
| 1.3.1 Optimization Problem Fundamentals  | 37        |
| 1.3.2 Development of modern ASO  | 41        |
| 1.3.3 State-of-the-art: High-fidelity gradient-based ASO for subsonic and transonic configurations     | 42        |
| 1.3.4 Multimodality  | 47        |
| 1.3.5 Supersonic aircraft optimization   | 48        |
| 1.3.6 The morphing wing concept  | 52        |
| 1.4 Research questions   | 54        |
| <b>2 Methodology</b>   | <b>57</b> |
| 2.0.1 MACH framework   | 57        |
| 2.1 Shape Parametrization Scheme: <i>Free-Form Deformation</i> (FFD)                                   | 59        |
| 2.1.1 Mathematical formulation of Free-Form Deformation Scheme   | 60        |
| 2.1.2 Applications and comparison with other approaches  | 60        |
| 2.2 Meshing  | 61        |
| 2.2.1 Mesh deformation Scheme  | 62        |
| 2.3 High-Fidelity Flow Solver  | 62        |
| 2.3.1 Validation for Supersonic Regime   | 64        |
| 2.4 Optimization algorithm   | 65        |
| 2.4.1 Gradient-Based optimization  | 66        |
| 2.4.2 Strategy comparison  | 67        |

|          |   |            |
|----------|---|------------|
| <b>3</b> | <b>Problem Formulation</b>  | <b>69</b>  |
| 3.1      | Investigation Approach and Baseline Geometry . . . . .                    | 69         |
| 3.1.1    | Meshing and Grid Convergence Study . . . . .                              | 72         |
| 3.2      | Design Variables . . . . .  | 74         |
| 3.2.1    | Local shape variables. . . . .  | 75         |
| 3.2.2    | Morphing Capabilities Implementation . . . . .                            | 75         |
| 3.2.3    | Twist. . . . .  | 76         |
| 3.3      | Flight Envelope . . . . .   | 77         |
| 3.4      | Constraints . . . . .   | 77         |
| 3.4.1    | Geometry Constraints . . . . .  | 78         |
| 3.4.2    | Performance constraints. . . . .  | 79         |
| 3.5      | Optimization Problem Definition . . . . .                                 | 80         |
| <b>4</b> | <b>2D Optimization Results</b>  | <b>83</b>  |
| 4.1      | Single-Point Supersonic Optimization. . . . .                             | 83         |
| 4.1.1    | 2D non-lifting minimum drag shape . . . . .                               | 83         |
| 4.1.2    | Influence of Physical Factors . . . . .                                   | 85         |
| 4.1.3    | Parametrization Study and Unimodality Assessment . . . . .                | 86         |
| 4.2      | Multipoint Optimization . . . . .   | 88         |
| 4.2.1    | Equal-weights testcase . . . . .  | 88         |
| 4.2.2    | Transatlantic path testcase . . . . .                                     | 90         |
| 4.2.3    | Boom-less vs conventional transonic flight . . . . .                      | 93         |
| <b>5</b> | <b>3D Optimization Results</b>  | <b>97</b>  |
| 5.1      | Supersonic Optimization . . . . .   | 97         |
| 5.1.1    | Twist Optimization . . . . .  | 97         |
| 5.1.2    | Twist and Shape Optimization . . . . .                                    | 99         |
| 5.2      | Multipoint Optimization . . . . .   | 104        |
| 5.2.1    | Clean wing . . . . .  | 104        |
| 5.2.2    | Morphing wing . . . . .   | 105        |
| <b>6</b> | <b>Conclusions</b>  | <b>111</b> |
| 6.1      | Limitations and Recommendations for Future Research. . . . .              | 114        |
|          | <b>Appendices</b>   | <b>117</b> |
| <b>A</b> | <b>Brief review of parametrization methods for ASO</b>                    | <b>118</b> |
| <b>B</b> | <b>Discretization Error Estimation for CFD Meshes</b>                     | <b>121</b> |
| <b>C</b> | <b>Notes on Gradient-Free Optimization</b>                                | <b>123</b> |
| <b>D</b> | <b>The adjoint method and applications to gradient-based optimization</b> | <b>125</b> |
| D.1      | Mathematical formulation. . . . .   | 125        |
| D.2      | Implementation through Automatic Differentiation . . . . .                | 127        |
| D.3      | Automatic Differentiation . . . . .                                       | 127        |
| D.4      | Observations on flow solver and optimizer settings. . . . .               | 128        |

# Abstract

The second-generation of supersonic civil transport has to match ambitious targets in terms of noise reduction and efficiency to become economically and environmentally viable. High-fidelity numerical optimization offers a powerful approach to address the complex trade-offs intrinsic to this novel configuration. Past and current research however, despite proving the potential of such design strategy, lacks in deeper insight on final layouts and optimization workflow challenges. Stemming from the necessity to quantify and exploit the potential of modern design tools applied to supersonic aircraft design, this work partially fills the gap in previous research by investigating RANS-based aerodynamic optimization for both supersonic, transonic and subsonic conditions. The investigation is carried out with the state-of-the-art, gradient-based MDO framework *MACH*, developed at University of Michigan's MDO Lab - which hosted the author for the 14-month research stint. Details of the tool and a brief overview of supersonic aircraft design and modern aerodynamic optimization strategies are reported in the first part of this manuscript.

After circumscribing the research niche, I perform single and multi-point optimization to minimize the drag over an ideal supersonic aircraft flight envelope and assess the influence of physical and numerical parameters on optimization accuracy and reliability. Leading and trailing edge morphing capabilities are introduced to improve the efficiency at transonic and subsonic flight speed by relaxing the trade-offs on clean shape optimization. Benefits in terms of drag reduction are quantified and benchmarked with fixed-edges results. It is observed how the optimized airfoils outperform baseline reference shapes from a minimum of 4% up to 86% for different design cases and flight conditions. The study is then extended to the optimization of a planar, low-aspect-ratio, and low-sweep wing, using the same schematic approach of 2D analysis. I investigate the influence of wing twist alone and twist and shape on cruise performance, obtaining a drag reduction of 6% and 25% respectively as the optimizer copes with both viscosity and compressibility effects over the wing. Results for 3D multi-point optimization suggest that the proposed strategy enables a fast and effective design of highly-efficient wings, with drag reduction ranging from a minimum of 24% up to 74% for cruise at different speeds and altitudes, including edge deflection.

Ultimately, this work provides an extensive and, to the best of author knowledge, unprecedented insight on the optimal design solutions for this specific aircraft configuration and the challenges of the optimization framework. The benefits of RANS-based aerodynamic shape optimization to capture non-intuitive design trade-offs and offer deeper physical insight are ultimately discussed and quantified. Given the promising results in terms of performance improvements and design efficiency, it is hoped that this work will foster the implementation of this method for more comprehensive full-configuration, multidisciplinary supersonic aircraft optimization studies.

Cover picture: Pressure and Mach number distribution over an optimized wing layout.  
(Credits: Marco Mangano)



# Acknowledgements

Completing this MSc has been a much longer and more intense ride that I could have ever conceived when I first entered the Aerospace department in Kluyverweg, almost four years ago. An adventure that spanned three countries and two continents, a seemingly-endless climb that has disclosed newer and broader perspectives to me, anytime I felt I was close to my admittedly unresolved target. Everything I experienced during my time as a TU Delft student had a substantial role in shaping me as a more mature engineer and, maybe, as a more adult person. I learnt how to take the most from all the opportunities I am able to grab, to never really settle and go for the easy way, and to always try and “break” things apart, just to take a peek at what is inside - and finally understand it.

The more I go forward the more I feel like a drop of water in a sea of immense knowledge, made by outstanding scientists and human beings that I have the privilege to learn from. I feel like I am on the verge of a cliff, getting ready to dive into this ocean: I am scared, thrilled and relieved at the same time. Although I still can't believe what I have done so far and what I am going to do next, I feel so happy to end this phase of my life in what I hope it is the best way possible, while looking at the future with renovated energy, awareness, and hunger for knowledge.

Nevertheless, I cannot pretend these have not been the most demanding, mind-blowing, and exhausting years of my life so far. I have been very close to my mental and physical limits in a number of occasions, and I want to sincerely thank (and apologise to!) all of people who showed their support or shared these moments: I would have probably never gotten so far without your help, support, and love.

First and foremost, I need to express my gratitude to my advisors, who made this project possible. Thanks to Prof. Gianfranco La Rocca, who has introduced me and many other colleagues to MDO and design optimization with his enthusiasm and challenging tasks, showing me the first of many novel career perspectives. His discreet and long-distance support has been fundamental to not lose sight of the final objective, during my long time abroad. My greatest gratitude goes to Prof. Joaquim Martins, who opened the doors of his research group and hosted me as if I was one of his students since the beginning, motivating me and giving the opportunity to express myself at the best of my abilities. I am so proud and excited to join again his research group and have him as mentor, this time for a toughest challenge, and I am looking forward to our future collaboration!

The work presented here could have not been possible without the patient support of all the colleagues from MDO Lab, who never complained when I bugged them for more or less stupid questions, and always offered their warm support. In particular, I want to thank Nick and Anil for their game-saving coding tips, together with John, Neil, Sham and Eirikur for not just the insightful technical comments, but the relieving and sometimes rambling chats, just to remember ourselves to not get lost through the papers and the endless lines of code. Thanks to Cristina for bearing my rants and comforting me with her wisdom, and to my

visiting colleagues Jichao, Mads and Mostafa for sharing their positivity and apprehension while living in a place so strange for us.

Going back to Delft, I cannot but express my love to my buddies Giacomo, Marco, Francesco and Cristiano, with whom I shared more studying nights than we would like to admit. We have been to hell and back! I can't imagine having gone through all that classes without our support group, even if we could have done some things.. a little less Italian-style. We are not colleagues anymore but I will always look for your support!

Thanks to all my "chickens" from Pollaio, who always offer me a second home close to home, and an opportunity to feel like I never left and grew away. Thanks to Stefano, a lighthouse of poetry and sophistication in the long and dull work periods, who constantly inspires me and feeds me with food (not only) for thoughts. Thanks to all the houses that hosted me and the people who filled them: your energy made everyday life lighter and always more unpredictable. Thanks to Pierre, who never ceases to surprise and inspire me with his positive energy: apparently life always put us on parallel but close tracks, and I am looking forward to see what amazing things you are going to pull out of the hat, hoping that life could bring us closer again. Thanks to Alberto, who has already given me enough suggestions and recommendations for an entire life, even if I wish so hard he could give me just one more. I hope you would have been proud of me.

Thanks to my life-long soulmates Francesca, Matteo and Giuseppe, who never made me feel like I was missing-in-action while they were back at home and I was "fighting" in my outpost. Any additional word is redundant with them, as we can understand each other already from how the voice trembles at the first "Hello", the missing commas in the late-night text messages, or the weight of our breaths on the phone while we look for ourselves on Google Maps. Thanks to my best (dis)adventure buddy Giulia, who has never been as close as in the last year, maybe because finally we did not have so many time zones between us, maybe because we both shared the same burden of absence. I can't be sad with you around and your energy will never fail to kickstart me! Thanks to Maria Teresa, Andrea, and Nicola for never letting me forget my roots or my childhood slip away. There is always going to be a spot available for you in any place I am going to move in. After this I know for sure that, wherever I will go, I will always feel at home with all of you.

Last but absolutely not least, thanks to my family, who fully trusted me and believed my enthusiasm since I first shared with them my plans of going abroad, and then even further. Your support made me feel like I could have never really failed, and still makes me burst of joy every time I step on a plane to fly back home.

Ultimately, thanks to all the people who have been part of this ride, whose names and faces are more or less unforgettable: to those who were there since the beginning and even before, to those who joined for the last charge, and to those who I lost along the way.

The more I go forward the more I bring you inside me.





# List of Symbols and Abbreviations

|       |   |
|-------|---|
| ADODG | <i>Aerodynamic Design Optimization Discussion Group</i>   |
| AIAA  | <i>American Institute of Aeronautics and Astronautics</i> |
| ASO   | Aerodynamic Shape Optimization                            |
| BWB   | Blended Wide Body configuration                           |
| $C_d$ | Drag coefficient  |
| $C_f$ | Skin friction coefficient                                 |
| $C_l$ | Lift coefficient  |
| $C_m$ | Pitching Moment coefficient                               |
| $C_p$ | Pressure coefficient                                      |
| CAD   | Computer Aided Design                                     |
| CFD   | Computational Fluid Dynamics                              |
| CP    | Control Point   |
| CRM   | <i>Common Research Model</i>                              |
| D     | Drag  |
| DV    | Design variables  |
| FFD   | Free-Form Deformation                                     |
| L     | Lift  |
| LE    | Leading Edge  |
| M     | Mach number   |
| MDO   | Multi Disciplinary Optimization                           |
| MTOW  | Maximum Take-Off Weight                                   |
| NACA  | <i>National Advisory Committee for Aeronautics</i>        |
| NASA  | <i>National Aeronautics and Space Administration</i>      |
| NLF   | Natural Laminar Flow                                      |
| OBW   | OBlique Wing configuration                                |

|      |                                 |
|------|---------------------------------|
| OML  | Outer Mold Line                 |
| PDE  | Partial Differential Equation   |
| ROM  | Reduced Order Model             |
| BBW  | Strut-Braced Wing configuration |
| SSBJ | Supersonic Business Jet         |
| SST  | Supersonic Transport            |
| TE   | Trailing Edge                   |

# List of Figures

|      |  |    |
|------|--|----|
| 1.1  | Past and future of supersonic aviation. Two of the most iconic supersonic aircraft from XX century: (a) the Aérospatiale-BAC Concorde (captured while flying at Mach 2) [15] and (b) the Lockheed SR-71 Blackbird [16], together with (c) latest concept of the Aerion AS2 as reported on company website [17] as of April 2019 and (d) a rendering of Lockheed-Martin QueSST low-boom experimental aircraft [18]  | 24 |
| 1.2  | Graphical representation of the Mach cone and silence zone at $M > 1$ by Von Karman [39]   | 28 |
| 1.3  | (a) Sketch of the conical camber concept from [53] and (b) a sketch of the related spanwise lift distribution [56]   | 31 |
| 1.4  | Detail of F-102 wing showing the conical camber of the leading edge, by Prof. Mason [41]. According to the author, this feature is so evident because it was added at a later design stage, with a trial-and-error approach typical of these early supersonic aircraft projects.   | 33 |
| 1.5  | Aerion Supersonic and its Natural Laminar Flow technology: (a) a snapshot from experimental campaign on NLF highlighting laminar flow (light grey) and transition to turbulent boundary layer, from [73] and (b) the expected laminar flow area extension on Aerion AS2 [74]   | 36 |
| 1.6  | Concorde navigation map for transatlantic routes [81], <i>Sierra Mike</i> in green (westbound), <i>Sierra November</i> in cyan (eastbound), and <i>Sierra Oscar</i> in purple (bidirectional).   | 37 |
| 1.7  | Geometrical representation of an optimization problem design space from [82], with $x_1$ and $x_2$ design variables, $c_1$ and $c_2$ (inequality) constraints, $f$ objective function and $x^*$ constrained optimum.   | 38 |
| 1.8  | Results from early ASO studies. (a) Hicks and Henne [94] performed a supersonic airfoil optimization study using a primitive analysis tool, that however provided consistent results with analytical and experimental data for this simple case study. In (b) Drela [5] presents results for subsonic, multi-point airfoil optimization as part of a broader analysis of the influence of problem formulation on optimal designs. The optimizer induced a number of bumps on the suction side (highlighted by arrows) that would delay flow separation at different design conditions - for single-point, two-point, and six-point respectively. | 42 |
| 1.9  | Comparison between baseline and optimized wing by Lyu et al. [10]. The optimizer has been able to virtually eliminate shockwaves over the wing at cruise conditions.   | 44 |
| 1.10 | An example of airfoil optimization from [117] comparing shapes (a) and pressure distributions (b) for single-point and multi-point optimized airfoils. The impact of different objective functions on final shapes is highlighted by different $C_p$ distributions.  | 46 |

|      |  |    |
|------|--|----|
| 1.11 | An example of multimodality by Bons et al. [37]. A lift-constrained ( $C_l=0.2625$ ) inviscid aerodynamic shape optimization of a wing, starting from randomly generated baseline shapes, converges to different local minima. . . . .   | 48 |
| 1.12 | Detail of the SST configuration optimized by Reuther et al. [124]. Authors used SYN87-MB solver coupled with a gradient-based optimizer using adjoint method and code parallelization to increase computational performance. . .   | 49 |
| 1.13 | A snapshot of the structural topology of the SST configuration from Laban et al. [131]. Their high-fidelity MDO framework was developed in the context of European HISAC project. . . . .  | 51 |
| 1.14 | Schematics of a gap-less LE flap designed to ensure laminar flow over the wing of an efficient supersonic aircraft, from [75] . . . . .  | 53 |
| 2.1  | <i>MACH</i> ASO solver scheme, from Martins et al. [93]. Geometry and mesh block includes both the <i>PyGeo</i> and <i>IDwarp</i> modules, while the flow and adjoint solvers are both part of <i>ADflow</i> . . . . .   | 58 |
| 2.2  | A not-strictly aeronautical application of Free-Form Deformation technique, from [158]: the Stanford bunny is twisted and stretched after being embedded and mapped into an FFD control volume. . . . .  | 59 |
| 2.3  | An example of a full aircraft configuration parametrized with FFD scheme, highlighting deformation control volumes (on the left) and B-spline surfaces (on the right) [158] . . . . .  | 61 |
| 2.4  | An example from Lyu et al. [10] shows <i>ADflow</i> converging for a randomly distorted initial geometry (reference: CRM wing at $M=0.85$ ). Coupling the flow solver with an adjoint solver for flow sensitivities reduces computational cost and ultimately makes gradient-based strategies the most efficient option for high-fidelity ASO. . . . .   | 63 |
| 2.5  | <i>ADflow</i> is validated against NASA's CFL3D solver with data from Rodriguez et al. [180]. Pressure distributions and aerodynamic coefficients show excellent match. . . . .  | 64 |
| 2.6  | Optimization algorithm performance comparison. The influence of design variables number is tested against the computational cost in terms of number of evaluations for a Rosenbrock function minimization case [1]. Gradient-based strategies with analytical derivatives show the best scalability. . . . .   | 65 |
| 3.1  | The four main airfoil geometries used as baseline for the 2D optimization study: (a) NACA 2S-(40)(015)-(40)(015), a biconvex airfoil with 3% thickness located at 40% of the chord, according to the nomenclature presented above; (b) RAE2822, typical supercritical airfoil developed by the Royal Aircraft Establishment; (c) NACA 0012, symmetrical with 12% thickness with canonical NACA 4-digit shape definition; (d) NACA 66-206, a NACA 6-digit with 6% airfoil designed to enhance laminar flow over the wing. . . . . | 70 |
| 3.2  | Baseline wing geometry used for the 3D optimization studies. (a) the trapezoid planform inspired by Aerion AS2 configuration (details in Tab. 3.1) and (b) a detail of the wing tip leading edge . . . . .   | 71 |

|     |   |    |
|-----|---|----|
| 3.3 | Example of non-uniform point distribution over a RAE2822 airfoil. For better visualization, 30 points are distributed over the spline curve using a linear (a), cosine (b), and highly-conical (c) distribution. This approach has been used to refine the surface meshes close to LE and TE, as illustrated in Fig. 3.4. . . . .   | 72 |
| 3.4 | Baseline mesh for a NACA 2S-(40)(1.5)-(40)(1.5) airfoil (a) and detail of its rounded leading edge, R=0.4mm (b) . . . . .   | 73 |
| 3.5 | 2D grid convergence study for baseline NACA 2S-(40)(1.5)-(40)(1.5) mesh, for (a) supersonic regime, (b) high-transonic regime, (c) transonic regime, and (d) subsonic regime. Meshes have 520K elements (L0), 130K elements (L1), 32K elements (L2) and 8K elements (L3) respectively. . . . .  | 73 |
| 3.6 | Mesh family for baseline wing with biconvex wing section. Grid sizes are respectively (a) L0: 22M elements, (b) L1: 6M elements, (c) L2: 750K elements . . . . .  | 74 |
| 3.7 | Example of full wing parametrization, including both local control points (orange) and child grids (cyan) for leading and trailing edge deflection (a), and a snapshot of a deformed wing (b) with $\beta_{LE}=\beta_{TE}=10^\circ$ and a twist of $10^\circ$ , $5^\circ$ , and $0^\circ$ at the three spanwise stations, from tip inboard. Root section twist is fixed. . . . .  | 75 |
| 3.8 | Example of morphing leading and trailing edge for NACA 2S-(40)(015)-(40)(015) (a) and detail of airfoil deformation around the front virtual hinge (b). Deflection is $\beta_{LE}=\beta_{TE}=15^\circ$ . . . . .  | 76 |
| 3.9 | Visualization of the four target flight regimes identified for an SST ideal mission, reported on an altitude vs. Mach plot. . . . .   | 77 |
| 4.1 | Comparison between optimal shape for non-lifting viscous optimization and theoretical minimum drag 2D section, derived from Sears–Haack body. Figure highlights both the discrepancy from analytical reference due to non-linear effects (a), and the influence of shape parametrization at the leading edge on the final layout (b). . . . .   | 84 |
| 4.2 | Snapshots of Mach contours for baseline (a) and optimal shape (b) for drag minimization at $C_l=0$ . The different intensity of leading edge shock is highlighted. 16 chordwise design variables are used in the optimization. Scaling is identical for both figures. . . . .   | 84 |
| 4.3 | Set of optimization results for (a) fixed flow conditions ( $M=1.45$ @ 45000ft) and variable $C_l$ constraint and (b) fixed $C_l=0.236$ and altitude (45000ft), and variable freestream Mach. While thickness distribution is mostly unaffected, increase in $C_l$ tends to shift the maximum camber position closer to the leading edge, while an increase in freestream Mach has the opposite effect. Lift constraint has the biggest impact on camber magnitude. . . . . | 85 |
| 4.4 | Computational time and discrepancy for a single-point supersonic optimization, starting from different baseline airfoils and using different FFD grids. Optimization runs are performed on University of Michigan’s HPC cluster (FLUX) using 12 processors for each case. . . . .   | 86 |
| 4.5 | Drag minimization of an airfoil for $M=1.45$ at 14500m, $C_l=0.236$ , starting from NACA2S-(40)(1.5)-(40)(1.5), NACA0012, NACA66-206, and RAE2822. . . . .  | 87 |
| 4.6 | Shape comparison between clean, fixed-edges and morphing airfoil multi-point optimization. Supersonic, transonic and subsonic flight regimes from Tab. 3.2 are taken into account with same weight in the objective function. . . . .   | 89 |

|      |  |     |
|------|--|-----|
| 4.7  | Shape comparison for both clean and morphing airfoil multi-point optimization starting from NACA2S-(40)(1.5)-(40)(1.5) and NACA66-206 respectively. Morphing results refer to the same optimization case and are reported in different plots for clarity purposes. Supersonic, high-transonic and subsonic conditions from Tab. 3.2 are weighted for CDG-JFK flight route. . . . . | 92  |
| 4.8  | Shape comparison for two clean airfoils optimized for CDG-JFK route, considering transonic (conventional) and high-transonic (boomless) overland cruise speed respectively. . . . .  | 93  |
| 4.9  | $C_l$ vs. $C_d$ polars for clean, optimal airfoils reported in this section. Case names refer to Tab. 3.2. Note that in the legend <i>SP</i> stays for single-point and <i>MP</i> stays for multi-point. . . . .   | 94  |
| 5.1  | Spanwise lift and twist profiles for twist-only, supersonic optimization of a planar wing, using 3,5, and 7 twist design variables respectively. Twist sections are linearly spaced along the span. . . . .  | 98  |
| 5.2  | (a) Lift and drag spanwise distribution for the biconvex and NACA 66-206 test-cases and (b) comparison of wing shape and pressure distribution at mid span. Despite a small geometry difference due to manipulation issues, the fluid over the wing has the same behaviour in both cases. This supports the confidence of the final design as a global optimum. . . . .            | 99  |
| 5.3  | Spanwise lift, drag and twist distributions for twist-only and twist+shape single point, supersonic wing optimization case. . . . .  | 101 |
| 5.4  | Local wing section and supersonic pressure distribution comparison between baseline, twist-only, and twist+shape optimized wing. Sections reported are highlighted in Fig. 5.5 . . . . .   | 102 |
| 5.5  | Pressure distribution comparison between baseline and twist+shape optimized wing at reference supersonic regime. . . . .   | 103 |
| 5.6  | Spanwise, lift and drag distribution for clean, optimized wing at supersonic, transonic, and subsonic regime; objective function is weighted according to the reference Paris-New York route. Elliptic lift distribution is reported as a reference. . . . .   | 105 |
| 5.7  | Spanwise lift, drag and twist distributions for multi-point morphing wing optimization. Objective function is weighted according to the reference Paris–New York flight route, with conventional transonic overland flight. . . . .  | 106 |
| 5.8  | Comparison between clean and morphing wing drag improvement at different flight conditions for the test cases reported in Fig. 5.6 and Fig. 5.7. . . . .   | 107 |
| 5.9  | Spanwise, lift and drag distribution comparison between clean, optimized wing and morphing optimized wing at reference supersonic, transonic, and subsonic cruise conditions. . . . .  | 108 |
| 5.10 | Local, mid-span wing section and pressure distribution comparison between clean optimized wing and morphing optimized wing at reference cruise conditions. . . . .   | 108 |
| 5.11 | $C_l$ vs. $C_d$ polars for single-point and multi-point optimized wings. Edges deflection for multi-point, morphing layout is kept fixed to cruise-optimized values reported in Tab. 5.3. Flight conditions refer to Tab. 3.2. . . . .   | 109 |

D.1 Example of odd airfoil shape evaluated during early optimization steps. AD-flow fully converged for this supersonic simulation. . . . . 129

# List of Tables

|     |  |    |
|-----|--|----|
| 2.1 | Aerodynamic coefficient comparison between Rodriguez et al. [180] data and ADflow simulations with current settings. ADflow overestimates total drag coefficient by 0.6% . . . . .   | 65 |
| 3.1 | Baseline wing geometry data. Aerion AS2 renderings have been used as reference. . . . .  | 72 |
| 3.2 | Optimization problem definition. Parameters in blue on the table apply to wing optimization, while the additional design variables for morphing edges are highlighted in green. . . . .  | 81 |
| 4.1 | Angle of attack variation for optimal layouts with varying design $C_l$ , and comparison with linearized supersonic theory prediction. Analytical results become less accurate with higher $\alpha$ , as expected from model assumptions. . . .  | 86 |
| 4.2 | Results for single-point, supersonic optimization starting from different initial airfoils reported in Fig. 4.5. $C_d$ is provided in drag counts ( $C_d \times 10^4$ ) . . . . .  | 88 |
| 4.3 | Baseline and optimized shape drag for multi-point optimization, comparing clean and morphing airfoil cases. Flow conditions refer to Tab. 3.2 and have the same weight in the objective function. Drag coefficient is provided in drag counts ( $C_d \times 10^4$ ). . . . .   | 89 |
| 4.4 | Results relative discrepancy for multi-point optimization, starting from NACA2S-(40)(1.5)-(40)(1.5) and NACA66-206. Both clean and morphing airfoil results are taken into account: supersonic, high-transonic and subsonic conditions refer to Tab. 3.2 and are weighted for CDG-JFK flight route. In $\beta$ rows, leading and trailing edge deflections are reported ( $\beta_{LE}/\beta_{TE}$ respectively), with counter-clockwise positive deflection. * high relative deflection discrepancies highlighted with the asterisks do not undermine the overall excellent match of the results, as the absolute difference in deflection is in the order of $1^\circ$ . Final shapes consistently overlap, as illustrated in Fig. 4.7. . . . . | 91 |
| 4.5 | Performance comparison between clean and morphing airfoil optimization along the reference CGD-JFK route, for cases reported in Fig. 4.7. Reference initial drag refers to NACA2S-(40)(1.5)-(40)(1.5). . . . .   | 91 |
| 4.6 | Results comparison for airfoils reported in Fig. 4.8. Optimization for CDG-JFK route, considering transonic (conventional) and high-transonic (boomless) overland cruise speed respectively. Case names refer to Tab. 3.2. Results highlighted in gray refer to flight conditions outside the specific optimization case. Drag coefficients are provided in drag counts ( $C_d \times 10^4$ ). . . . .   | 94 |
| 5.1 | Results for twist-only optimization of a planar wing for supersonic regime. Twist sections are linearly spaced along the span. Pitching moment constraint is active for this design problem. . . . .   | 99 |

|     |  |     |
|-----|--|-----|
| 5.2 | Drag and optimal angle of attack for two identical supersonic shape-and-twist optimization of the reference wing, one with a biconvex wing section (same case presented in Tab. 5.3) and a NACA 66-206 wing section. Results highlight how, despite parametrization-induced discrepancies compensated by a different $\alpha_{\text{optimal}}$ , the two cases converge to approximately the same optimal design. Multimodality does not affect this specific optimization case. . . . . | 100 |
| 5.3 | Results comparison between twist-only optimization and twist-and-shape single point, supersonic wing optimization case. As for previous case, pitching moment constraint is active. . . . .  | 101 |
| 5.4 | Performance improvement of a multi-point optimized reference wing, highlighting drag reduction and final angle of attack for supersonic, transonic, and subsonic regime. . . . .   | 104 |
| 5.5 | Drag, angle of attack and edge deflection for multi-point wing optimization with morphing capabilities - same test case reported in Fig. 5.7. . . . .  | 107 |



# 1

## Introduction

In recent years, numerical optimization has been extensively applied in the aerospace sector to improve aircraft performance and extend the design space beyond the boundaries of more traditional design approaches. Aircraft design in particular, because of its intrinsic complexity and multidisciplinary nature, can consistently benefit from the application of optimization strategies that simultaneously take into account different disciplines and subsystems - namely, the fundamental concept behind MDO architectures.

The first studies focused on structural and aerodynamic optimization date back to the 1970's [1]. Since then, the improvements on hardware computational power, together with the development of both efficient simulation software and optimization strategies, have allowed engineers to improve the accuracy and reliability of their frameworks without dramatically increasing computational time [2]. Aerodynamics is likely the engineering discipline that has most benefited of this substantial reduction in design effort [3]. From early works based on low-fidelity panels-method based tools [4, 5], academic interest shifted towards more reliable prediction software, exploiting the capabilities of CFD tools into broader design frameworks. The publicly available literature related to aerodynamic optimization is indeed rich in examples of high-fidelity shape optimization studies for subsonic and transonic regimes [6–11], also considering aero-structural coupling to model aeroelastic effects [12–14].

However, a relatively small number of publications focus on the challenge of extending this high-fidelity approach to supersonic aircraft configurations, especially when it comes to exploit the most recent and accurate analysis and optimization tools. Such inherently complex and relatively novel aircraft configuration can hugely benefit from the design insight and performance enhancement enabled by MDO strategies. Additionally, topics as robustness and accuracy in supersonic transport (SST) optimization have not been extensively investigated so far, with a lack of literature sources that provide both physical and numerical modelling insight on high-fidelity optimized layouts. Thus, an investigation on this specific subject would be of significant interest, both to enrich the current knowledge base and provide a consistent benchmark reference for future studies at academic and industry level. The rising interest in a new generation of civil supersonic transport aircraft by research institutes and private companies acts as further motivation for such a research effort.

Indeed, even if the last supersonic commercial flight, made by the world-famous Concorde (Fig. 1.1(a)), dates back to the early 2000s, the research related to supersonic aircraft concepts for civil transport did not experience major setbacks. Sonic-boom reduction and flight efficiency improvement are referenced as major issues in the design of the next generation of SST. These engineering challenges are directly related to both environmental concerns and operating costs. Reducing supersonic cruise in particular fuel burn is a complex design problem that has to be addressed while also taking into account the impact of off-design, low-speed flight segments on the overall fuel consumption. Furthermore, current regulations forbid supersonic flight overland due to the damage and discomfort caused by sonic-boom at ground level. This implies that novel designs have to consider both noise reduction strategies and, more realistically in the short term, aerodynamic trade-offs to reduce drag penalty when flying at transonic regimes over populated areas. Setting aside the design effort for cleaner and faster jet engines, achieving high aerodynamic efficiency for such a peculiar mission is a major bottleneck towards a sustainable and market-competitive aircraft.

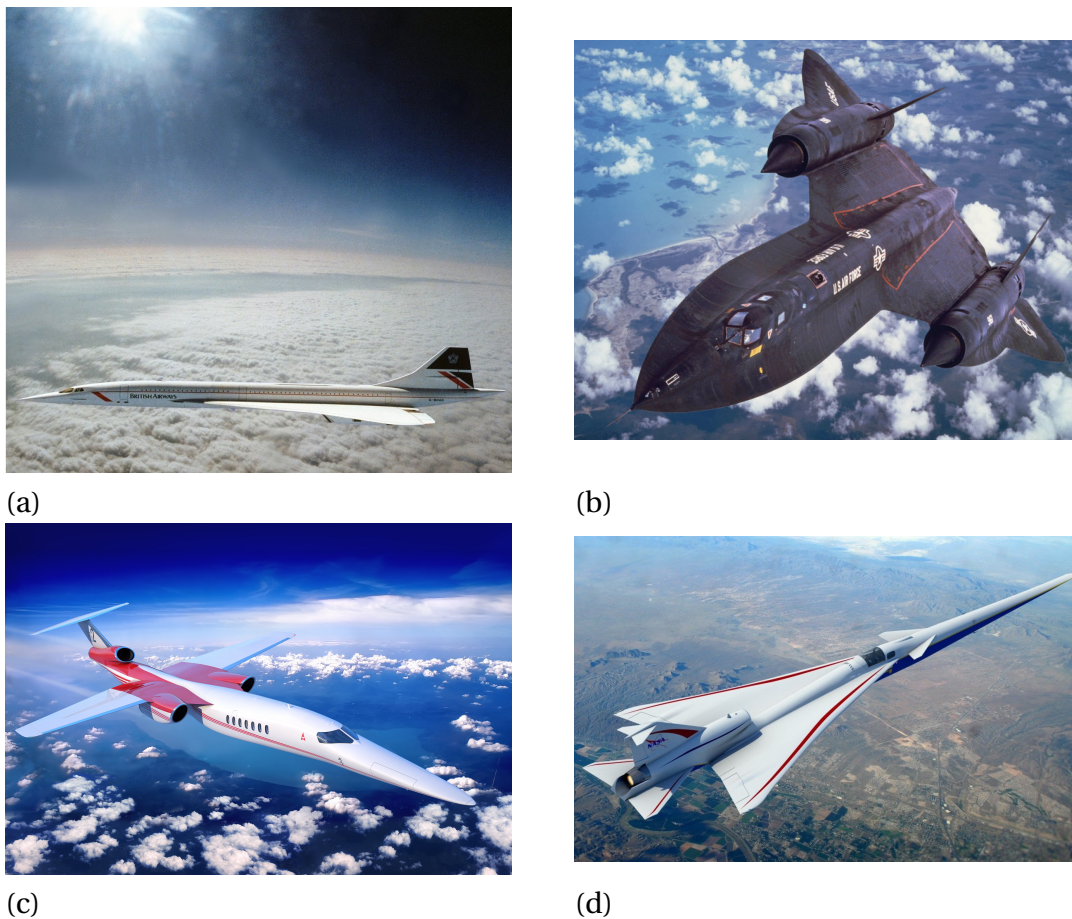


Figure 1.1: Past and future of supersonic aviation. Two of the most iconic supersonic aircraft from XX century: (a) the Aérospatiale-BAC Concorde (captured while flying at Mach 2) [15] and (b) the Lockheed SR-71 Blackbird [16], together with (c) latest concept of the Aerion AS2 as reported on company website [17] as of April 2019 and (d) a rendering of Lockheed-Martin QueSST low-boom experimental aircraft [18]

In this sense, research agencies such as NASA and JAXA have spent significant effort and resources in the last decades aiming to make commercial supersonic flight a concrete possi-

bility. The main challenges involve cost reduction, environmental impact and public acceptance, with particular focus on sonic-boom reduction, as for example the X-59 experimental plane (Fig. 1.1(d)). In the industry, a number of companies currently claim to be involved in designing the next generation of SST. According to market analyses, even if the global trend for commercial aviation has shifted on sustainability and highly-efficient transportation, a profitable market share has been forecasted for Supersonic Business Jets (SBJJ) in the next 20 years [19, 20], Fig. 1.1(c).

Although a rising interest in supersonic and hypersonic experimental and computational aerodynamics, there have been few attempts by academia to consistently extend the most innovative optimization tools to SST design. A number of relevant studies on high-fidelity supersonic aerodynamic optimization [21–28] and multifidelity [29–33] have indeed proven the feasibility and hinted the potential effectiveness of this approach. However, they did not produced relevant insights on the key features that affect routine reliability nor explained the results from a fluid dynamics and computational point of view. Moreover, to the author best knowledge, none of the previous research on supersonic aerodynamics combines the key features embedded in MACH (*MDO of Aircraft Configurations with High fidelity*) framework, developed at University of Michigan’s *MDO Lab*, which hosts and supports this research. This state-of-the-art optimization framework, which capabilities have been exploited by a number of recent publications [10, 11, 34–37], includes a Free-Form Deformation scheme for geometry and mesh manipulation and a fast and accurate flow solver with adjoint-based viscous sensitivity calculations. It can thus be efficiently coupled with a gradient-based optimizer to perform fast and accurate aerodynamic shape optimization (ASO) and multidisciplinary optimization (MDO) studies.

This master thesis project proposes to fill the presented literature gap in ASO applied to SST specifically, by using MACH framework and focusing on airfoil and wing aerodynamic drag minimization as first step of a more comprehensive multidisciplinary, full-configuration study. The investigation initially focuses on 2D cases, to prove the effectiveness of the strategy on relatively simple cases, draw useful design guidelines and develop intuition on both the physical and numerical parameters that drive the optimization process. This includes both focusing on how fluid dynamics “shapes” the optimal solution in a consistent fashion with the problem formulation and identifying how the framework enhances and limits the final design solution. The extension to full-wing configuration comes as a natural development of the airfoil analysis and offers some more meaningful engineering insight on SST configurations. A set of cases is indeed presented and discussed, both considering optimization for pure supersonic cruise and for a more realistic SST flight envelope that includes transonic and even lower, subsonic-speed regimes. The effectiveness of “morphing” wing devices, modelled as gapless leading and trailing edge flaps, is quantified and benchmarked with “clean”, non-morphing airfoil and wing configuration. Such broader design perspective is crucial to overcome the limitations of past projects (including the Concorde itself), that ultimately prevented the success of civil supersonic transportation. In particular, it is highlighted how non-linear viscosity and compressibility effects lead to non-intuitive design trade-offs. Framework reliability is investigated by evaluating the impact of parametrization on the optimal solution and the convexity of the design space, crucial for a consistent application of gradient-based strategies. Multiple baseline geometries are used to rule out the presence of local minima with a satisfying degree of accuracy. A fundamental “behind-the-

scenes” effort has focused on tuning the algorithms embedded in the tool, from the mesh deformation scheme to the optimizer and CFD settings. Some general-interest considerations are noted down in this report. However, the most blatant proof of robustness of the framework is represented by the huge number of cases hereby discussed and the physical and numerical consistency of the results. In the next chapters, the considerations and observations briefly reported here will be extensively dissected and justified with a mix of literature sources and result analysis.

As final remark, most of the research results discussed in this manuscript are part of a paper presented at 2019 AIAA SciTech Forum and Exposition [38].

### **1.0.1. Research aim**

In synthesis, the scope of this work is addressed by the following research question, which will be further expanded at the end of this introduction chapter:

*What is the degree of accuracy, reliability and performance improvement that can be obtained by a high-fidelity gradient-based aerodynamic shape optimization framework, aiming at the design of low-drag airfoils and wings for a supersonic aircraft throughout its flight envelope?*

This project, as just introduced, is rooted in the broader and innovative subject of high-fidelity optimization, namely the design of complex engineering systems by means of numerical optimization methods coupled with high-fidelity simulation tools. There is a single numerical tool for the discipline analysis, a CFD solver, being the focus on solely aerodynamic characterization and performance analysis. The accuracy and reliability of the tool will be assessed by performing numerical convergence analyses and exploring a set of design conditions starting from different baseline geometries. There is a limited number of sources that provide relevant data for benchmark, thus comparisons with analytical results and numerical error estimation techniques will be used to further validate results and assess the well-definition of the optimization problem. The focus on low-drag supersonic airfoils and wings circumscribes the research interest to (constrained) efficiency maximization at flow regimes with freestream  $M > 1.2$ , without compromising the performance at lower, subcritical speeds. This implicitly excludes from the investigation an analysis of the aeroacoustic effects of supersonic flight, i.e. the so-called *sonic-boom*, leaving the study and optimization of SST noise footprint - a current “hot topic” in aerospace community - to future work. Moving back to the analysis framework, the optimization routine typology (gradient-based) is a fundamental assumption at this stage, excluding a priori a benchmark study between different optimization strategies. Further considerations to support these conceptual assumptions are drawn in Chap. 2.

### **1.0.2. Report Overview**

The present report offers an extensive overview of the design problem, the methodology and ultimately the results of the optimization campaign. The introduction chapter describes the engineering problem in terms of fluid dynamics phenomena and optimization numerical modelling, before circumscribing the research objective presenting a comprehensive

literature study on ASO. A chapter is dedicated to tool and modelling methodology description, Chap. 2, spanning from the parametrization scheme to the optimization algorithm. Additional and specific modelling details and observations are provided in the Appendices section. The problem formulation and approach to case studies is discussed in detail in Chap. 3 before presenting and analysing optimization results in Chap. 4 and 5 for airfoils and wing respectively. Conclusive Chap. 6 sums up the observations and the answers to research questions, while also underlining project limitations and suggesting future research opportunities.

As mentioned above, the present chapter will focus on a short recap of the key features of compressible fluid dynamics Sec. 1.1. Following that, an historical review (Sec. 1.2.1) will provide the background to dive into an overview of supersonic flight perspective in the near future, Sec. 1.2.2, and into the current research and development efforts at both industry and academic level, Sec. 1.2.3. In the following Sec. 1.3 the optimization problem is presented in its fundamentals (Sec. 1.3.1) and discussed in its notable applications - Sec. 1.3.3– 1.3.4 -, with a focus on state-of-the-art tools and ultimately previous applications to SST ASO, in Sec. 1.3.5. The morphing wing concept used in the present investigation is also briefly presented in Sec. 1.3.6 before the research questions are listed and discussed in Sec. 1.4.

## 1.1. Brief review of compressible aerodynamics

Compressible aerodynamics is a vast and complex topic that has been the subject of decades of research and a huge number of books and publications; the author has not the hubris to present a complete overview on this subject. Von Karman [39], Anderson [40], Mason [41] and Kroo [42] offer an excellent review of the topic and are used as technical reference. In this section fundamental features and formulas of supersonic aerodynamics are summed up, to introduce relevant concepts that will be useful for both project planning and results interpretation.

**Supersonic flow** The physics of a body moving into a fluid at supersonic speeds is substantially different from subsonic fluid mechanics, as compressibility effects become dominant. Considering the speed of sound as the velocity at which the pressure disturbances are propagated into the surrounding fluid, it is evident that if the body moves faster than sound it is unable to send signals ahead (“*Rule of Forbidden Signals*”) [39], thus creating a zone of silence as illustrated in Fig. 1.2. The presence of a conical zone of action behind the body, whose half vertex angle is trigonometrically derived as  $\beta = \sin^{-1}(1/M)$  - the *Mach angle*, implies that pressure effects are concentrated inside and especially at the border of this “Mach cone” (“*Rule of Concentrated Action*”). Von Karman [39], considering horizontal momentum transfer inside a control volume, showed how this non-uniformity introduces a specific form of drag called *wave drag*, practically the momentum loss due to the presence of shock-waves at both supersonic and transonic speeds. Drag rise is particularly relevant between  $0.8 < M < 1.2$  due to unsteady phenomena and the presence of both subsonic and supersonic flow regions.

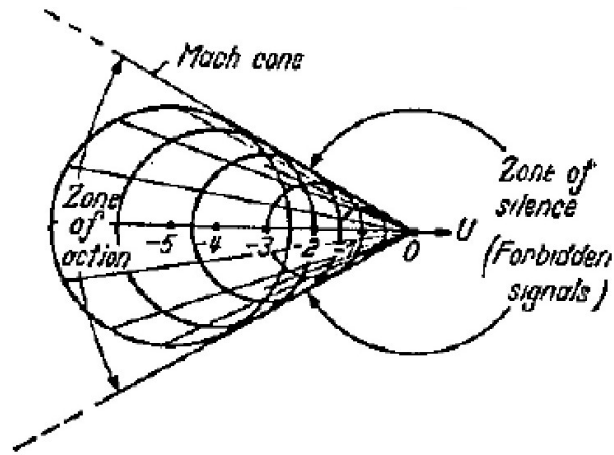


Figure 1.2: Graphical representation of the Mach cone and silence zone at  $M > 1$  by Von Karman [39]

In order to analyse total drag at supersonic regime, some additional considerations have to be made. Generally trailing edges are supersonic as sweep angle is smaller than Mach angle [41], so upper and lower surfaces are (locally) decoupled and Kutta condition is no longer applicable. At leading edge however, flow is supersonic or subsonic depending on the leading edge sweep being lower or higher than  $\beta$  respectively. If the LE is inside the Mach cone, lower and upper surfaces can “communicate” inducing the typical subsonic singularity related to  $C_p$  peak; otherwise, spanwise pressure remains constant. Sharp edged airfoils and wings anyway show reduced subsonic performance due to the minimum effect of this LE suction singularity, which, in more common thick-nosed shapes, produces a thrust force that alleviates overall drag [42]. Concerning viscosity effect, boundary layer is mostly subsonic and so skin friction drag is modelled according to approximations based on chord-based Reynolds number:  $C_{f_{laminar}} = \frac{1.328}{\sqrt{Re_c}}$  and  $C_{f_{turbulent}} = \frac{0.074}{Re_c^{1/5}}$ . It has to be highlighted that for high supersonic ( $M > 2$ ) and hypersonic speeds ( $M > 5$ ) thermal effects come into play and alter boundary layer characteristics and behaviour [19]. Moreover, shockwave boundary layer interaction, getting closer to transonic region, can induce flow separation as additional source of drag and instabilities. In this sense, viscous CFD codes are crucial to assess the occurrence of these phenomena.

As additional distinctive feature, aerodynamic center shift may indirectly affect drag and overall performance when accelerating from subcritical to supersonic speeds. Due to the different chord-wise pressure distribution on the wings at supersonic speeds, the virtual point of application of aerodynamic forces, used as reference for pitching moment calculation, moves from the typical quarter-chord location to half of the chord. This translates into a dangerous pitching-down attitude that has to be compensated when accelerating through transonic region. As trimming the aircraft would easily lead to poor performance, this issue is commonly tackled by moving fuel between different tanks along the wings and fuselage, shifting the center of gravity and thus minimizing the pitching behaviour. However, this factor should be taken into great account during aerodynamic design to guarantee consistent flight characteristics over the whole flight envelope.

**Sears–Haack Body** Studies on the theoretical bodies of revolution with minimum drag have been carried out since the early stages of supersonic flight. Sears [43] and Haack [44] in two separate studies defined the shape of minimum drag for a given volume as:

$$y(x) = \sqrt{\frac{16V}{3\pi^2} [4x(1-x)]^{\frac{3}{4}}} \quad (1.1)$$

whose (inviscid) drag is equal to  $C_D = 24V$ . This “simple” shape is used as reference to compare drag of general configurations in supersonic flow and ultimately represents the ideal volume distribution for area ruling, discussed later in this chapter. In recent years, Palaniappan and Jameson [45] used numerical methods to revisit the theory considering non-linear phenomena. Small differences due to leading edge shocks were noticed in maximum thickness position and overall drag. This work is considered as benchmark for 2D non-lifting optimization study.

**Supersonic Thin Airfoil Theory** Anderson [40] in his renowned book provides an extensive explanation of the compressibility effects on fluid dynamics and their implication on aircraft design. Considering the approximation to linear potential flow, the change in sign of Prandtl correction term  $(1 - M^2)$  substantially alter the nature of the PDE for supersonic regimes. An approximation of the pressure coefficient  $C_p$  is derived in the form presented on the left hand of Eq. 1.2. Lift and drag coefficient are obtained by integrating  $C_p$  along the airfoil surface, leading to approximated formulas reported on the right hand of Eq. 1.2.

$$C_p = \frac{2\Theta}{\sqrt{M_\infty^2 - 1}} \Rightarrow \begin{aligned} C_l &= \frac{4\alpha}{\sqrt{M_\infty^2 - 1}} \\ C_d &= \frac{4}{\sqrt{M_\infty^2 - 1}} (\alpha^2 + g_c^2 + g_t^2) \end{aligned} \quad (1.2)$$

$\Theta = \partial z / \partial x$  is the local surface angle with respect to free stream and  $g_c^2, g_t^2$  the camber and thickness effect respectively. These two terms coalesce into  $\bar{\delta}^2$  according to Von Karman [39] formulation, where  $\bar{\delta}$  is the mean of the airfoil surface angles with respect to chord line. For a double wedge airfoil it is equivalent to  $\frac{t}{c}$ . Due to the fundamental model assumptions, these equations hold for small flow perturbations, thus sharp, thin airfoils at low angles of attack.

**Wing-body supersonic drag** The extension of approximations for lift and drag to wing-body configurations has been carried out with a combination of experimental campaigns and analytical derivations based on potential methods. Although nowadays CFD solvers are accurate and efficient enough to get information on supersonic drag of a complete aircraft relatively quickly, it is worth to report few useful equation that estimate maximum achievable performance. As previously introduced, drag can be broken down as [42]:

$$\text{Total Drag} = \text{friction} + \text{vortex} + \text{lift-dependant wave} + \text{volume wave}$$

Friction drag formulas are reported in the previous paragraph. A major step forward in understanding wave drag came from Whitcomb [46, 47] who introduced the “area ruling” concept, based on the fundamental idea that drag is related to cross-sectional area  $S(x)$  changes along the freestream direction  $x$ . Volume wave drag is calculated as:

$$D = -\frac{\rho_{\infty} U_{\infty}^2}{4\pi} \int_0^l \int_0^l S''(x_1) S''(x_2) \ln|x_1 - x_2| dx_1 dx_2 \quad (1.3)$$

Mach does not appear in this formulation because it is derived from slender body theory [41]. Küchemann [48] studies on slender wing based on area ruling have been successfully implemented to supersonic and transonic configuration - the renown “Küchemann carrots” - highlighting the impact of Whitcomb intuition. A general approximation for combined vortex and lift-induced wave drag has been formulated by Jones [49], assuming an elliptical lift distribution:

$$C_D = \frac{C_L^2}{\pi AR} \sqrt{1 + (M^2 - 1) \left( \frac{\pi AR}{2} \right)} \quad (1.4)$$

Jones and Smith concepts are further extended on [42]; lift-induced wave drag of a general shape can then be calculated, with good match with well designed wings, with:

$$C_{D_{\text{lift}}} = \frac{\pi l^2}{16S} C_L^2 \left[ \sqrt{1 + (M^2 - 1) \left( \frac{4S}{\pi l^2} \right)^2} \right] \quad (1.5)$$

given  $S$  the wing planform area and  $l$  its length. For an elliptical planform wing with  $a$  and  $b$  semi-minor and semi-major axis respectively and symmetrical biconvex airfoils of thickness  $\frac{z}{z_{\text{max}}} = 1 - \frac{x^2}{a^2} - \frac{y^2}{b^2}$ , Jones [50] derived the following formula for volume wave drag from area ruling:

$$C_{D_{\text{vol}}} = 4 \frac{z_{\text{max}}^2}{a^2} \frac{1}{\sqrt{M^2 - 1 + \frac{a^2}{b^2}}} \left( 2 - \frac{M^2 - 1}{\sqrt{M^2 - 1 + \frac{a^2}{b^2}}} \right) \quad (1.6)$$

Moreover, the author estimates the overall volume drag of a wing-body configuration according to mutual drag theorem as:  $D_{\text{tot}} = D_{\text{fuselage}} + 2 * D_{\text{interference}} + D_{\text{wing}}$ , with  $D_{\text{interference}}$  analytically approximated for simple shapes. This small set of equations can be easily implemented to estimate both 2D and 3D supersonic drag, providing a reference value to estimate the influence of non-linear effects on analysis and optimization results. Fortran-based applets for supersonic drag estimations, developed with Mason contributions, are available for download at [51].

**Conical camber distribution** Between the 50s and the 60s, with increasing experience in high-performance supersonic design, more advanced solutions were included into aircraft aerodynamic layouts. Together with the ground-breaking area ruling concept, the F-102 was the first supersonic aircraft to introduce the so called *conical camber*, later applied to multiple fighter and bombers generations, from B-58 to F-15 [52]. As defined by Morris et al. [53] “the technique involves a sharp cambering of the leading edge of an airfoil such that it follows the contour of a cone emanating from the wing apex toward the wing tip”, as shown in Fig. 1.3(a). Introduced by Hall and further studied by Boyd and Smith among others [54–56], the concept aims to forcibly introduce leading edge suction benefits when the flow is (locally) subsonic, while avoiding flow separation. The locally forward-facing upper surface thus reproduces the beneficial effects of thick noses at low speed. This feature improves performance at both subsonic and supersonic speeds for highly swept delta wings [56]. Resulting ideal “conical” spanwise distribution is illustrated in Fig. 1.3(b)

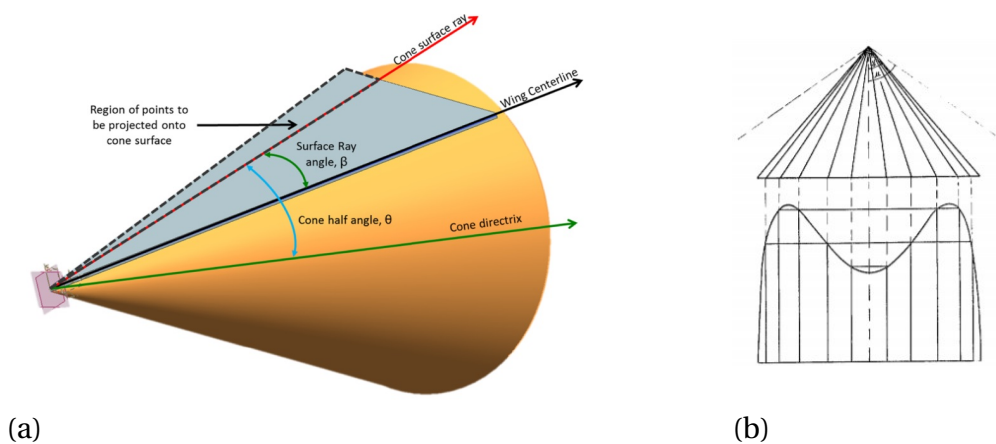


Figure 1.3: (a) Sketch of the conical camber concept from [53] and (b) a sketch of the related spanwise lift distribution [56]

Menees [57] carried out wind tunnel campaign assess the replicability conical camber effects by using movable surfaces, so to avoid detrimental effects of leading edge camber for supersonic regime (in a similar fashion to what suggested decades later by Tracy, as reported in Sec. 1.3.6). The successful implementation of this design gimmick supports the implementation of a “morphing” wing strategy in the optimization framework, proposed later in this chapter, to improve performance throughout the entire flight envelope.

## 1.2. Past, Present, and Future of Supersonic Transportation

Since the first milestone flight beyond the once known as “sound barrier”, made by Chuck Yeager on 14<sup>th</sup> October 1947, supersonic aircraft technology has made enormous leaps forward. Flying faster than sound has become a standard routine in military environment, with resounding examples as the SR-71, Fig. 1.1(b), able to reach Mach 3 [16], and the modern F-22, specifically designed for *supercruise* capability [58]. However, commercial transport requirements are substantially different from military standards, and somehow are even more difficult to be satisfied. According to Anderson [40]: “In today’s energy-conscious world,

*[the fuel consumption] constraint can be as much a barrier to high-speed flight as the sound barrier was once envisaged"*. The already mentioned Concorde made use of an advanced technology that was however no longer sustainable by the time of its decommissioning. Nonetheless, the research on the commercial supersonic technology has been carried out relentlessly since the early 90's [20]. Flight efficiency (intended both for environmental issues and operational cost) and sonic-boom reduction are indeed referenced as major challenges in the design of the next generation of supersonic transport. Thus, even if projects in the long term aim at the design of a 200-seats aircraft configuration, the most promising concept in terms of short term feasibility and market share predictions is Supersonic Business Jet (SSBJ), with passenger capability ranging from 6 to 20 seats. Multiple sources [19, 59] provide a consistent review of the last developments and engineering challenges involved in the design of SSBJ incoming generation. At current stage there is a number of companies and research institutions that are actively working on innovative technologies and advanced design tools, raising the interest of major aerospace players such as Boeing, General Electric [17] and Lockheed Martin [18]. However no prospects of flight activities before the early 2020s.

Supersonic flight is thus currently living a rather undetermined phase. The pursuit of speed, started soon after second world war, lost its impetus in the following decades. On the one hand, strategic and economical reasons prevented the implementation of faster and faster aircraft in air forces fleets of both western and eastern block during the Cold War. Costs escalation related to complex design challenges and the advent of ballistic missiles indeed led to funding cuts on a number of projects for aircraft flying at more than Mach 3. On the other hand, the shift towards fuel-burn reduction of commercial aviation, due to both environmental concerns and fluctuating oil prices, hindered the emergence of civil high-speed flight. Struggles in making the Concorde profitable and the enormous development costs prevented its sales to a large group of airlines; concurrently, the only potential rival, the TU-144, was never put into regular service due to project flaws. Public concern has also played a major role in operation disruption: at the beginning of 2000s aviation market crisis after 9/11 attacks and the tragic crash of a Concorde near Paris airport gave the final blow to the already troubled SST situation.

However, even without short-term industry projects, the research on supersonic aircraft technologies has been continuously carried out in the last 20-30 years. Modern computer-aided design techniques and the increasing "value of time" in an always faster and more interconnected world are bringing a new perspective over development and market potential of civil supersonic transport [19]. While more detailed review of ASO applied to SST is reported in Sec. 1.3.5, in the following paragraphs past applications and future projects for SST are briefly illustrated, highlighting how the niche research of the this research project can have an impact on near and far future of high-speed flight. Particular focus is put on aircraft aerodynamic characteristics, while observations on propulsive and structural features are out of the scope of this review. Most of the material consulted for the historical review is suggested by the exhaustive Prof. Mason's Configuration Aerodynamics course notes at Virginia Tech [41].

### 1.2.1. Historical background on supersonic flight

The first years of supersonic flight were characterized by feverishly research, as early experimental and theoretical investigations (Sec. 1.1) explored this previously-unknown field and took apart the initial scepticism of part of aviation community [40]. Just over 10 years after the first supersonic flight, third-generation jet fighters such as McDonnell-Douglas F-4 were able to reach Mach 2.5. Different configurations have been successfully implemented on operative aircraft, from low-sweep and low-aspect ratio such as Lockheed F-104, to variable sweep such as the Grumman F-14 or the General Dynamics F-111, to delta wing, including the Concorde itself. An unconventional but promising configuration was proposed by Jones [60] to reduce both abrupt lengthwise cross-sectional area changes and structural loads on the wing root: the oblique wing (OBW) aircraft. To provide a minimal background on historic applications, aerodynamic details of few relevant supersonic aircraft are reported below.

**Military applications** Supersonic flight have been a prerogative of air forces since the very first prototypal types, as speed is a crucial factor for both raid, interception and survivability characteristics. The F-102 and its successor F-106 (the “ultimate interceptor”) made use of both area ruling and conical camber, this last feature extending on the most external 15% of the semi-span. The 60° swept, 2.2 aspect ratio delta wing made use of a modified 4-digit NACA airfoil, the 0004-65, comparable to a biconvex airfoil [61]; LE radius-to-chord ratios varied between 0.13–0.17%. Few years later, innovations in materials, engine layout, and aerodynamics played a key role to make the SR-71 Blackbird cruise at Mach 3, close to hypersonic region. Its baseline delta planform (with 60° and -10° LE and TE respectively) was enhanced by a blended-fuselage configuration to ensure stability at supersonic regime while minimizing trim penalty and aerodynamic center shift [62].



Figure 1.4: Detail of F-102 wing showing the conical camber of the leading edge, by Prof. Mason [41]. According to the author, this feature is so evident because it was added at a later design stage, with a trial-and-error approach typical of these early supersonic aircraft projects.

Biconvex airfoils were used at all wing sections and conical camber is introduced at wing tips to reduce aeroelastic effects. Today, one of the most advanced fighters, the Lockheed-Martin F-22, still uses of biconvex airfoils and conical camber, but has sufficient thrust-minus-drag

margin to fly supersonic without using afterburners [63]. However, even nowadays, efficiency is not primary concern for military aircraft, with developments focused on engine development and low-radar signature [64].

**Civil Transport: the *Concorde*** Civil supersonic transport has a solely resounding example: the Aerospatiale-Bac Concorde, designed in the 60s and in service from 1976 to 2003. Designed to fly at Mach 2 at more than 50000ft to maximize range [65], it was characterized by a tailless ogive delta wing planform, obtained by modifying a standard delta shape with fuselage-blended canards to find the best compromise between airfield and cruise requirements. This approach minimized detrimental canard vortices and avoided the implementation of a closely-coupled tail surface. The high-sweep angle and long root chord, which forced a “narrow body” configuration, were aimed at providing good supersonic cruise capabilities and at the same time to generate vortex lift at subsonic regime. No trailing-edge flaps were implemented, but a set of spanwise control surfaces ensured manoeuvrability at low speed and high angles of attack. A number of challenges had to be faced to ensure appropriate stability margins and landing and take-off performance for a civil aircraft, together with complex system integration that is out of the scope of this review: a detailed overview of Concorde design is provided by Leyman [65]. Overall, despite the incredible technological achievement at the time, the Concorde had high-operative costs and its off-design performance, in terms of fuel efficiency, was extremely poor [19]. The aim of this project - along with other studies carried out in recent years - is to improve overall performance of SST considering subcritical performance, a crucial factor to make SST viable and marking a fundamental step forward with respect to previous applications.

### 1.2.2. Perspective on supersonic transportation in the XXI century

As previously introduced, sonic-boom reduction and flight efficiency improvements are referenced as major issues in the design of the next generation of SST, concerning both environmental impact and operating costs. Reducing supersonic cruise fuel burn is a complex design problem that has to be addressed while also taking into account low-speed and off-design flight segments on the overall fuel consumption. Furthermore, current regulations forbid supersonic flight overland due to the damage and discomfort caused by sonic-boom at ground level. This implies that novel designs have to consider both noise reduction strategies and, more realistically in the short term, aerodynamic trade-offs to reduce drag penalty when flying at transonic regimes over populated areas.

Welge et al. [20] provide an extensive and reasonably recent (2010) overview of the NASA-sponsored projects in the 2020-2035 timeframe. Considering noise and efficiency, N+2 (2020-2025) 25-100 passenger aircraft would most likely focus on the two extremes of the “Pareto front”, with separate studies on drag and noise reduction. Forecasted technological development should allow higher MTOW N+3 layouts, with up to 200 seats, to match both requirements consistently. These projections, after less than 10 years, seem optimistic for what concerns the time schedule in the long term. The N+2 generation seems almost ready for its timely debut (Sec. 1.2.3), with witness the rebirth of commercial supersonic flight in the 2020s. Large SST design however does not currently raise interest at industrial level, and will probably taken into consideration once smaller aircraft applications prove successful.

According to multiple market and technology assessments indeed “[...] *it is apparent that a small-size supersonic transport could be the first step into a new supersonic era*” [19]. High-end customer have economical resources to afford SSBJ in the short term and take advantage of reduced flight times, while lower MTOW makes feasible to reduce fuel-burn and noise impact without developing ground-breaking technologies in the short-term. Sun and Smith [19] quantify the benefits of drag reduction for SSBJ configuration: according to Breguet’s formula derivation, an increase in aerodynamic efficiency alone of less than 15% from a starting  $\frac{L}{D} = 7$  (considered a feasible target with current technology) could extend the aircraft range by 4000nm. Concerning noise signature, Aerion Supersonic [17] and Spike aerospace [66] claim the implementation of “Boomless cruise” technology, allowing cruise at  $M=1.1-1.2$  (under certain altitude and atmospheric conditions) without disrupting noise perceived at ground-level. Such feature, if approved by FFA and EASA, could imply the possibility to fly along conventional flight routes at higher speed, leading to mileage reduction and especially relaxing low-transonic efficiency requirements. Incoming industry projects, presented in Sec. 1.2.3, plan first prototypal test flights from the next decade.

### **1.2.3. Current experimental research topics and industry concepts**

While a limited number of numerical optimization studies on SST has been published in the last decades, as presented in Sec. 1.3.5, few extensive experimental campaigns in recent years have provided valuable information for future SST development. NASA has cooperated with companies since the High Speed Civil Transport program during the 90s, laying the groundwork for current research. Investigations focused on Mach 2.4, 300-passenger aircraft that had minimum economical and technological viability at the time, but that valuable experience lead to a more rational approach to future SST and paved the way to current models implementation and critical technology development [20, 67]. European efforts on the HISAC project [68], focused explicitly on MDO techniques to address conceptual design challenges, although using low-fidelity tools. Parallel projects such as the Silent Supersonic Technology Demonstration Program by JAXA [69] have focused on the development of a scaled demonstrator for low-boom technology obtained with inverse-designed aerodynamic layout. At the time of writing (early 2019), NASA and Lockheed-Martin are currently engaged in the development of quiet transport flight demonstrator QUESST [18], that will be used to both validate design tools and test community response to reduced boom levels.

Drag reduction problem has been tackled by recent joint US industry and academic efforts which have focused on the in-flight validation of the natural laminar flow (NLF) wing. The concept, extensively addressed by Peter Sturdza in his PhD thesis [70], is based on minimizing laminar boundary layer disruption over wing surface by prioritizing favourable pressure gradients during design process. The resulting wing layout is characterized by a low-sweep angle to minimize cross-flow induced transition. Low aspect ratio comes as direct consequence of structural trade-off with slenderness ratio [71], although this last study by JAXA proposes a highly-swept configuration. The Japanese agency has indeed validated a CFD-inverse designed full-aircraft configuration aimed at NLF wing design, starting from a user-defined pressure distribution [72].

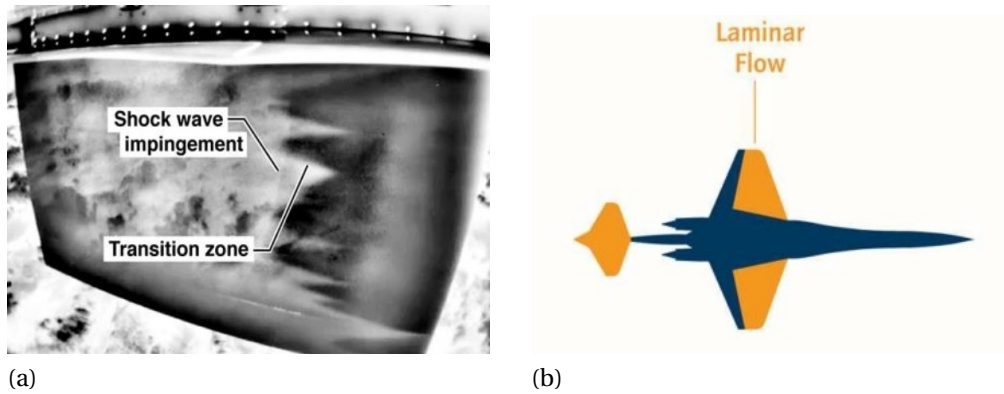


Figure 1.5: Aerion Supersonic and its Natural Laminar Flow technology: (a) a snapshot from experimental campaign on NLF highlighting laminar flow (light grey) and transition to turbulent boundary layer, from [73] and (b) the expected laminar flow area extension on Aerion AS2 [74]

However, NASA campaigns [73, 74], as reported in Fig. 1.5(a), show how the configuration proposed by Sturdza and Aerion supersonic has solid chances of success. The company, founded by Richard Tracy, has founded its roots in NLF technology and efficient off-design transonic flight, also implementing “morphing” control surfaces and other technical gimmicks to ensure consistent performance throughout the whole flight envelope [75–77]. Fig. 1.5(b) highlights how the whole configuration aims at postponing turbulent transition. According to Sun and Smith [19], there is a number of companies that claim to be involved in SBJJ development, such as Boom supersonic [78] and Spike Aerospace [66]. Aerion corporation however has at the time of writing the most promising SST project, with first flight planned for early 2020s. Nevertheless, Lockheed effort with both Aerion AS2 and QueSST development [18], together with the “dormant” interest of major companies such as Boeing and Gulfstream, suggest that soon the competition for next generation of SST could be much more intense.

#### 1.2.4. Supersonic Mission Profile

As short digression, it is of interest to provide a brief overview of SST flight envelope. Leyman [65] in his Concorde review underlines how supersonic and subsonic flight segment have almost equal importance at design stage, with however the subcritical part unavoidably split into a number of sub-sections (take-off, climb, hold, diversion to alternate airport) that are hard to accurately include in the model. Typical mission envelopes reported in [33, 79, 80] and others feature a constant-lift high altitude supersonic cruise section between M-1.4–1.6; emissions concerns regarding the impact on high atmosphere limit the maximum operative altitude to 55000ft( $\approx$ 16800m) [20], while on average cruise altitude is around 45000ft. What is peculiar of SST mission is the quick dive-acceleration from subsonic to supersonic speeds once received high-speed flight clearance, to minimize the time spent in the high-drag transonic region. Due to overland speed restrictions, Concorde transatlantic route, as illustrated in Fig. 1.6 was longer than conventional paths in order to accelerate to supersonic regime as soon as possible. Change in regulations and concurrent sonic-boom minimization could play a crucial role towards shorter and more efficient SST mission routes.



Figure 1.6: Concorde navigation map for transatlantic routes [81], *Sierra Mike* in green (westbound), *Sierra November* in cyan (eastbound), and *Sierra Oscar* in purple (bidirectional).

### 1.3. Aerodynamic shape optimization: conceptual approach and applications to supersonic aircraft design

In this section the fundamentals of computer-based aircraft design and optimization are presented and the potential of these strategies is demonstrated by a review of most notable literature examples. Before I discuss previous MDO studies applied to aircraft and, more in particular, SST design, I briefly present a broader optimization problem definition (Sec. 1.3.1) and its intrinsic challenges. State-of-the-art tools and applications are presented in Sec. 1.3.3 to outline the current MDO capabilities and the scope of the analyses carried out in this project. A dedicated section is focused on the “curse of local minima” addressing multimodality issues in gradient-based aircraft optimization (Sec. 1.3.4), before discussing more in detail the core research background related to this thesis project. Relevant examples of ASO and MDO applied to supersonic aircraft are reported and analysed in Sec. 1.3.5, while a short ending section illustrates the fundamental concept beneath the morphing wing technology I implement in the optimization problem.

#### 1.3.1. Optimization Problem Fundamentals

The optimization problem, from a mathematical point of view, consists in the minimization (or maximization) of a function subject to constraints [82]. The problem can be described in the following form:

$$\begin{aligned}
 &\text{Minimize} && F(\bar{x}) \\
 &\text{Subject to} && g_j(\bar{x}) \geq 0 \quad j = 1, \dots, J \\
 & && h_k(\bar{x}) = 0 \quad k = 1, \dots, K \\
 & && X_{i_{min}} \leq X_i \leq X_{i_{max}} \quad i = 1, \dots, N_{DV} \\
 &\text{with} && \bar{x} = \{X_1, \dots, X_{N_{DV}}\}
 \end{aligned} \tag{1.7}$$

where  $F(\bar{x})$  is the objective function,  $g_j(\bar{x})$  and  $h_k(\bar{x})$  are the equality and inequality constraints respectively and  $X_i$  are the components of the design vector, which are bounded by  $X_{i_{min}}$  and  $X_{i_{max}}$ .

The objective function quantifies the performance of the system under investigation. For aircraft optimization it is in general a functional of the system state variables  $\omega$ . Drag coefficient, for example, depends on state variables value distribution over the flow field, so that the previous function  $F(\bar{x})$  could be made explicit as  $F(\bar{x}) = C_d(\omega, \bar{x})$ . Comparable functions, such as lift, pitching and bending moment (or even more complex phenomena such as buffet [83]) are evaluated to define non-linear constraints, which brings additional challenge when calculating objective sensitivities and defining optimization steps, as discussed in Sec. 2.4 and D.

All optimization algorithms have an iterative scheme [82]. As the objective function and constraints can often be non-linear, ASO algorithm has to be selected accordingly. A comparison between different optimization schemes is reported in Sec. 2.4. According to Wolpert [84] there is not a specific algorithm that is an all-around best choice and thus the optimizer choice has to be tailored to the specific class of problems. The solution of an optimization problem must satisfy the so-called *optimality conditions*, which vary with the algorithm structure itself. For example, in gradient-based optimization the optimality condition is generally a threshold on the norm of the gradient calculated at the last design point.

A visual representation of a simple optimization problem for a constrained design space is illustrated in Fig. 1.7.  $X_1$  and  $X_2$  are the design variables,  $c_1$  and  $c_2$  the constraints and  $x^*$  the optimal solution. This must necessarily lay in the feasible region, thus (active) constraints force the optimizer to converge to an optimal feasible solution rather than the minimum (or maximum) of the unconstrained design space. A robust framework must be able to quickly reach constrained optimum in multidimensional design spaces regardless of the initial design point [82].

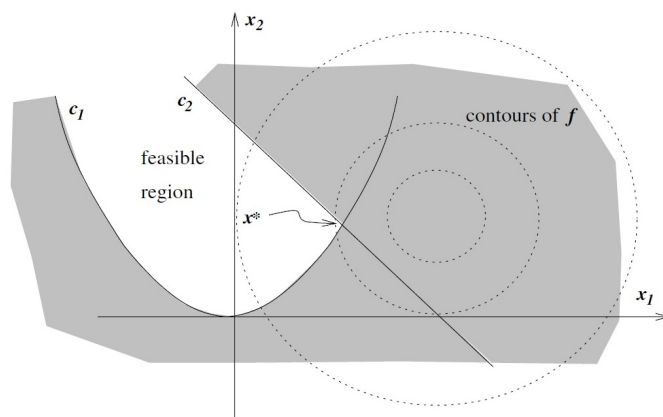


Figure 1.7: Geometrical representation of an optimization problem design space from [82], with  $x_1$  and  $x_2$  design variables,  $c_1$  and  $c_2$  (inequality) constraints,  $f$  objective function and  $x^*$  constrained optimum.

**Design vector** A design variable is defined as a parameter which is explicitly under the control of the optimizer [2]. The design vector is the array that wraps all the design variables

and thus mathematically define the design space in all its degrees of freedom. For the specific case of aircraft aerodynamic design, the optimizer has the control of the external shape of the vehicle or outer mold line (OML). A well-posed problem presents mutually orthogonal (namely, linearly independent) design variables [85]. As a point-by-point definition of the shape is unnecessarily complex if not unfeasible, geometry definition is addressed by defining a suitable parametrization scheme (notable examples discussed in Appx. A). Practically speaking, the design vector contains control points position or polynomial coefficients that provide direct control on the geometry. Thus, the choice of the scheme implicitly defines the design space topology [86].

The design vector size has a first-order impact on the optimizer overall performance, as discussed later in Sec. 2.4. There is a trade-off to be considered between reducing the number of parameters to increase the convergence speed or increasing them to ensure higher design freedom and, potentially, accuracy. Using an insufficient number of variables can forbid the optimizer to improve the current design; nevertheless, an excessive number of control points can lead to convergence problems due an overly complex design space, given by intractable coupling effects among parameters [86] or excessively small modifications to be properly evaluated by the flow solver, especially on coarse grids.

For MDO problems, the design variables are generally classified as global or local if they are shared among multiple disciplines or relate to a single discipline respectively [2]. However, a different definition proposed by Bons et al. [37] is more suitable to the solely ASO problem. The authors define as *global* the variables which simultaneously act on a number of control points (as for example for wing twist modifications), while *local* variables are related to single control points displacements.

Setting consistent upper and lower bounds for design variables is crucial, as shown in early studies such as Drela [5]. In general, when optimizing a wing or a wing section based on the solely aerodynamic discipline, constraints are set to ensure the feasibility of the final shape in terms of structural and (as far as possible) manufacturability. Benchmark cases defined by ADODG [87], given the initial geometry, suggest to maintain the same initial thickness (case 1), airfoil area (case 2), internal wing volume and local thickness (case 4 and 5), wing planform area (case 6) or limit wing tip twist (case 3). However, when it is of interest to start from different initial shapes, the use of “absolute”, dimensional value constraints is necessary.

**Constrained optimization** Aircraft design is an inherently constrained problem and numerical methods have to ensure a robust handling of these conditions. Indeed, even if the problem does not include “performance” constraints, geometry definition itself poses constraints that have to be satisfied by the design variables [86]. A detailed constrained optimization theory review is out of the scope of this survey, as it is exhaustively covered in publicly available books [82, 88]. However, it is useful to recall some basic concepts for later discussion.

A generalized objective function defined according to lagrangian theory, is reported using the same notation used in Eq. (1.7):

$$I = F(\bar{x}) + \sum_{j=1}^{N_1} \gamma_j g(\bar{x})_j + \sum_{k=1}^{N_2} \hat{\gamma}_k (h(\bar{x})_k - s_k^2) \quad (1.8)$$

where  $\bar{\gamma} = \{\gamma, \hat{\gamma}\}$  are the so called lagrangian multipliers, which allow to “adjoin” the constraints to the unconstrained objective function. When solving the problem analytically, these coefficients must satisfy the *Karush–Kuhn–Tucker* conditions [89, 90] and have to be considered as additional variables, increasing the dimensionality of the problem.  $s_k$  are the so-called slack variables. These variables are used to transform an inequality constraint into an equality constraint and are defined so that the initial inequality is satisfied:  $h(\bar{x})_k - s_k^2 = 0 \Rightarrow h(\bar{x})_k \geq 0$ . When solving the problem with numerical approaches, the same mathematical form is used to define a merit (or cost) function where the lagrangian multipliers and the slack variables act as penalty factors [86] on the unsatisfied constraints, as for example done for SNOPT algorithm [91] used at MDO Lab. With this strategy, any constrained optimization problem can be turned into a corresponding unconstrained problem and solved with a range of numerical algorithms. Quoting Drela [5]: “*The net effect is to project all changes in the design space onto the admissible constrained subspace*”. So, the optimization steps are taken strictly along the allowable subspace of the control function, allowing to find a solution to the problem even when the (unconstrained) optimum is unattainable [92].

**Problem convexity and topology** A design space is defined *convex* if the  $N_{DV}$ -dimensional linear segment between two design points lies entirely inside the design space itself [82]. Currently, there is not a mathematical proof that can prove the convexity of the design space for ASO problems and thus the presence of a global optimum. For this reason, ASO solutions are defined as “optimal” in a local sense [2]. However, it is possible to reduce the uncertainty about the “globality” of a solution by benchmarking the problem with different optimization strategies and baseline configurations [1, 86, 93]. The smoothness of the design space and the objective function is a fundamental condition that ensures the predictability of the function [82], especially when a gradient-based optimizer is used. Discontinuities lead to meaningless sensitivities value and eventually (depending on the relative position of the initial point and the local minimum) prevent the problem from converging. This very same consideration also explains why gradient-based algorithms cannot handle discrete variables. This is not the case for ASO problems however, which are in general defined by the use of continuous variables. The concern about design space convexity has to be addressed to prove the accuracy and robustness of the optimized designs. Studies regarding the presence of multiple local minima in ASO problems are presented in Sec. 1.3.4.

**Multipoint optimization** The necessity to design an aircraft for a range of different conditions is intrinsic to its own engineering concept and becomes more important when numerical methods are implemented in design process, as discussed in Sec. 1.3.2. An aircraft indeed spends part of its typical flight envelope flying at lift, speed and altitude conditions that are other from nominal design values, as during take-off, landing or holding. Moreover, it is not guaranteed that a plane could always cruise at the exact design conditions,

also including uncertainties in atmospheric conditions and design and manufacturing process - leading to broader considerations over uncertainty quantification, outside the scope of the present report. ASO is particularly effective to minimize, for example, drag at a certain design point, but often this performance improvement is related to detrimental effects at off-design conditions, thus becoming potentially counterproductive. It is particularly interesting to notice that two studies carried out at almost 20 years apart with different tools, Drela [5] and Kenway and Martins [83], show comparable results in this sense. Multipoint optimized shapes in general tend to sacrifice the single design point to improve the average net performance.

From a mathematical point of view, multipoint optimization consists in the formulation of an objective function which is the weighted sum of the different objective functions evaluated at single-point. The weights choice for the different design points is up to the designer itself [8], that once more have to creatively formulate the problem in a meaningful way for practical application. The optimizer then runs and assess the sensitivities by simultaneously averaging the improvements and detrimental effects between single point cases. If properly formulated, the problem can be parallelized [6, 7], further saving computational time. Relevant examples are reported in following Sec. 1.3.3.

### 1.3.2. Development of modern ASO

The first numerical simulation tools were initially developed to obtain better insight on complex fluid dynamics phenomena and estimate the flow behaviour of different designs, without the necessity to run wind tunnel experiments. Being able to predict the characteristics of alternative layouts, engineers soon started questioning themselves about how to take advantage of this capability and automatically modify the design to improve its performance. Despite the accuracy and flexibility of these early flow solvers were not comparable to current software, the nature of the engineering and mathematical problem is substantially identical.

On the practical side, a useful and effective design tool, regardless of the selected physical model and fidelity level, “[...] *must also be robust, not liable to fail when parameters are varied, and it must be able to treat useful configurations, ultimately the complete aircraft. Finally, reasonable accuracy should be attainable at reasonable cost.*” [3]. As additional feature, the method should be also flexible enough to be applied to a range of physical conditions, shapes and constraints.

Early works by Hicks et. Al [94, 95] represent a first relevant example in terms of usability and effectiveness. The practical method for ASO of non-lifting transonic airfoils presented in [94] and wings [95] made use of an already existing inviscid aerodynamic analysis tool coupled with a feasible-directions-method-based optimizer. These early publications lead the way by showing promising results, but were inevitably affected by accuracy and reliability problems. In the following decade, Jameson [3] gave fresh impetus to research by applying the control theory to aerodynamic design and thus introducing the “adjoint method” (Appx. D), cornerstone of current gradient-based ASO strategies. The aim of this study was to prove the “[...] *benefits in regarding the design problem as a control problem in which the control is the shape of the boundary*” [3], where the design problem itself involves a system governed

by PDE. It was indeed shown that such an approach can be used to formulate optimization problems with reduced computational cost.

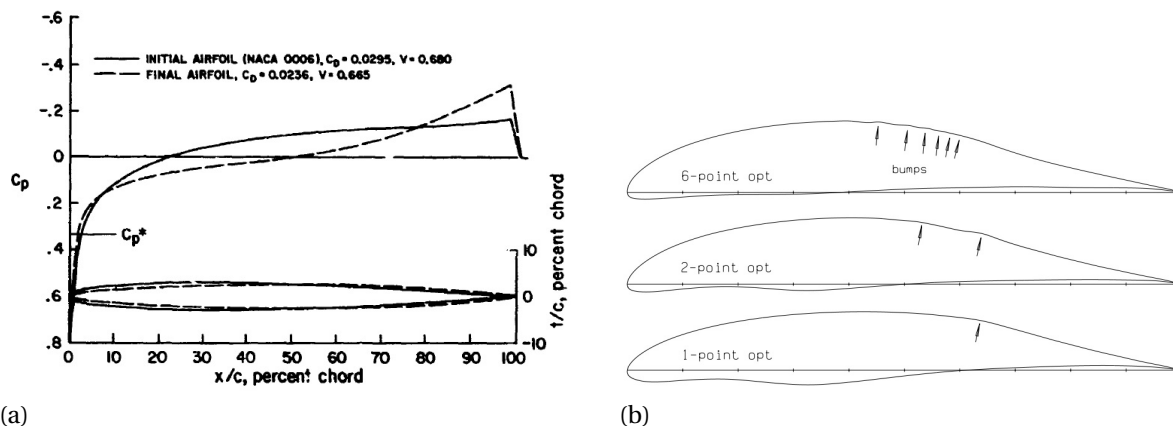


Figure 1.8: Results from early ASO studies. (a) Hicks and Henne [94] performed a supersonic airfoil optimization study using a primitive analysis tool, that however provided consistent results with analytical and experimental data for this simple case study. In (b) Drela [5] presents results for subsonic, multi-point airfoil optimization as part of a broader analysis of the influence of problem formulation on optimal designs. The optimizer induced a number of bumps on the suction side (highlighted by arrows) that would delay flow separation at different design conditions - for single-point, two-point, and six-point respectively.

Comparable studies from the 90s, such as Drela [5], shifted the focus from the numerical consistency of the tools to the actual engineering problem definition and the related design “creative” process. A lift-and-pitching-moment-constrained airfoil drag minimization problem was investigated using an Euler-solver coupled with a boundary layer model and an interactive optimizer. Even for the simplest design cases then, it becomes clear how crucial it is to ensure proper bounds and limit the design space so to exclude a-priori any unfeasible layout. Consistent constraint definition however does not guarantee robust results: single-point optimized shape provided poor off-design performance. If this on the one hand proves once more the effectiveness of ASO, at the same time highlights the necessity of multi-point optimization to improve the robustness of final design. The author itself when it came to explain the unexpected results stated: “*The real deficiency here is not with the optimization technique, which gives the demonstrably correct answer, but rather with the formulation of the optimization problem itself.*” [5]. Such conceptual errors are more actual than ever at both industry and academic level, as often designers rely too much software capability to converge without actually ensuring a consistent problem definition.

### 1.3.3. State-of-the-art: High-fidelity gradient-based ASO for subsonic and transonic configurations

The first pioneering works presented in Sec. 1.3.2 have introduced the challenges of numerical modelling for aerodynamic shape optimization. Since early 2000s, with the leap forward made by both hardware and software and the implementation of new numerical approaches, the research on MDO and ASO has been significantly boosted. To illustrate the latest advancements in this sector, given the lack of recent high-fidelity ASO for SST that

fosters this very research project, a number of relevant studies on transonic and subsonic configurations are hereby presented, to be later used as qualitative benchmark. Two crucial topics such as parametrization, Appx. A, and multimodality of the design space, Sec. 1.3.4, are discussed in dedicated sections.

The efficiency, accuracy and explorative design capabilities of low and especially high-fidelity numerical optimization tools are exploited when applied to aerodynamic design of lifting surfaces. Wing design is indeed one of the most blatant and effective applications of ASO. Its complexity and crucial role in characterizing the system performance are well described by a veteran Boeing 747 engineer in [96] (as reported in [93]) who compares the aircraft wing itself to a “*Savile Row suit*” in terms of “*literally thousands of decisions*” and “*many invisible tricks built into its shape*”. This design complexity, which is simplified (especially at conceptual design level) by the use of low-fidelity tools and more simple parametrization approaches, translates into a vast number of design variables and system analyses that have to be handled, when it comes to high-fidelity optimization.

Notable works have been produced by Prof. Zingg and his colleagues at University of Toronto, focusing in particular on the manipulation capabilities. Hicken and Zingg [97, 98] developed a (inviscid) high-fidelity gradient-based optimization tool with a sophisticated spline-based mesh deformation module. The proposed approach guarantees high-quality meshes while reducing specific CPU time by two or three orders with respect to comparable schemes, now estimated about less than 5% of the overall computational time. Gagnon and Zingg [99] proved that with this methodology it is possible to obtain a BWB configuration starting from a sphere, however neglecting the impact of viscous phenomena. This latest study however Independent work at McGill University by Nadarajah and Tatossian [100] extended gradient-based optimization to viscous unsteady flows. Unsteadiness issues however are not a primary concern for cruise drag minimization studies. Despite the relevance of capturing unsteady phenomena such as wake and boundary layer separation in aerodynamic (and aerostructural) design, steady numerical approaches are considered satisfying in a broader sense. The additional drag estimated by forcedly-steady flow separation is high enough to prevent the optimizer to look for an optimal solution in these areas of the design space.

In the last decade, University of Michigan’s *MDO Lab* research group has developed a powerful optimization framework named MACH (described in Sec. 2.0.1), raising the bar in terms of accuracy, scalability and constraint handling for high-fidelity aerodynamic and aerostructural optimization. Mader et al. [101] developed an hybrid sensitivity analysis method that coupled a selective automatic differentiation code with an adjoint method to efficiently calculate the required partial derivatives. This approach can be applied to arbitrary set of governing equations and boundary conditions, with measurable advantages in terms of required memory and computational cost. After the first application to an Euler-based CFD tool, Lyu et al. [102] extended the methodology to a RANS-solver using TAPENADE [103], thus implementing the calculation of viscous and turbulence model sensitivities. Kennedy et al. [104] enabled the parallelization of the aerostructural optimization framework improving the scalability of coupled and complex optimization problems with a high number of design variables.

Lyu et al. [10] present a interesting reference case in terms of quality and breadth of the analysis. A series of benchmark optimization for the CRM wing only geometry are presented

with plentiful information on design variables and optimization trends, allowing an insightful comparison of baseline and optimal shape.

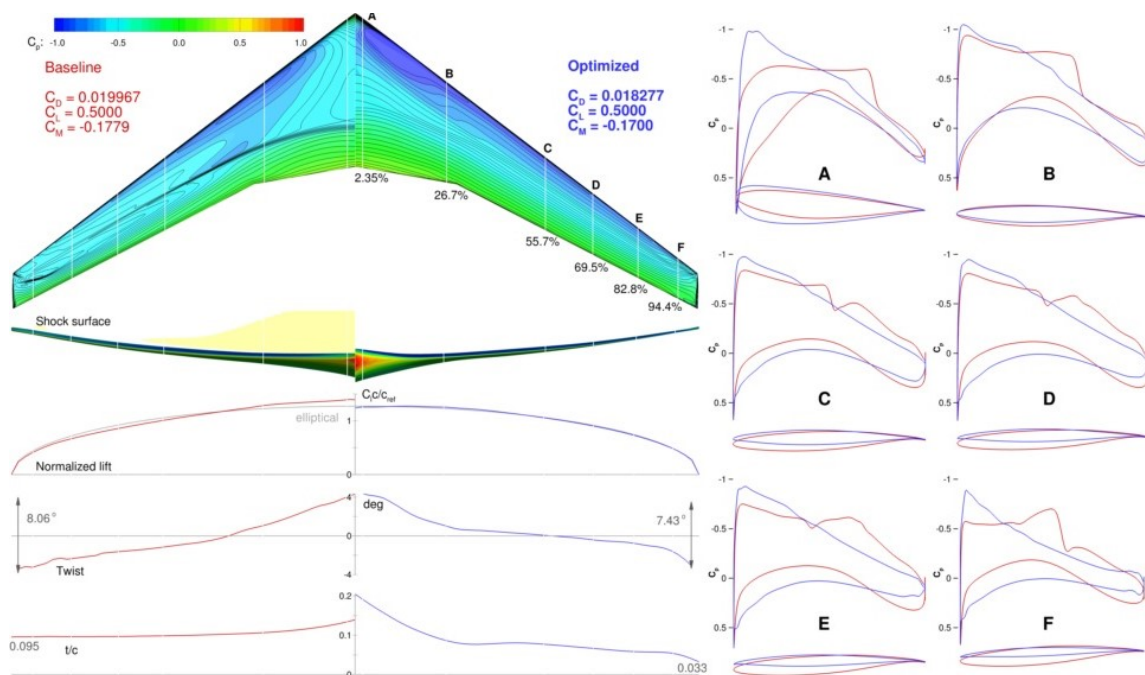


Figure 1.9: Comparison between baseline and optimized wing by Lyu et al. [10]. The optimizer has been able to virtually eliminate shockwaves over the wing at cruise conditions.

To provide a practical example, in Fig. 1.9, results for single-point transonic case are presented comparing baseline and optimized full-wing and cross sectional shapes with relative lift, twist, thickness, and pressure distribution. Data is complete and easy to interpret and comment. It emerges that, for the specific case, the optimal shape has an almost elliptical lift distribution and a virtually shock-less upper surface thanks to a combination of twist and shape variations. The final target of the master project is to produce a similar analysis for one or multiple supersonic wing configurations, including single-point and multi-point optimization cases, also including morphing capabilities.

**Constraints implementation** The feasibility of the optimized configurations has been regarded as a relevant obstacle that prevents the extensive application of MDO techniques at industry level. Among other issues discussed in this survey, the definition of more physics-based constraints plays a crucial role in this sense. Mader and Martins[105] first applied stability constraints and bending moment constraints to ASO while Ning and Kroo [106] implemented a stall speed constraint based on maximum local  $C_{l_{max}}$ . Kenway and Martins [83] formulated a less intuitive separation-based buffet constraint that is directly evaluated from the steady-RANS solution, while Bons et al. [107] have successfully coupled flight envelope constraints such as climb rate and take-off field length. Again, these studies prove the maturation of high-fidelity MDO tools and their ability to take into account complex design requirements. The benefits in (future) extension of similar methodologies to supersonic aircraft configuration are particularly marked due to the intrinsic diversity of its flight envelope in terms of speed and altitude.

**Multipoint optimization applications** The relevance of multipoint optimization to improve the robustness of optimal layouts has been already discussed in the previous sections. Among most cited examples of high-fidelity studies taking into account multiple design conditions, Nemec et al. [8] investigated 2D multipoint gradient-based optimization with RANS solver, including high-lift conditions and extending the problem to multiple objective functions. Results show how multipoint optimized airfoil drag divergence Mach number is increased by 0.05 (approx.7%) without drag penalties at lower speed. Peigin and Epstein [108, 109] took a different approach using genetic algorithms and reduced order models with massive parallelization to improve the performance of a wing-only and wing-body configuration. Despite the lower accuracy if compared to full high-fidelity, results again show how this approach can postpone drag divergence for transonic configurations by up to  $\Delta M=0.1$ . A more articulated approach based on historical operational data and surrogate models for mission analysis has been used by Liem et al. [110]. Authors proposed an automated selection of design points and relative weights for high-fidelity aerostructural optimization, making use of surrogate models to approximate the performance throughout the flight envelope. This increases design robustness of the final design with relatively reduced computational cost - which however still requires the use of supercomputers. Detailed analysis of MACH multipoint aerostructural optimization capabilities, backbone of this study, has been reported by Kenway and Martins [11, 12]. A less accurate but meaningful mission performance estimation is derived from Breguet's range equation, once more proving the soundness of this approach if compared to single-point studies. The results of these few examples suggest how performance and design robustness improvements given by aerodynamic (and structural) multipoint optimization are even greater when the strategy is applied to "diverse" flight envelopes, such as the typical SST mission illustrated in Sec. 1.2.4.

**Unconventional configurations** MDO and ASO techniques have been successfully used to explore design spaces for unconventional configurations, suggesting a great potential to improve the fidelity of the studies on supersonic configuration later presented in Sec. 1.3.5. Hicken and Zingg [98] investigated wake and lift-induced effects on aircraft fuel consumption given by winglets and non-planar configurations, exploiting non-planar wing-tip wakes to reduce induced drag. The use of high-fidelity tools is crucial for this study because it allows to model high-order effects such as wake shape and induced lift, although accuracy is limited by the use of Euler-based CFD. Gagnon and Zingg [111], focusing on comparable non-planar layouts, make use of a combination of axial and FFD design variables to perform a full-configuration ASO study, obtaining drag values lower than up to 46% when compared to reference civil aircraft. An high-fidelity ASO of a Blended-Wide-Body configuration has been carried out by Lyu and Martins [112], who used MACH framework to study the trade-offs between drag minimization and trim, stability and bending moment requirements (the last to address structural concerns). Secco and Martins [113] used the same framework to optimize a strut-braced wing aircraft, using overset meshes and component based parametrization to minimize detrimental effects due to strut and wing interaction. The examples hereby briefly summarized prove how high-fidelity tools provide an unmatched insight on non-intuitive trade-offs when it comes to conceptual and preliminary design of novel configuration, dramatically reducing design time and costs if compared to more traditional approaches.

**Modern airfoil shape optimization** Airfoils have been used as simple and lightweight design case to test optimization techniques and framework since the early stages of ASO, (Sec. 1.3.2) and are subject of relevant publications still today. Focusing on recent publications, Buckley et al. [114] performed an 18-point multipoint optimization comparing an unconstrained approach with automatic weight update, to get insight on single points relevance, with a SNOPT-based approach where off-design manoeuvrability constraints are explicitly handled, thus improving convergence. Broader aerodynamic considerations and the presence of local minima suggest that however final design is not as robust as intended and the problem should be extended to the wing, raising however computational cost constraints due to the (excessively) high number of design points. The weighted-integral-objective-function approach suggested for comparable design cases in [115] however appears promising, especially when considering multi-objective optimization.

Other recent investigations on 2D ASO robustness by Poole et al. [116, 117] highlight once more how different single-point and multi-point RANS-based optimization result are for a lift-constrained drag minimization problem, as illustrated in Fig. 1.10. Authors in particular stress on the relevance of an optimal solution with shocks for better off-design performance. An interesting comparison is made between these results and a range-maximization ( $\max F = M \frac{C_l}{C_d}$ ) problem using non-dimensional wing loading constraint ( $MC_l^2 = l$ , with  $l$  constant non-dimensional lift). The design point is included among the design variables - as for flight envelope optimization - and an induced drag penalty factor to model detrimental effects of high  $C_l$  on full wing drag. Results show potential advantages in terms of robustness due to shocked optimal layouts and postponed drag divergence, although more detailed insights should be obtained by future work.

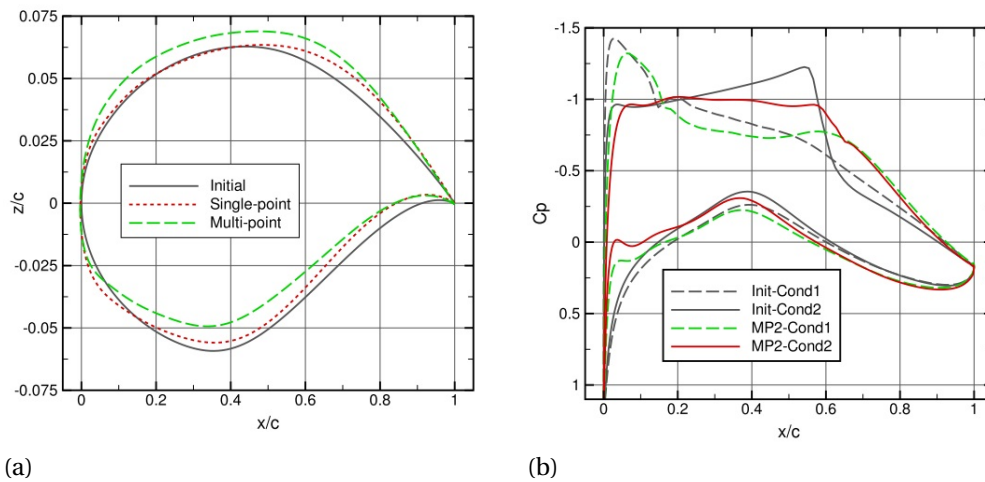


Figure 1.10: An example of airfoil optimization from [117] comparing shapes (a) and pressure distributions (b) for single-point and multi-point optimized airfoils. The impact of different objective functions on final shapes is highlighted by different  $C_p$  distributions.

Introducing a different example of airfoil optimization, Li et al. [118] recently performed a surrogate-based drag minimization study that showed a relatively small error if compared to RANS-based optimization. Despite this kind of approach is out of the scope of this survey, it is interesting to notice how airfoil ASO is still a relevant benchmark case for innovative

methodologies. However, extending this strategy to wings and full configurations for diverse flight conditions (including supersonic) with comparable accuracy and time saving is a challenging task that has to be tackled by future research.

### 1.3.4. Multimodality

In Sec. 3.5, the concept of design space convexity has been introduced. The presence of local minima in aircraft optimization problems is a non trivial issue that has been carefully investigated in recent years. The dependency of gradient-based algorithms on initial starting point and algorithm line search makes these approaches vulnerable to get stuck into sub-optimal configurations. However, according to Martins et al. [1] “[...] *the existence of multiple local minima (multimodality) has been overstated*” for these approaches. This relatively limited risk, together with the advantages in terms of computational cost and scalability for a high number of design variables, makes them the preferred choice for most 3D ASO studies and a relevant fraction of 2D studies.

Although the existence of a global optimum cannot be proved analytically, researchers usually validate and benchmark their results to minimize this uncertainty around the accuracy and robustness of the solution. For an airfoil problem, early works [119] suggested the possibility of multiple optimal solutions for wing sections, as low-drag shapes distant from the initial design point were found with gradient-free optimization methods. The already mentioned Buckley and Zingg [114] claim to have individuated local minima for 2D ASO as well. More recent research by Chernukhin and Zingg [120] (based on the ASO tool by Hicken and Zingg [97]) however showed that, despite coming to similar conclusions of [37] for 3D problems: “*typical two-dimensional airfoil-optimization problems [subsonic and transonic] are unimodal*”. Varying initial shapes, design variables number (B-spline control points), sub-critical Mach number and objective function do not induce additional local minima and gradient-based optimization proves to be the most efficient. Thus, it seems unlikely that supersonic airfoil design space could be affected by local minima, unless for minor discrepancies given by parametrization scheme. However, this possibility has to be investigated by starting from different initial airfoil configurations or randomly generated shapes as done in [10, 37, 120].

It emerges from [120] how for full-configuration optimization the design space is prone to be multimodal. The reported blended-wing-body ASO presents 8 radically different local minima due to the high geometric flexibility of the problem. Such moderate multimodality however could be induced by the use of inviscid flow solver and not tightly converged solutions, two crucial factors that will be largely taken into account for the thesis project. Nevertheless, authors conclude that “local” gradient-based optimization is generally adequate for high-fidelity ASO due to the relative proximity to the optimum and the strict geometry constraints. A specific ADODG[87] case, No.6, has been formulated to study the presence of local minima for transonic rectangular wing drag minimization. Bons et al. [37] investigated the issue in depth using a multifidelity approach and individuating several critical issues, as illustrated by the example in Fig. 1.11.

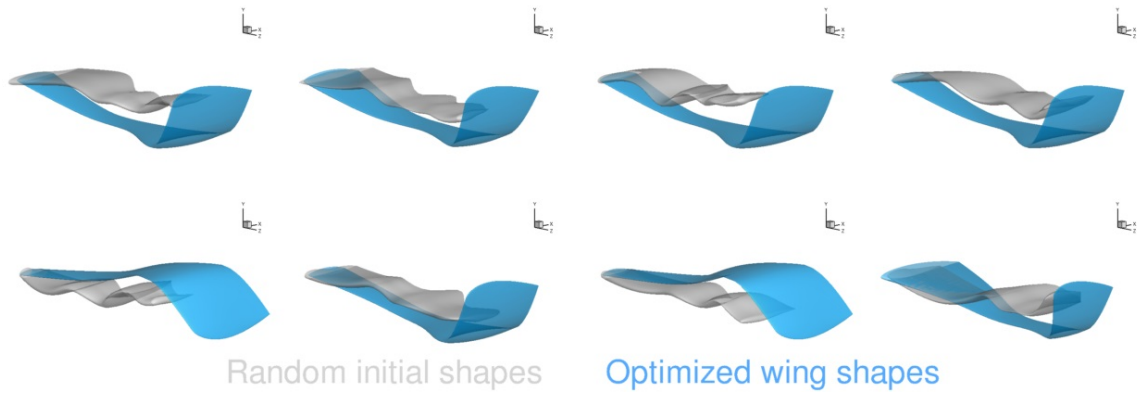


Figure 1.11: An example of multimodality by Bons et al. [37]. A lift-constrained ( $C_l=0.2625$ ) inviscid aerodynamic shape optimization of a wing, starting from randomly generated baseline shapes, converges to different local minima.

It is shown how the introduction of chord and dihedral variables induces local minima in the design space, together with the strong influence of the lift coefficient. This test case moreover appears to be dominated by trade-offs between viscous and induced drag. If multiple inviscid optimal solutions as those reported in Fig. 1.11 cannot be physically explained, the introduction of viscous effects produces more meaningful results - even if may add additional multimodality. Lyu et al. [10] find local minima in the design space when starting from randomly deformed initial shapes. However, optimal layouts differ by max 0.1 drag counts and no more than 0.4% of the mean aerodynamic chord: such small differences in authors opinion do not justify an extensive search for a global optimum. This supports the use of RANS-based optimization tools to explore wing design spaces. Moreover, it suggests that a more reality-based problem formulation, taking into account multiple flight conditions, coupling with a structural model, and more meaningful geometric constraints, could significantly reduce multimodality. Finally, as suggested by previous works [86, 120], it is also crucial to carefully assess parametrization scheme and solution convergence level to rule out “fake” local minima due to poor quality of the results.

### 1.3.5. Supersonic aircraft optimization

The development of analytical models based on linear flow theory by Von Karman [39], Munk [121] and Tsien [122] has fostered the research on supersonic aerodynamic performance since the 1950s. With the advent of numerical optimization, Hicks and Henne [94] applied their novel ASO approach to the design of a supersonic airfoil, highlighting how, despite the good approximation, theory could not predict more complex compressibility and viscosity effects, even for simplified cases. Reuther et al. [22, 123, 124] first used Euler-equations-based optimization strategies, as shown in Fig. 1.12, to improve the L/D of an SST configuration considering nonlinear aerodynamic effects, using adjoint-method approach from control theory [3] and parallel computing to reduce computational cost. The inviscid drag of a generic SST configuration was reduced by up to 8% by solely optimizing wing sections shape and local twist [124].

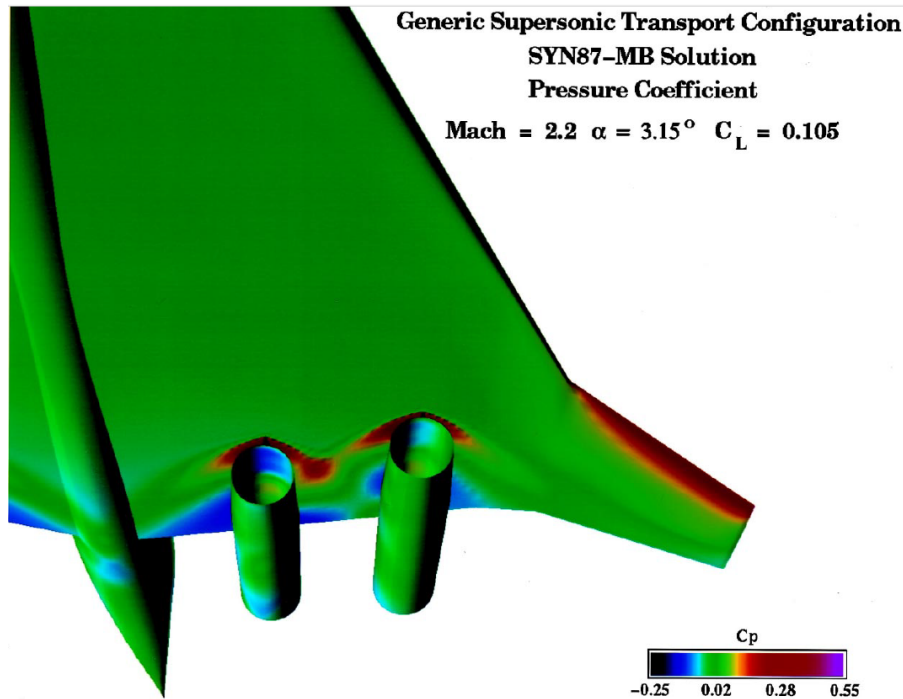


Figure 1.12: Detail of the SST configuration optimized by Reuther et al. [124]. Authors used SYN87-MB solver coupled with a gradient-based optimizer using adjoint method and code parallelization to increase computational performance.

Similar approach was also used by Kim et al. [125], who obtained comparable results for a wing-body-nacelle configuration. A concurrent study by Cliff et al. [126] investigated the benefits of considering multiple flight conditions for SST design optimization, using inviscid gradient-based ASO tools developed under NASA's high-speed research programme. They demonstrated how simultaneous multipoint optimization could improve the performance of a highly constrained configuration at all design conditions, with better results than a sequential shape and trim optimization.

In the late 90s European industry and academia exploited the potential of multipoint [23, 68, 127, 128] and multidisciplinary [129] optimization strategies to reduce supersonic aircraft drag at high and low speed, showing however limits in terms of framework efficiency and accuracy. The aim was to obtain better insight at conceptual and preliminary design level: viscous effects were neglected or approximated and few variables were taken into account due to expensive sensitivities calculation methods implemented. More advanced MDO tools have been developed to perform consistent mission optimization of different SST configurations [130–132]. Considering the aerodynamic analysis modules implemented in these frameworks, inviscid CFD tools were used for cruise condition only, with viscous effects and performance at off-design conditions estimated by analytical and semi-empirical approaches. CFD computational cost and the weakness of mesh perturbation modules prevented a wider application of high-fidelity approaches. Global optimization was performed with gradient-free approaches to avoid additional complexity given by coupled disciplines sensitivities.

The use of genetic and evolutionary algorithms for supersonic ASO has been studied by

Sasaki and his colleagues [24, 133], who were able to explore a large design space and obtain a design that outperformed a traditionally developed supersonic wing. This approach allows to better identify design trade-offs and define reasonable Pareto solutions, at the cost however of an elevated number of expensive CFD analyses. A comparative study with gradient-based algorithms [134] applied to supersonic wings underlined benefits and drawbacks of the two strategies, remarking the efficiency of adjoint method to compute sensitivities but at the same time the potential risk to incur in local minima when exploring complex design spaces. Gradient-free methods that use surrogate models have a reduced computational cost, achieved however by means of high-fidelity data approximation. Kim et al. [135] performed a multipoint aeroelastic optimization for a supersonic fighter wing using a response surface model to approximate aerostructural coupling effects, while Seto [136] exploited the efficiency and explorative design capabilities of an MDO tool using Kriging based multi-objective genetic algorithm.

The excessive cost of gradient-free methods to perform high-fidelity aerodynamic shape optimization, especially when the problem is extended to a high number of design variables, limits the application of these algorithms to low-fidelity analyses. Gradient-based optimization conversely provides an accurate and efficient approach to ASO and has been profitably applied to a range of studies on subsonic and transonic aircraft (refer to [86], Sec.3, for examples). Chernukhin and Zingg [120] among others addressed the challenge given by the possible presence of local minima in the design space and demonstrated the advantages of this approach. Notable applications of gradient-based algorithms to SST optimization, after the previously mentioned works by Reuther et al., are given by Martins et al. [25], who performed aerostructural optimization of a supersonic business jet (SSBJ) by successfully implementing coupled aerodynamic and structural adjoint equations to calculate sensitivities, further showing how computational cost is nearly independent from the number of design variables with this approach. The pure aerodynamic optimization of a basic SBJJ configuration resulted in an overall inviscid drag reduction of 5.8% at Mach 1.5 thanks to spanwise lift redistribution, wing mounting angle of attack, and fuselage camber modifications. Jameson et al. [137] were able to reduce the drag of an SBBJ configurations by minimizing weak shocks over the wing, using a continuous adjoint formulation for the optimization algorithm. However, they reported results below the expectations because of limitations in flow solver and parametrization scheme of a framework initially developed for transonic configurations, once more highlighting the relevance of sub-routines accuracy in the global framework performance. A comparable high-fidelity optimization strategy has been coupled to low-fidelity response-surface-based approaches by Choi et al. [26], who presented a conceptual and preliminary design tool that embedded an Euler-based adjoint optimization module as highest accuracy approach in a two-level multifidelity framework. They were able to further reduce the low-fidelity optimized configuration drag by 7.6%. Even if noise signature considerations are out of the scope of this work, it is worth mentioning that the adjoint method has been successfully applied to sonic-boom reduction studies [138–140], further proving the potential of gradient-based optimization applied to SST configurations.

In the last decade, new MDO frameworks have been developed specifically for supersonic aircraft design. Kroo et al. [21] presented an extensive NASA-funded study focused on multifidelity MDO approaches including model uncertainty. Promising results were shown in terms of computational cost reduction for conceptual design and mission optimization,

however still lacking in aerodynamic analysis accuracy and robustness at high-fidelity level. As conceptual level MDO tools are more focused on an efficient integration of aircraft design sub-disciplines, aerodynamic analysis accuracy is often sacrificed for the benefit of computational cost [29], with CFD tools used at a latter stage to validate final designs [30, 31]. Results show a relatively small error in terms of overall drag prediction. However, previously mentioned works show how high-fidelity optimization consistently improves a low-fidelity optimized configuration. More recent works by Kiyici and Aradag [28] and Sun and Howard [33] present a combination of literature-based models for aircraft sizing routine and aerodynamic analysis, do not include viscous effects in their tools. Li et al. [141] investigated wing shape and twist optimization on a full-configuration SST using FFD parametrization. This work however makes use of a combination of surrogate, Kriging-based and CFD-trained models and particle swarm algorithms and, although the practical and insightful approach, is not directly comparable with the methodology proposed in this research.

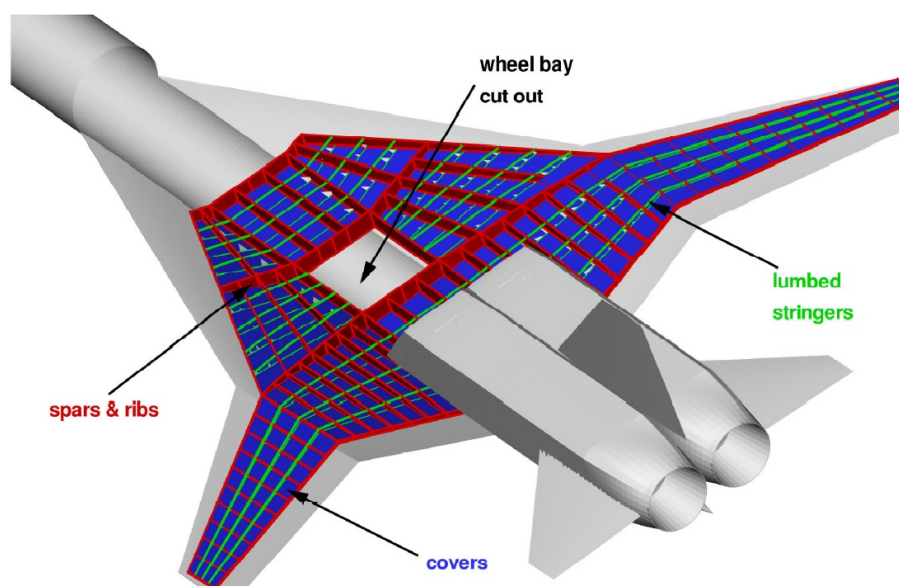


Figure 1.13: A snapshot of the structural topology of the SST configuration from Laban et al. [131]. Their high-fidelity MDO framework was developed in the context of European HISAC project.

The specific airfoil optimization problem has been generally included in the broader wing design, but few relevant works focused specifically on the 2D problem. After the already mentioned [94], Pittman [142] extended the drag minimization study to lifting airfoils with a fully potential aerodynamic solver and using a linear interpolation of a given set of airfoils as parametrization scheme, showing promising but yet inaccurate results. Kroo et al. [21] considered an airfoil optimization problem to benchmark different optimization strategies in their multifidelity MDO study, without however discussing the optimal shape performance. In recent years, Hu et al. [143] applied the adjoint method to an inviscid CFD solver to optimize a Busemann-biplane wing section to reduce noise and drag with respect to a standard shape, while minimizing configuration specific flow hysteresis phenomena. Optimized airfoil show benefits with respect to a standard diamond shape, however friction drag penalty due to the additional wetted area is not taken into account. Suga and Yamazaki [144] used a similar test case to investigate uncertainty quantification, suggesting a more robust although expensive design strategy.

Conversely, Lattarulo et al. [27] optimized a NACA0012 airfoil at fixed angle of attack using a metaheuristic optimization algorithm and Hicks-Henne functions for shape deformation. Although main focus was on algorithm validation, a specific but relevant case study is presented, Authors also highlight the offset between Euler-based and RANS-based analysis, which supports the idea of performing supersonic ASO considering viscous phenomena. Kiyici and Selin [28] finally report an inviscid-CFD-based airfoil optimization with Hicks-Henne parametrization to verify their conceptual design tool, able to reduce the drag of a NACA 6-digit of more than 20% while maintaining the same  $C_l$ . Final shape reportedly resembled a typical diamond shape wing section.

Considering the use of less conventional design solutions, the concept of a “morphing wing”, more practically the implementation of slot-less and gap-less high lift devices on supersonic aircraft wings, has not been thoroughly investigated with modern high-fidelity tools. This technology is explicitly described as a solution to improve efficiency at low speeds in multiple patents [75, 145]. In addition to off-design L/D increase, control surfaces can also be used to limit the shift center of pressure between supersonic and subsonic flight regime, reducing detrimental aeroelastic effects on thin low-torsional-stiffness supersonic wings [146]. Varying wing camber at  $M \leq 1$  potentially allows to relax the aerodynamic trade-off between subsonic and supersonic performance on clean airfoil shape, with limited mechanical complexity if compared to variable-sweep-wing configuration. The absence of steps on the surface is meant to prevent the disruption of laminar flow on the wing. Preliminary transonic L/D improvement were estimated by more than 14% [68, 128], subject however to uncertainties around flow solver accuracy. Relevant work on the topic was made by Kim et al. [147], who investigated transonic cruise performance improvement of an SST with 10 flaps equally distributed on wing trailing and leading edges. The analysis was limited by constraints on flow separation, enforced in the form of maximum Mach numbers over the wing surface, to not overcome Euler solver capabilities. Authors highlighted the potential design improvements of using a couple of inboard and outboard leading edge flaps, estimating a decrease in transonic drag of 17%. Neglecting viscous effects however poses a significant limitation to the analysis and suggests that more relevant and accurate results could be obtained by means of RANS-based ASO.

### 1.3.6. The morphing wing concept

A detailed multidisciplinary review of morphing aircraft technologies is out of the scope of the present survey. The author opts to discuss a few relevant publications that underline the benefits of this design approach and justify the assumptions of the morphing capabilities implementation in the optimization framework.

The definition of morphing wing can be ambiguous. In general, the term refers to flexible and “bird-inspired” wings that provide “efficient, multi-point adaptability” and may include macro, micro, structural and/or fluidic approaches” [148]. While camber modifications to increase lift during landing and take-off are common practice, the application of this approach to improve off-design performance has not been applied to in-service military or civil aircraft. Testing campaigns carried out between the 80s and 2000s on a modified F-111 [149] and F-18 [150, 151], focusing adaptive camber and aeroelastic twist modifications respectively, have shown an improved aerodynamic performance while highlighting weight

and packaging issues.

An energy cost function modelled on both components strain energy and aerodynamic loads was introduced by Namgoong [152] for 2D optimization. Considering this additional energy minimization problem, the author suggests that morphing wings could be particularly suitable for supersonic aircraft, as more extensive shape modifications could lead to greater aerodynamic benefits with smaller relative costs in terms of actuator energy. The effectiveness of morphing topologies for diverse (low-speed) flight envelopes has been further proven by Fincham and Friswell [153], who were able to reduce low-speed reconnaissance UAV wing section drag by more than 30%. High-fidelity studies on CRM configurations, aiming at multipoint aerodynamic [35, 154] and aerostructural [36] optimization, estimated an aircraft drag reduction on the entire flight envelope up to 5% and a fuel burn reduction of more than 1% for ASO and up to 5% if structural load alleviation is taken into account. Such figures are promising, as they prove the impact of such technology on a full-aircraft configuration with a relatively restricted flight envelope at cruise.

However, despite morphing wings being such a promising technology, its implementation will not be mature for industrial-level application before 2030-2040 [155]. Considering the use of less-advanced and short-term-feasible design solutions for SST, the concept of a more practical (although less effective) morphing wing - consisting in the implementation of slot-less and gap-less high lift devices on supersonic aircraft wings Fig. 1.14 - has not been investigated in the past decades but not thoroughly assessed with modern high-fidelity tools. This technology is explicitly described as a solution to improve efficiency at low speeds in multiple patents [75, 145]. In addition to off-design L/D increase, control surfaces can also be used to limit the shift center of pressure between supersonic and subsonic flight regime, reducing detrimental aeroelastic effects on thin low-torsional-stiffness supersonic wings [146]. Varying wing camber at subcritical flight conditions potentially allows to relax the aerodynamic trade-off between subsonic and supersonic performance on clean airfoil shape, with limited mechanical complexity if compared to variable-sweep-wing configuration. The absence of steps on the surface is meant to prevent the disruption of laminar flow on the wing.

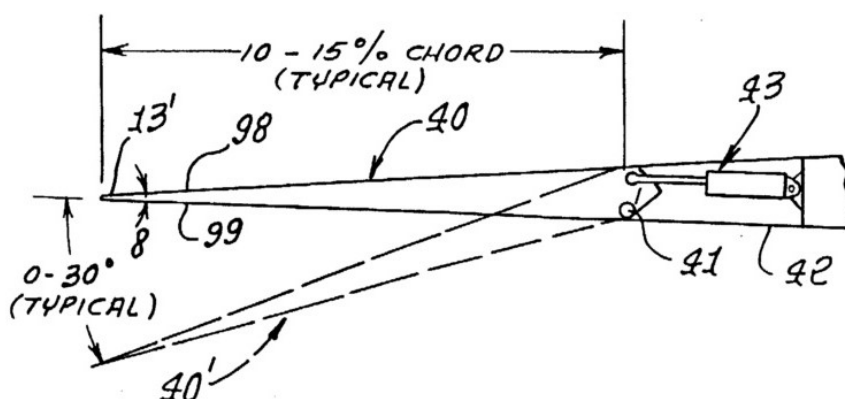


Figure 1.14: Schematics of a gap-less LE flap designed to ensure laminar flow over the wing of an efficient supersonic aircraft, from [75]

Preliminary transonic L/D improvement were estimated by more than 14% [68, 128], subject however to uncertainties around flow solver accuracy. Relevant work on the topic was made by Kim et al. [147], who investigated transonic cruise performance improvement of an SST with 10 flaps equally distributed on wing trailing and leading edges. The analysis was limited by constraints on flow separation, enforced in the form of maximum Mach numbers over the wing surface, to not overcome Euler solver capabilities. Authors highlighted the potential design improvements of using a couple of inboard and outboard leading edge flaps, estimating a decrease in transonic drag of 17%. Neglecting viscous effects however poses a substantial physical limitation to the analysis and suggests that more accurate results have to be obtained by means of RANS-based ASO. The benefits of morphing capabilities for an SSBJ wing and wing section are thus a very promising research topic to be investigated in the master thesis project with MACH framework, leaving however any structural or technological considerations to future works.

## 1.4. Research questions

Given the historical, technical and mathematical insight provided earlier in this chapter, it is possible to break down the thesis objective presented in Sec. 1.0.1 into a set of more detailed research questions:

1. *What are the main bottlenecks in the optimization workflow? What are the potential weaknesses of the different modules and how can they be addressed?*
  - (a) *What is the best trade-off in terms of accuracy and computational cost for supersonic ASO? How can mesh refinement, CFD solver, and optimizer settings be selected for best results?*
  - (b) *What is the influence of the selected CFD solver on the reliability of the specific optimization problem? Can it correctly capture supersonic flow characteristics for different airfoil shapes and flight configurations?*
  - (c) *What are the critical factors that affect flow solver and optimizer convergence? How can I increase the robustness of the routine?*
2. *How can Free-Form Deformation scheme be tailored to the specific problem, in order to improve the optimizer manipulation capabilities and at the same time ensure the optimization framework robustness?*
  - (a) *Which is the best control points distribution and number that maximizes manipulation capabilities and routine robustness with a minimum impact on computational cost and design feasibility?*
  - (b) *How can I set-up the FFD framework to ensure a smooth and consistent deflection of the control surfaces?*
3. *How do different boundary conditions, constraints and morphing capabilities affect the optimized airfoil and wing, and what is the justification from a physical and numerical*

*perspective?*

- (a) *How much does multi-point optimization improve the overall performance, with respect to single-point optimization? Can it effectively extend the configuration operational flexibility without excessively compromising the performance at supersonic regime?*
  - (b) *How does the choice of the flight envelope and the relative weight of the flight phases affect the optimal shape?*
  - (c) *How does the addition of movable leading and trailing edge devices increase the efficiency of the airfoil and wing for a wider range of flight conditions? And which is the influence of the deflection angles on the performance at subcritical flight regimes?*
  - (d) *Do the investigated optimization problems show evidence of multimodality? Are the possible inconsistencies given by the non-convexity of the design space or are they related to numerical errors?*
4. *What design-specific conclusions are drawn from this study, in particular for the full wing case?*
- (a) *What are the shape differences between optimal airfoils and the wing sections of the optimized wing?*
  - (b) *What is the optimal spanwise lift distribution at supersonic regime?*
  - (c) *What is the twist distribution that provides the most benefits at both supersonic and subsonic regimes?*
  - (d) *How do the 3-dimensional flowfield at supersonic regime affect the local airfoil shape along the wing span?*
  - (e) *Do the additional variables introduce multimodality in the design space?*

The answers to these questions will be addressed in Chap. 4-5 and ultimately summed up in the conclusive chapter.



# 2

## Methodology

In the previous chapter, the conceptual approach and notable examples of computer-based aerodynamic shape optimization have been presented. MDO and ASO strategies are demonstrating the potential to foster a major breakthrough towards more advanced and efficient aircraft design, both in terms of engineering effort and operative performance. While the advantages and challenges of such methodologies have thus been already clarified, it is at this point necessary to dive deeper into the intrinsic software features and gain a more profound understanding of the tools involved in the optimization process. The inner core of this methodology has indeed a substantial applied mathematics foundation that spans through a range of sub-topics, from PDE solving techniques and flow modelling to optimal control theory and geometry mapping and manipulation. The following chapter will tackle more in detail some core aspects involved in the numerical modelling of the most advanced optimization frameworks, from parametrization schemes and (hints of the) flow solver capabilities, to optimization algorithms and sensitivities calculation, with particular focus on the methodologies implemented in *MACH* framework used for thesis research project.

After a short summary of the optimization framework characteristics in Sec. 2.0.1, the Free-Form deformation scheme is introduced and compared against other approaches in Sec. 2.1. A short overview of mesh generation scheme and grid convergence strategies, Sec. 2.2 is provided, together with a will be brief discussion of key flow solver features, Sec. 2.3 to provide a solid discipline background. Following that, optimization algorithms are discussed in Sec. 2.4, providing an overview of the pros and cons of gradient-based and gradient-free strategies and ultimately supporting the choice of SNOPT algorithm for the thesis project. For further insight, adjoint method formulation and implementation are introduced and in Appx. D.

### 2.0.1. MACH framework

To contextualize the features discussed in this section, I briefly introduce the optimization framework that has been used for this research project, namely University of Michigan's *MACH*. The ASO suite has been recently made available in an open-source format on the MDO Lab Git Hub page (click on link). While the fundamental works that document its de-

velopment are already highlighted in Sec. 1.3.3, in this section the focus is narrowed down to its founding elements and algorithms. The tool currently includes a free-form deformation geometry parametrization scheme *PyGeo*, dedicated modules for mesh generation and warping *IDwarp*, and *ADflow* flow solver. This powerful framework provides efficient and accurate gradient computation strategy for each of its blocks based on adjoint method coupled with automatic differentiation. The source code of this tool is based on Fortran language. However, on user front-hand, workflow settings and run files are handled as a set of Python scripts.

The starting geometry is provided in the form of a surface mesh, generated by the user with a range of approaches. Airfoil grids are generally built with python scripts combining reference databases and spline interpolation to customize chordwise elements distribution. 3D surfaces are conversely handled with off-the-shelves software such as ICEM. This input file is then passed to a 3D hyperbolic, structured mesh generator named *pyHyp*, based on [156], that provides as output a *.cgns* file which is read by any commercial flow solver. The CFD tool embedded in *MACH* is based on a finite-volume method: thus, even the airfoil grid must be 3-dimensional with (at least) a one-cell span. From a computational point of view, this quasi-2D shape is turned into an infinite span wing due to the symmetry conditions along the side boundaries, while the wing (when fuselage and engines are not taken into account, as for this project) is mirrored with respect to the vertical plane intersecting the wing root.

The baseline shape is parametrized and manipulated using the FFD scheme described in Sec. 2.1. An interpolation algorithm method based on [157] - Sec. 2.2 - is used by mesh deformation module *IDWarp* to displace the (structured) volume mesh matching the updated surface mesh, indirectly manipulated by the optimizer at each iteration using the geometry deformation module *pyGeo*. *MACH* framework is optimizer independent; however, for ASO problems it is usually coupled with a gradient-based algorithm named SNOPT [91] (see Sec. 2.4), which handles constraints with an augmented lagrangian approach as presented in Sec. 3.5.

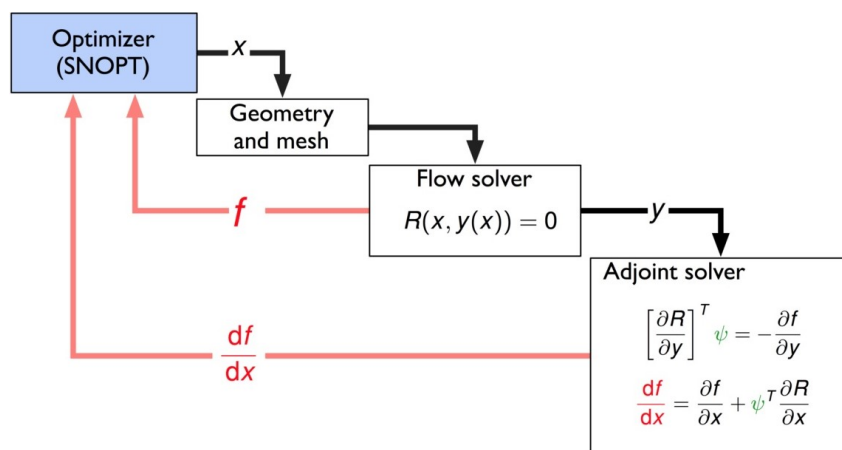


Figure 2.1: *MACH* ASO solver scheme, from Martins et al. [93]. Geometry and mesh block includes both the *PyGeo* and *IDwarp* modules, while the flow and adjoint solvers are both part of *ADflow*.

The typical block structure related to aerodynamic shape optimization is schematized in

Fig. 2.1. The optimizer passes the design vector  $x$  to the geometry manipulation module, then the mesh structure is deformed accordingly. The flowfield discretized governing equations  $R$  for the deformed mesh are then solved by *ADflow*, which provides the target functional values  $f$  back to the optimizer and the flowfield state variables  $y$  to the adjoint solver. This last module, using the methodology described in Appx. D, sends back to the optimizer the information on flow sensitivities  $\frac{df}{dx}$ , so that the gradient-based optimizer has all the necessary information to elaborate the following design vector step. This sequential loop iterates until the optimality conditions on local objective function gradient  $\frac{df}{dx}$  are satisfied together with all the equality and inequality constraints.

## 2.1. Shape Parametrization Scheme: *Free-Form Deformation* (FFD)

Among the most common parametrization approaches, further discussed in Appx. A, Free-Form Deformation scheme is nowadays one of the most widely applied in ASO [86]. Its deformative nature is particularly suitable for CFD-based optimization due to the huge amount of mesh points involved, which coordinates are then just translated instead of being recalculated, while guaranteeing machine precision accuracy [85]. This method provides a more efficient set of design variables and becomes particularly effective with complex configurations. Multiple disciplines, such as structures and aerodynamics, are handled at the same time [158].

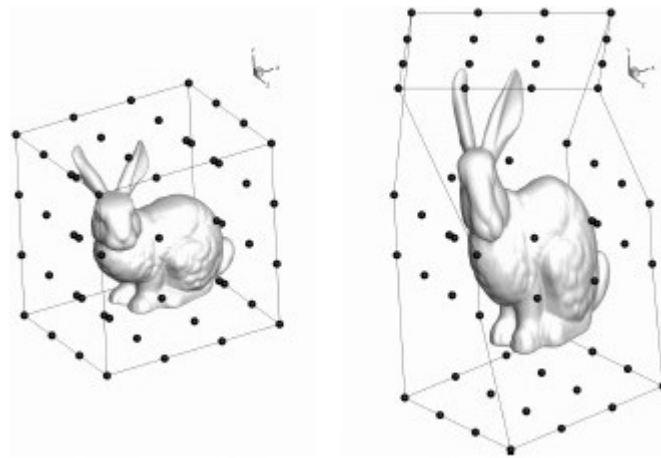


Figure 2.2: A not-strictly aeronautical application of Free-Form Deformation technique, from [158]: the Stanford bunny is twisted and stretched after being embedded and mapped into an FFD control volume.

The baseline geometry is enclosed within a hull control volume against which the mesh points are mapped, something that is described “*as embedding an object in a clear, flexible, rubber-like material*” [158] - as is intuitively shown in Fig. 2.2. Control points are defined along the surface of this volume and their displacement can control both local and global variables. The propagation of local deformation is affected by control points local density [35]. The model is both “*applied locally while maintaining derivative continuity with adjacent, undeformed regions of the model*”, or hierarchically, embedding child grids with

additional control points [159]. The formulation of this approach implicitly impose constant topology in the optimization process [86]: the embedded geometry cannot be “broken” as continuity is maintained inside the volume. This assumption however is not limiting for high-fidelity optimizations, as baseline shape are generally relatively close to the optimum [10].

### 2.1.1. Mathematical formulation of Free-Form Deformation Scheme

According to Sederberg and Parry [160], who first introduced the scheme in the 80st: “*Mathematically, the FFD is defined in terms of a tensor product trivariate Bernstein polynomial*”, thus consisting in a  $\mathbb{R}^3 \rightarrow \mathbb{R}^3$  map that is defined as [85]:

$$P_{\text{ffd}} = \sum_{i=0}^l \sum_{j=0}^m \sum_{k=0}^n B_{i,l}(x) B_{j,m}(y) B_{k,n}(z) \mathbf{Q}_{i,j,k} \quad (2.1)$$

$$\text{with } B_{a,b}(t) = \frac{b!}{a!(b-1)!} t^a (1-t)^{b-a} \quad (2.2)$$

where  $l, m$  and  $n$  are the number of design points (minus 1) along each control volume reference axis,  $x, y$  and  $z$  the embedded point coordinates,  $\mathbf{Q}_{i,j,k}$  the normalized coordinate of the control point and concurrently the coefficients of Bernstein polynomial (in generic form)  $B_{a,b}(t)$ . Embedded coordinates are mapped in the control volume system of reference and their modification is calculated as a function of the control point displacement  $\mathbf{Q}_{i,j,k}$ . One of the greatest advantages for application to gradient-based optimization is that geometrical derivatives are calculated analytically [158], improving efficiency and accuracy of the framework:

$$\frac{\partial X_{\text{pt}}}{\partial x_{\text{dv}}} = \frac{\partial X_{\text{coeff}}}{\partial x_{\text{dv}}} \frac{\partial X_{\text{pt}}}{\partial X_{\text{coeff}}} \quad (2.3)$$

with  $X_{\text{pt}}$  the coordinates of the embedded geometry,  $x_{\text{dv}}$  the design variables, and  $X_{\text{coeff}}$  the control points coordinates.

### 2.1.2. Applications and comparison with other approaches

An early example of FFD parametrization applied to an ASO framework was made by Andreoli et al. [161], with a promising work that hinted at the potential of multi-level approaches to increase convergence. Kenway et al. [158] implemented an FFD scheme in *MACH* and coupled it with a hybrid mesh deformation module to demonstrate its effectiveness for high-fidelity MDO of CRM configuration, as shown in Fig. 2.3 and assessing the efficiency of the method when dealing simultaneously with both CFD and FEM meshes. Lyu et al. [10] proved the flexibility and accuracy of this model by performing a shape recovery test from random initial geometries, with final results within 1 drag count and a mean aerodynamic chord variation of 1.2%. All the works performed with *MACH* presented in this survey are based on this powerful and effective implementation, including morphing aircraft

optimization [35, 36] using a hierarchical approach. A number of other relevant but specific applications of FFD, especially for space and hypersonic vehicles, is reported in [85].

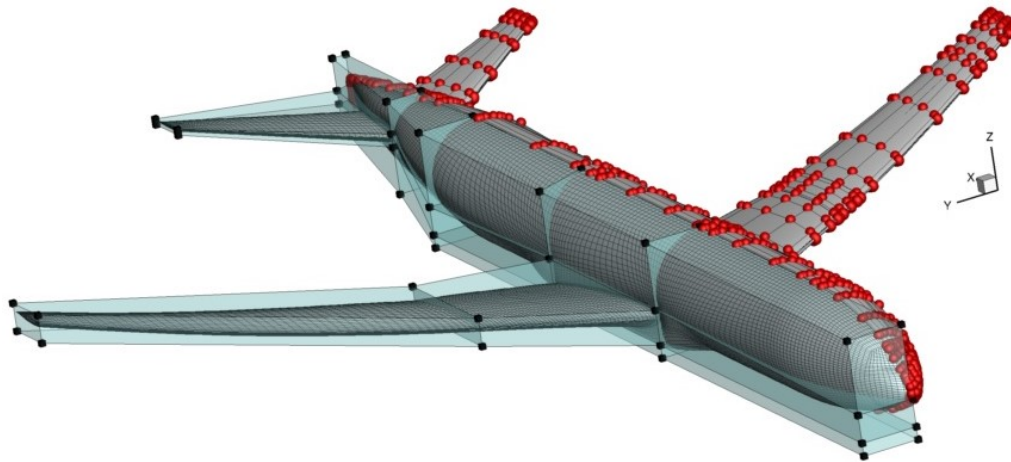


Figure 2.3: An example of a full aircraft configuration parametrized with FFD scheme, highlighting deformation control volumes (on the left) and B-spline surfaces (on the right) [158]

Two recent studies by Masters et al. [162, 163] presented a review and comparison of modern shape parametrization method, focusing on geometric shape recovery tests and ADODG [87] benchmark case 2 respectively. For the simple airfoil case B-spline and Hicks-Henne bump functions showed the best convergence performance with a relatively small number of design variables, after however having modified the basis functions to ensure smoothness and better follow adjoint sensitivities. FFD parametrization seems to be sensitive to the sharp trailing edge of the baseline NACA0012 airfoil and require a slightly higher number of DV, but is overall more robust than other splines methods. Moreover, splines and CST would be less efficient in modelling the sharp geometries typical of an SST. The shape recovery study [162] highlights the good performance of modes with respect to FFD: however, a more meaningful control points reciprocal constraint definition could have improved grid convergence rates by reducing the number of design variables and minimizing numerical errors.

Concerning supersonic optimization, the only works that explicitly use FFD approach are [28, 164], as this scheme has become popular in more recent years and is in general discarded for low-fidelity models and parametrizations. Given the examples provided in this report, I am confident that FFD remains the best approach for this kind of ASO study.

## 2.2. Meshing

The software for volume mesh generation included in *MACH* is called *pyHyp* and is based on Chan and Steger [156]. This hyperbolic mesh generator is faster than elliptic schemes and its smoothness and robustness is proven even for highly-convex corners, thus being suitable to generate high-quality body-fitted meshes for complex aerospace systems configurations. *pyHyp* generates by default an O-grid mesh topology; a C-grid is obtained by splitting the domain and rearranging the boundaries with tools such as [165]. According to Lutton [166], O-grid is superior in terms of accuracy close to the edges if the mesh is equally spaced, espe-

cially when shocks are present. However, it is pointed out how hyperbolic-generated meshes are affected by numerical instabilities around fine spaced trailing edges, together with poor wake modelling. Experience at MDOLab suggests that O-grids are more robust when manipulated and converge faster than C-grids, despite lower elements orthogonality in the wake region, which might be mitigated using blunt or round trailing edges. C-grid advantages in terms of mesh construction are annihilated by *pyHyp* performance.

### 2.2.1. Mesh deformation Scheme

Skinner and Zare-Behtash [86] in their survey report how mesh deformation schemes are common practice in high-fidelity aerodynamic and aerostructural optimization. However, grid modification remains a critical component in the optimization frameworks, affecting both reliability and accuracy of the algorithm routine. An optimization run could indeed fail to improve the design due to bad mesh warping, as experienced by the author, or even lead to false optimization with unrealistic results. Regardless of the method used to parametrize the geometry, there is the need to ensure a fast and robust mesh rearrangement along the updated boundary, namely the surface mesh modelled along the OML.

A range of methodologies has been used to propagate the surface deformation to the volume grid. Hicken and Zingg [97] and early works from MDOLab used a combination of linear elastic deformation and algebraic approach to model low and high frequency modifications respectively. Gagnon and Zingg [99], in a similar fashion, extended the FFD approach to a “second-level”, using multiblock FFD volumes to map the deformations and match them with surface changes using “first-level” geometry deformation control points, to better handle large shape changes.

Latest *MACH* version uses of a higher performance algorithm developed by Luke et al. [157]. Once the updated positions of the surface grid are passed from *pyGeo* to *IDwarp*, the volume nodes are rearranged accordingly using inexact explicit interpolation algorithm based on inverse distance weighting function. The scheme preserves boundary layer cells orthogonality and can be highly parallelized. This allows a fast mesh update, that takes in general less than 0.1% of the CFD computational cost [93].

## 2.3. High-Fidelity Flow Solver

The backbone of this single-discipline optimization study is the high-fidelity aerodynamic analysis. The structured multi-block flow solver developed at MDO Lab, named *ADflow*, is based on *SUmb* [167] numerical scheme, but has been substantially modified [105] and “now has a fully developed python API and operates as a python module for multidisciplinary analysis” [168]. The software can model the flowfield using both inviscid Euler, Reynolds-Averaged Navier–Stokes (RANS) and laminar NS, all of them with cell-centered scheme and a spatial accuracy of the second-order, supporting steady, unsteady and time spectral schemes, as thoroughly reported by Kenway et al. [168]. Moreover, overset mesh capabilities, based on implicit hole cutting to determine connectivities, have been recently implemented, to enable ASO on complex configurations [113, 169].

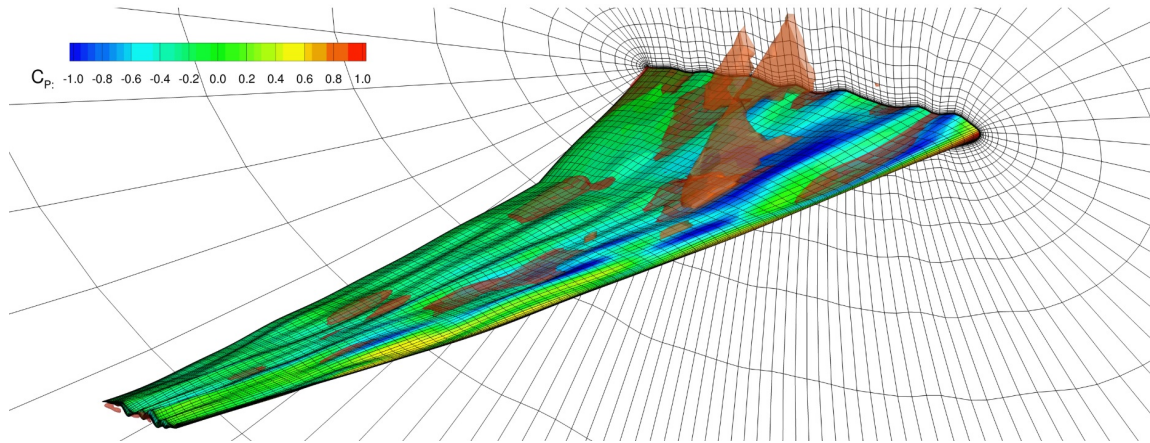


Figure 2.4: An example from Lyu et al. [10] shows ADflow converging for a randomly distorted initial geometry (reference: CRM wing at  $M=0.85$ ). Coupling the flow solver with an adjoint solver for flow sensitivities reduces computational cost and ultimately makes gradient-based strategies the most efficient option for high-fidelity ASO.

Discretized nonlinear residuals are solved in the  $R(q, w) = 0$  form, where  $w$  is the state variables vector and  $R$  is the aerodynamic residual including turbulent and viscous terms [104]. Steady-state simulations are initially solved with both explicit or implicit time-marching schemes such as Runge-Kutta or Diagonal Alternating Direction Implicit (DADI) [170] respectively. Once a user-defined tolerance on the time residual is reached, the convergence is accelerated by an approximate Newton–Krylov [171] (labelled ANK) and a full, preconditioned matrix-free Newton-Krylov (NK) algorithm [172, 173] solved with GMRES scheme [174]. NK approaches, of which detailed discussion is out of the scope of this survey, have proven to be consistently efficient for aerodynamic and aerostructural solvers. An inexact Newton method in the form [175]:  $\frac{\partial R}{\partial q} \Delta q^{(n)} = -R(q^{(n)}, w)$  (with  $\Delta q^{(n)}$  design vector update) is used to iteratively solve flow model equations at each grid node. As this system is linear, it is solved using Krylov methods such as GMRES, which are particularly efficient to reduce the computational cost of  $Ax = b$  linear systems with sparse  $A$  coefficient matrix. They are based on the concept that the solution of such system lies in the so-called Krylov subspaces (namely the subspaces given by linear combination of images of  $b$  with first  $r$  powers of  $A$  matrix,  $b, Ab, A^2b, \dots, A^{r-1}b$ ) whose dimension is much smaller than the original problem [176], thus leading to faster convergence. Matrix-vector products needed by GMRES is approximated using finite differences [172] or more efficiently using adjoint information, thus avoiding the computational burden to explicitly form the Jacobian of the state equations. This matrix-free approach minimizes the memory-requirements of the machine [104]. The Krylov space is further reduced by pre-multiplying this linear system so to make  $A$  behave as a diagonalizable matrix with few eigenvalues, thus reducing the number of iterations to get convergence. The preconditioner for GMRES is formed using a block-fill incomplete lower–upper factorization of an approximate Jacobian matrix [172, 174]. More detailed description of the implementation of these methodologies in *MACH* is reported in [104].

As mentioned in Sec. 1.3.3, an efficient adjoint method has been initially implemented by Mader et al. [101, 177] and then extended to RANS equations Lyu et al. [102] with one-equation turbulence model [178], increasing the accuracy and the fidelity range of the tool. This noteworthy feature, which allows a fast flow sensitivities calculation and thus make

possible an efficient coupling with gradient-based optimization algorithms (see example in Fig. 2.4 from a shape recovery test run), is further discussed in Appx. D. Adjoint equations, due to their linearity, are solved with GMRES algorithm as well.

### 2.3.1. Validation for Supersonic Regime

ADflow accuracy has been assessed by multiple studies aimed at subsonic and transonic optimization, some of which have been presented in Sec. 1.3.3. The selection of the Spalart–Allmaras (SA) turbulence model when ADflow is used for optimization purposes has been mostly driven by the relatively easiness of differentiating a one-equation model rather than a two (SST,  $k - \epsilon, k - \omega$ ) or more equation turbulence model. In this sense, MDO Lab has recently proposed a framework [179], tested on openFOAM, to provide rapid adjoint development for a wider range of primal solvers and turbulence models, overcoming this current limitation.

I use a test case from Rodriguez et al. [180] to assess the accuracy of ADflow viscosity and turbulence models for supersonic regime. Data for a relatively simple 2D case, a biconvex (*thickness-to-chord-ratio=3%*), sharp-edged airfoil at  $M=1.5$  and  $\alpha=3^\circ$  is provided for different solvers, but I focus specifically on the results from the sole RANS code reported, namely NASA-developed CFL3D.

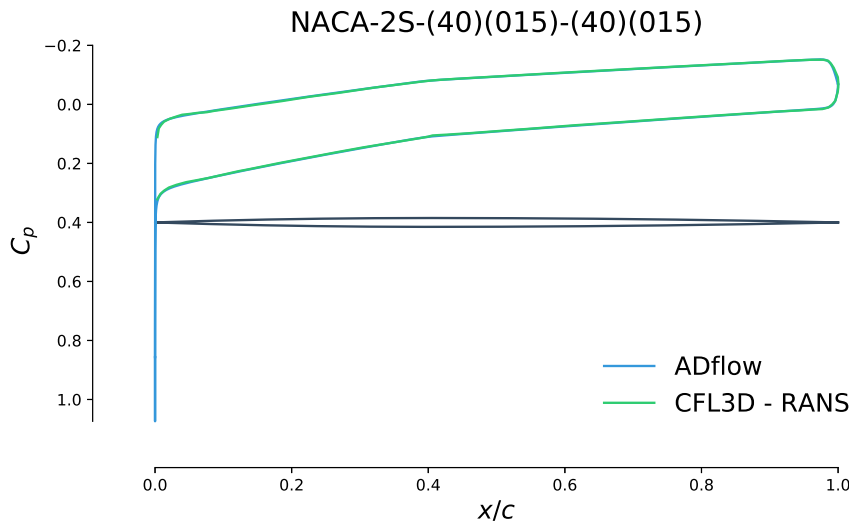


Figure 2.5: *ADflow* is validated against NASA’s CFL3D solver with data from Rodriguez et al. [180]. Pressure distributions and aerodynamic coefficients show excellent match.

Comparison in Fig. 2.5 and Tab. 2.1, shows an overlapping  $C_p$  distribution and a 0.4% mismatch on  $C_l$  and 0.6% on  $C_d$ , which we repute more than satisfying for our ASO study. Moreover, ADflow accuracy is particularly appropriate as other cases reported in [180] and other examples in literature are based on Euler solvers (often combined with boundary layer codes), showing much higher discrepancies. The choice of such solvers is usually justified by a reduced relevance of viscous phenomena at high speeds (although, as reported later in Sec. 3.5  $Re$  number is comparable to transonic cases) and a much reduced computational

cost. However, viscous effects become necessary when lower flight speeds are considered, as in the current work. The choice of ADflow RANS-SA code thus does not represent a limitation of this project and, furthermore, marks a step forward in physical accuracy for this kind of ASO studies (see Sec. 1.3.5).

Table 2.1: Aerodynamic coefficient comparison between Rodriguez et al. [180] data and ADflow simulations with current settings. ADflow overestimates total drag coefficient by 0.6%

| Solver | $C_l$  | $C_d$  | $C_{d_p}$ | $C_{d_v}$ |
|--------|--------|--------|-----------|-----------|
| CFL3D  | 0.189  | 219.5  | 147.5     | 72.0      |
| ADflow | 0.1898 | 220.87 | 148.34    | 72.53     |

## 2.4. Optimization algorithm

Optimization can be intended as “*the process of obtaining the most suitable solution to a given problem*” [86], where “most suitable” indicates that the optimal result may not necessarily be the exact best solution, but could be considered “sufficiently superior” with respect to the initial state of the problem [82]. As discussed since early ASO and MDO studies (Sec. 1.3.2), a numerical algorithm must converge with reasonable computational effort, be accurate enough to capture relevant variations in the design space and be robust enough to minimize user intervention and be used for a vast range of problems. Moreover, due to the physical complexity of aircraft design, the algorithm must be able to handle non-linearity for both objective functions and constraints [1].

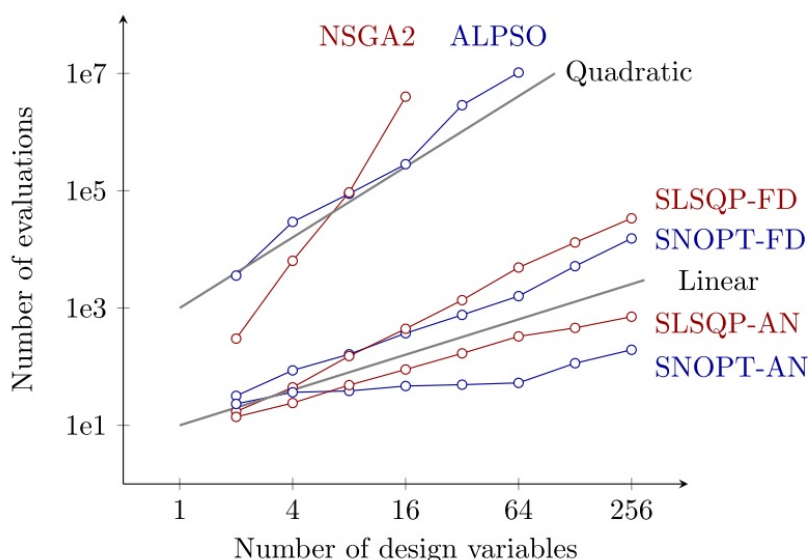


Figure 2.6: Optimization algorithm performance comparison. The influence of design variables number is tested against the computational cost in terms of number of evaluations for a Rosenbrock function minimization case [1]. Gradient-based strategies with analytical derivatives show the best scalability.

According to the *Free lunch theorem* [84], there is not an ultimate algorithm that outper-

forms all other possible candidates, as all algorithms that minimize (or maximize) a cost function have the same performance if averaged over all possible objective functions. The choice of the algorithm thus is strictly related to the specific problem. Global, gradient-free optimizers, for example, are less prone to incur in local minima due their more extensive exploration of the design space, while gradient-based approaches convergence rate is usually much higher thanks to additional information on local design space topology given by sensitivity analysis [2]. A number of promising hybrid strategies have been used for ASO, combining the broad search capabilities of heuristic methods with the efficiency of gradient-based approaches. However, for continuous design spaces typical of ASO problems, the initial gradient-free search is more efficiently replaced by a gradient-based multiple start strategy to investigate local minima and ensure the robustness of the optimal design.

In addition to robustness and accuracy, algorithm scalability plays a major role in the selection of the approach, as often MDO problems can have hundreds or thousands of design variables. Martins and Hwang [1] compared different gradient-free and gradient-based algorithms on a multivariate Rosenbrock function, Fig. 2.6: gradient-based optimizers with analytical derivatives (SNOPT-AN and SLSQP-AN in the figure) scale better than linearly, showing then little sensitivity to the number of design variables. Authors thus claim that *“our only hope for solving large-scale aircraft design optimization problems—problems with  $O(10^2)$  design variables or more—is to use a gradient-based optimization.”* [1]. A short overview and comparison of gradient-free and gradient-based algorithms is reported in the next sections.

### 2.4.1. Gradient-Based optimization

Examples of gradient-based (GB) optimization studies are extensively reported in this survey, thus a detailed performance analysis is redundant at this point. However, it useful to introduce some general observations. The iterative process of GB algorithms are simply summarized as:

$$x_{k+1} = x_k + \alpha_k p_k$$

with  $x_k$  the design vector,  $p_k$  the search direction and  $\alpha_k$  the step size. This formulation implies that the design space has to be continuous and derivable, an assumption that may be non trivial even for aircraft ASO and especially MDO problems [86]. The search direction of the algorithm  $p_k$  is obtained from first-order  $g = \nabla f$  (steepest-descent) and second-order  $H = \nabla^2 f$  derivatives, individuating the multidimensional direction towards with design variables modification are expected to induce maximum benefits. However, as gradient value is a local property of the design space, step  $\alpha_k$  has to be determined with a trade-off between potential objective function decrease, consistency of gradient information in the proximity of the current design point and evaluation time. Step-size selection, namely the line-search problem, is a delicate and complex mathematic topic that is thoroughly discussed in books such as [82].

The sensitivity calculation approach plays a key role for optimization performance, as pointed out in multiple recent reviews on the topic [181, 182]. The most intuitive numerical scheme to obtain total derivatives is finite differences, based on individual perturbation of each design variables by a fixed step and an additional function evaluation [6]. It is evident how

such an approach, whose cost scales linearly with design variables, is inefficient for large MDO problems; moreover, its accuracy is limited by the minimum size of the step due to numerical cancellation. In this sense, complex-step method [183] increases the accuracy of the derivatives by several significant figures with the same computational cost. It is derived from Taylor-series expansion of real function using complex variables, introducing a purely imaginary step  $ih$  rather than the usual real value. It is demonstrated that the order of convergence of the derivative is at least  $O(h^2)$  and step size is dramatically reduced due to the absence of numerical cancellation errors, as no subtractions are involved in the derivative evaluation. It however requires deep modifications of the code (functions have to be complexified, which is not always possible) instead of the “black box” approach of finite differences. Analytical derivatives, when highly non-linear systems are involved in the analysis, are obtained with the use of symbolic differentiation and coupled with powerful schemes such as the adjoint method, showing complex-step accuracy with much better scalability. This approach is discussed in detail in Appx. D. Gradient accuracy, especially for RANS-based ASO, is critical for the approximation of the Hessian made by quasi-Newton methods. For this reason, it is strongly recommended to avoid substantial simplifications (such as frozen turbulence) to reduce computational effort of the sensitivity analysis [181] and validate the code with cross comparison with finite-differences or complex-step approaches.

**SNOPT** The optimization algorithm most commonly used at MDOLab is *SNOPT* [91] (Sparse Non-linear Optimizer), specifically developed for the aerospace industry aiming at mission optimization problems with large numbers of variables and constraints. It is based on sequential quadratic programming (SQP), using a quasi-Newton method with Hessian approximation to solve convex sub-optimization problems at each iteration. This approach minimizes memory requirements due to the fact that sparse first and second derivative matrices do not need to be stored. Both linear and non-linear constraints are handled directly as the algorithm implements them in the form of a smooth augmented Lagrangian and address the infeasibilities by using penalty functions. Detailed and up-to-date user settings and useful comments are available in the publicly available software manual [184].

### 2.4.2. Strategy comparison

There is a number of publicly available studies that compare different algorithms on a benchmark problem, to test their performance and drive approach selection. For ASO, the current framework panorama is pretty diverse. Gradient-based approaches have proven their effectiveness but, due to their implementation complexity and the low per-evaluation cost of popular low-fidelity methods, gradient-free approaches are often preferred although their lower accuracy. Zingg et al. [185] benchmarked the two different optimization strategies for a range of 2D ASO problems, highlighting how GA require between 5 and 200 times more function evaluations than GB while producing essentially the same results. Even Pareto front estimation is possibly obtained much faster with gradient-based approach, although optimal solutions appear pretty wacky for this specific study, raising doubts on solver convergence. Similar considerations are made in the already discussed [120] for BWB optimization, where it is shown how multi-start gradient-based optimization can capture lo-

cal minima with lower cost than non-deterministic methods. More recently Lyu et al. [186] benchmarked several optimizers on both ASO problems and Rosenbrock function, once more proving how gradient-based algorithms enhanced with adjoint method are the best option for highly multidimensional optimization. With similar methodology, Yu et al. [187] optimized CRM benchmark model starting from random geometries, producing comparable results in terms of speed while showing slight discrepancies in optimal shapes (less than 0.05% drag difference). This apparent multimodality is interpreted as a consequence of numerical errors on substantially flat regions of the design space.

# 3

## Problem Formulation

In this chapter the approach to the optimization problem is discussed, including numerical methods and more practical tips. I first introduce the airfoils and wing planform I intend to optimize, including meshing approaches and expedients aimed at increasing optimization robustness. The strategies to assess mesh quality described in Appx. B are applied to find the best compromise to match different flow characteristics at different flight regimes. Design variables are presented and discussed for both 2D and 3D problem, also illustrating the morphing capabilities of the framework, before summarizing and characterizing the constraints imposed on the optimization process. The selected flight conditions are briefly discussed and the selection of the multi-point objective function is justified. Finally, the problem is schematically summed up to characterize the different case studies at a glance.

### 3.1. Investigation Approach and Baseline Geometry

The characteristics of the optimization framework used for this investigation pose a non-negligible relevance on the starting geometry selected for the optimization runs. The choice of parametrization scheme and the gradient-based search algorithm imply that, if not thoroughly investigated, final shapes may not represent the best configuration possible.

A first limitation comes from the geometrical relation between baseline and optimal layouts. The FFD scheme used in this study is, as its name suggests, a deformative parametrization approach. This implies that, in contrast to constructive schemes such as CST or B-splines, the initial geometry has a potential influence on the final shape [85]. The mathematical mapping from initial to final coordinates is thus potentially limited by numerical and fundamental assumptions; as discussed in Sec. 2.1, the initial topology (i.e. presence of holes, discontinuities) cannot be altered so to shift, for example, from sharp,  $C^0$  curves to round shapes - and potentially vice versa. Secondly, as discussed in Sec. 2.4, gradient-based strategies follow a “path” in the design space, from starting point to an objective function minima, driven by sensitivities information. Thus, they are prone to get stuck into local minima, if the objective function space is not strictly convex or smooth in proximity of the global optimum. Literature presented in Chap. 1- 2 and previous experience suggest that the specific design cases hereby presented are unimodal (= no local minima) but it is crucial to investigate this

aspect to ensure the consistency and reliability of optimization results.

To address these concerns, the 2D optimization cases start from multiple initial wing sections. This allows to assess the performance improvement relatively to a wide range of airfoils, test the flexibility of the tool, and at the same time to rule out the presence of local minima in the design space. Building the confidence in the obtained solution is critical for current and future optimization studies.

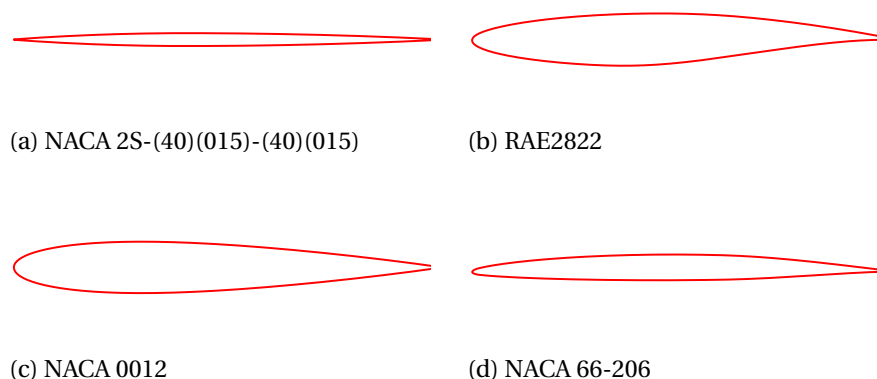
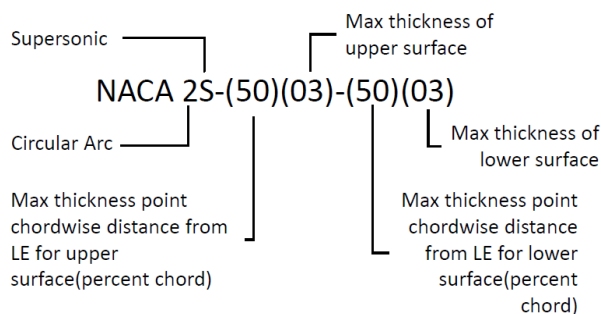


Figure 3.1: The four main airfoil geometries used as baseline for the 2D optimization study: (a) NACA 2S-(40)(015)-(40)(015), a biconvex airfoil with 3% thickness located at 40% of the chord, according to the nomenclature presented above; (b) RAE2822, typical supercritical airfoil developed by the Royal Aircraft Establishment; (c) NACA 0012, symmetrical with 12% thickness with canonical NACA 4-digit shape definition; (d) NACA 66-206, a NACA 6-digit with 6% airfoil designed to enhance laminar flow over the wing.

From a practical standpoint, some of the reference geometries are taken from well-known NACA 4-digit and 6-digit families, together with conventional transonic airfoils such as RAE2822, as briefly illustrated in Fig. 3.1. However, typical supersonic airfoils belong to two specific families: diamond-shaped geometries, with potentially lower performance but easier to manufacture, and biconvex shapes, composed by two circular arcs intersecting at leading and trailing edge. As the diamond shape cannot be effectively handled by FFD parametrization (the sharp edges on upper and lower surface cannot be smoothed with control points displacement), I opt to use the second type as the most efficient baseline geometry. A family of biconvex supersonic airfoils is thus purposely generated using an old-fashioned but effective NACA notation from [188], allowing to encode the geometry in a more conventional fashion. This notation is described below:



where the first digit is 1 or 2, indicating double-wedge or circular-arc baselines shapes respectively. The values into the brackets are in chord percentage, with thickness calculated from chord line. Note that upper and lower surface are parametrized separately, while camber line is implicitly defined.

The presence of sharp leading edges on the typical supersonic airfoil poses a challenge for the geometry deformation scheme. Control points displacement can sharpen a smooth round shape, but the reverse process is not guaranteed as the initial surface is not  $C^2$  continuous. For this reason, all biconvex airfoils generated for this study present a small round edge (as illustrated later in Fig. 3.4(b)) to replace the ideally sharp leading edges.

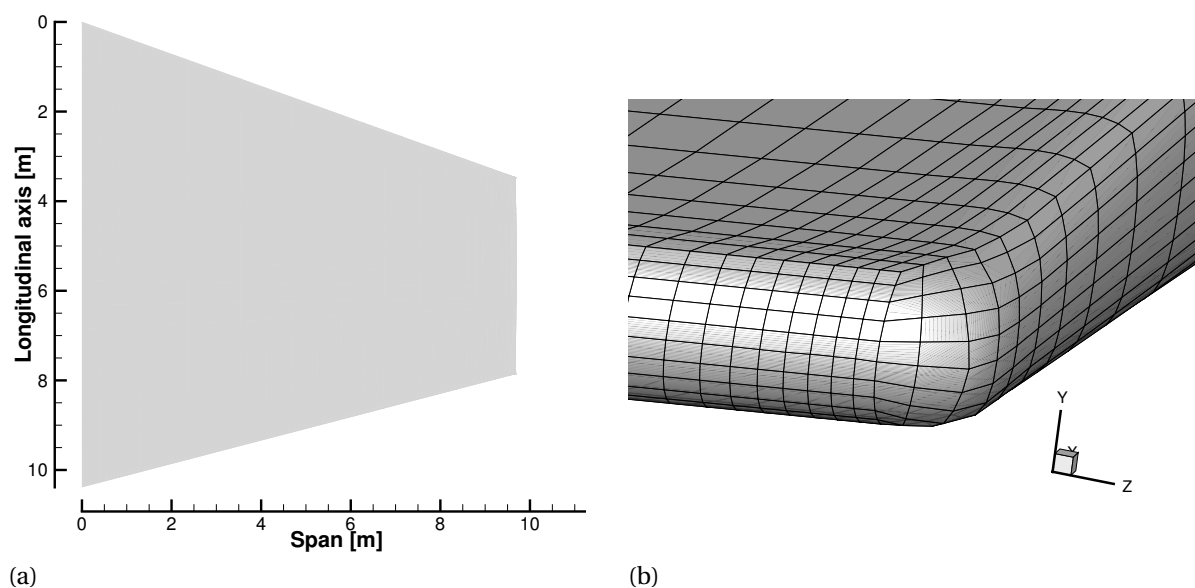


Figure 3.2: Baseline wing geometry used for the 3D optimization studies. (a) the trapezoid planform inspired by Aerion AS2 configuration (details in Tab. 3.1) and (b) a detail of the wing tip leading edge

Shifting to the 3D analysis, it is necessary to define a baseline planform geometry. Literature on this topic provides a range of different solutions, successfully implemented in current and past military aircraft. Delta wings are a common design option (from the F-102 to the Eurofighter Typhoon), together with variable geometry wings as present on the F-14 or the B-1. However, looking at the most promising configuration for SST in the near-future, Aerion AS2 concept as presented in Sec. 1.2.3 shows a low-sweep, low-aspect-ratio configuration, comparable to the renown F-104 design solution.

Investigating planform optimization or, without adding complexity to the design problem, optimal shape and twist for a range of planform geometries would have been a relevant research effort. Unfortunately, mostly due to time constraints, the current study has to be limited to a single, fixed baseline planform layout. Thus, for the baseline wing, I define a relatively simple trapezoidal planform using as reference the currently (April 2019) available information on the Aerion AS2 [17]. Snapshot of the baseline 3D geometry are illustrated in Fig. 3.2.

For mesh quality issues, the wing tip is modelled with a small curvature instead of a more

simple truncated tip, to guarantee mesh smoothness while modelling with ANSYS ICEM software. Quantitative details of this geometry are reported in Tab. 3.1. For principal optimization runs discussed in Chap. 5 , I select the same NACA 2S-(40)(1.5)-(40)(1.5) airfoil from the 2D case study as wing section, to be consistent with most typical supersonic designs.

Table 3.1: Baseline wing geometry data. Aerion AS2 renderings have been used as reference.

|              |                        |
|--------------|------------------------|
| Semi span    | 9.67[m]                |
| Semi area    | 71.48[m <sup>2</sup> ] |
| Aspect Ratio | 2.6                    |
| Root Airfoil | 10.38[m]               |
| Tip Airfoil  | 4.4[m]                 |
| LE sweep     | 19.7[°]                |

### 3.1.1. Meshing and Grid Convergence Study

As the CFD tool a finite volume solver is used, input grid file has to be generated accordingly even for a 2D case. User-defined surface meshes with arbitrary chordwise point distribution are passed to *pyHyp*, presented in Sec. 2.0.1. I chose O-grid topology due to its reduced computational cost and superior robustness when manipulated, if compared to C-grids [166]. The meshes for these “3-dimensional” airfoil, symmetrical along the spanwise direction, have been generated by means of a python script coded in collaboration with fellow lab members Neil Wu and Joshua Anibal. On-hands experience and preliminary tests showed the necessity to generate a non-uniform grid along the chordwise axis, to better capture leading and trailing edge shocks at supersonic regime without excessively increasing the overall number of grid elements. I single-handedly defined and tested a range of non-linear chordwise elements distributions that allowed to generate efficient meshes, without the necessity to use more complex software and user interfaces. My colleagues developed a fast, spline-based algorithm to define the node position directly on the curvilinear surface of the airfoil, rather than with a two-step procedure involving chordwise coordinate definition and a following projection on the geometry surface. The flexibility of the resulting algorithm is illustrated in Fig. 3.3. The difference between nodes distribution is emphasised for reader’s convenience.

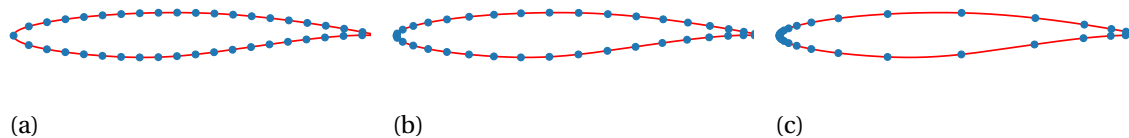


Figure 3.3: Example of non-uniform point distribution over a RAE2822 airfoil. For better visualization, 30 points are distributed over the spline curve using a linear (a), cosine (b), and highly-conical (c) distribution. This approach has been used to refine the surface meshes close to LE and TE, as illustrated in Fig. 3.4.

The advantage of this approach is the higher speed of user-generated grid with respect to

more conventional programming routines (seconds vs. minutes with a meshing software). An example baseline mesh for a supersonic airfoil is reported in Fig. 3.4(a), together with a detail of the above-mentioned thin rounded leading edge in Fig. 3.4(b). For wing meshes, as already mentioned, a more conventional and time-consuming methodology has been used, involving ICEM CFD software.

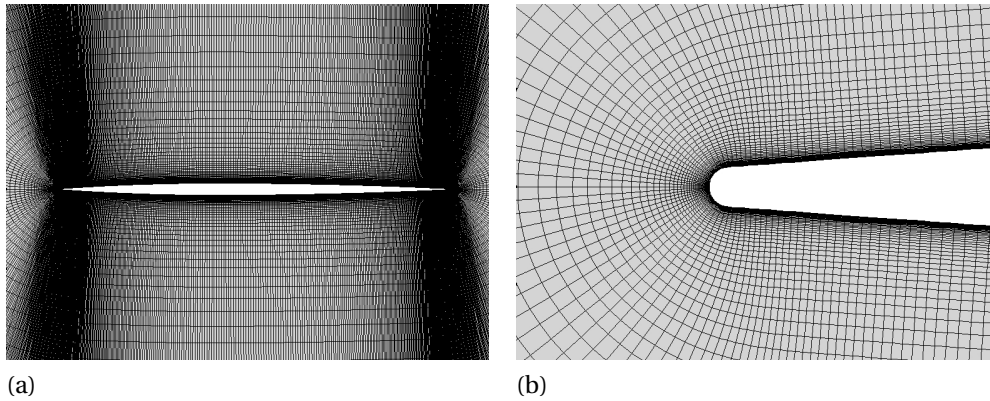


Figure 3.4: Baseline mesh for a NACA 2S-(40)(1.5)-(40)(1.5) airfoil (a) and detail of its rounded leading edge,  $R=0.4\text{mm}$  (b)

Mesh quality is assessed with the methodology described in Appx. B. I report an example of grid convergence study for our reference biconvex airfoil in Fig. 3.5.  $C_d$  is plotted against  $N^{-\frac{2}{3}}$  - where  $N$  is the number of mesh elements - to assess the asymptotic behaviour of  $C_d$  with mesh refinement.

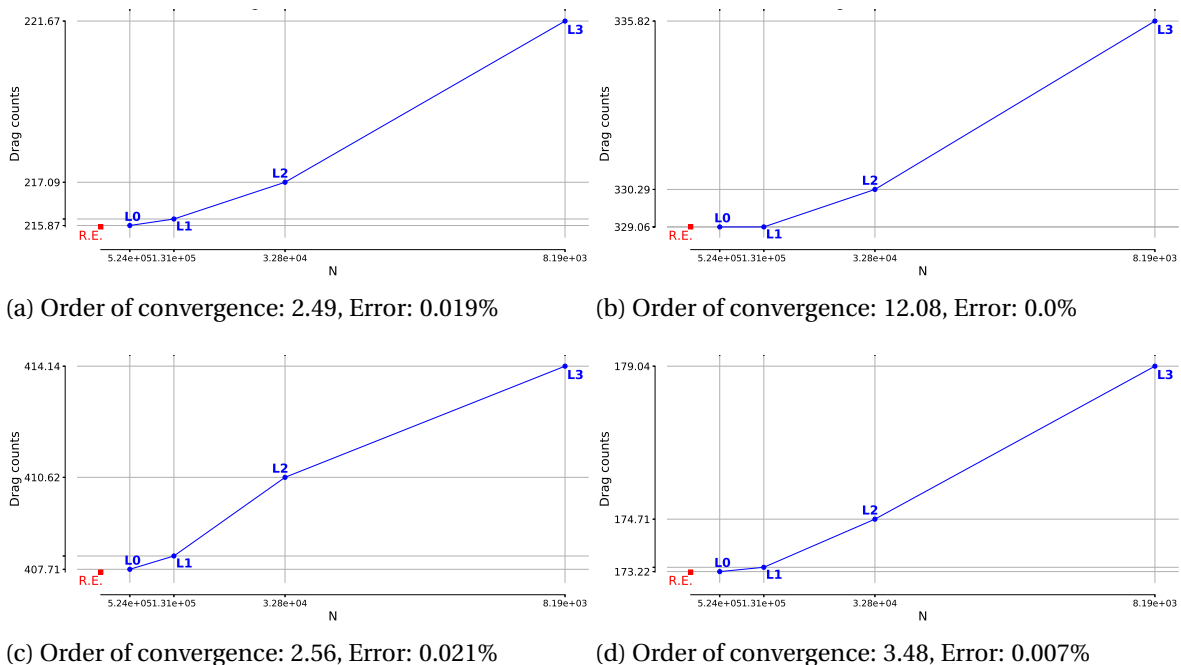


Figure 3.5: 2D grid convergence study for baseline NACA 2S-(40)(1.5)-(40)(1.5) mesh, for (a) supersonic regime, (b) high-transonic regime, (c) transonic regime, and (d) subsonic regime. Meshes have 520K elements (L0), 130K elements (L1), 32K elements (L2) and 8K elements (L3) respectively.

It is important to assess mesh quality at such different design conditions to ensure good accuracy of the multipoint optimization cases. To do so, I carefully tuned the chordwise elements distribution; ultimately, I select an elliptical distribution to refine the mesh close to the edges to better catch the shocks at supersonic and transonic regimes, while also better modelling wake and possible LE separation over sharp-nosed sections. For optimization purposes, I choose the L1 mesh (130K elements) for airfoils, focusing on accuracy, and L2 mesh (750K elements) for wing (Fig. 3.6), looking for a compromise that takes into account computational cost and physical accuracy.

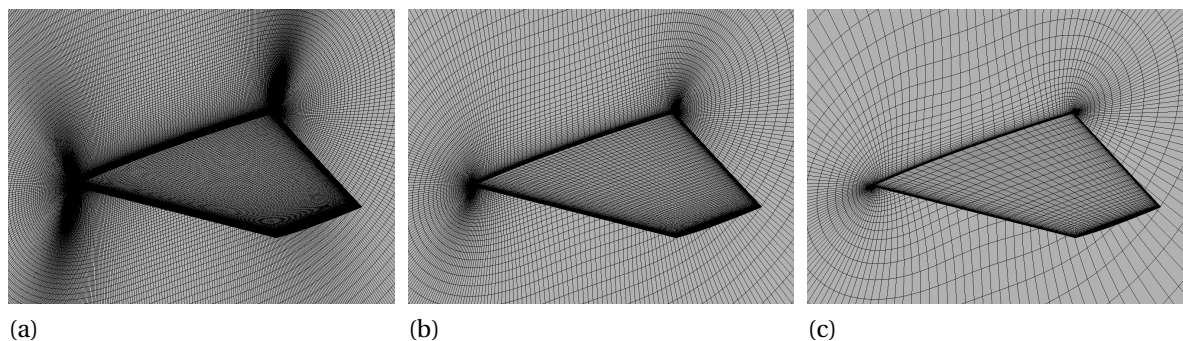


Figure 3.6: Mesh family for baseline wing with biconvex wing section. Grid sizes are respectively (a) L0: 22M elements, (b) L1: 6M elements, (c) L2: 750K elements

## 3.2. Design Variables

The design variables manipulated for an ASO study are mainly geometrical, as the optimization algorithm acts on the aircraft OML to match the constraints as the target function is minimized. As this investigation focuses on wings and wing sections, design parameters are limited to:

- Local airfoil shapes, to directly modify fluid behaviour over the wing and 2D airfoil. Control points distribution influences both manipulation capabilities and the propagation of the deformation along the geometry;
- Leading and trailing edge deflection, altering wing section camber at different flight regimes;
- Wing twist (on 3D cases only), to manipulate both local and full-wing fluid phenomena, and ultimately control spanwise pressure distribution.

The optimizer is also given control of the angle of attack  $\alpha$ , to match the different  $C_l$  constraints without excessively distorting the wing section and offer more realistic designs. As discussed in Sec. 3.1, planform modifications are outside the scope of this study, thus I neglect dihedral angle, sweep angle, and chord modifications. *MACH* framework allows the manipulation of such parameters, as shown in previous works from MDO Lab [37]. At this stage however, further extending this investigation would have exceeded the planned timing and possibly forced to a more superficial analysis and discussion of the huge amount of data and design cases thus produced.

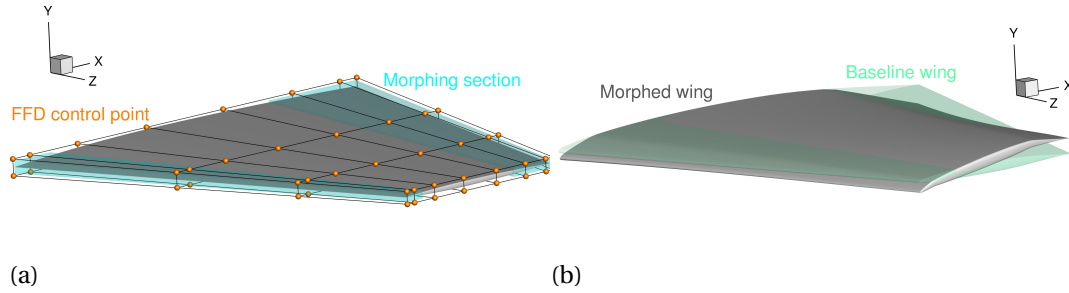


Figure 3.7: Example of full wing parametrization, including both local control points (orange) and child grids (cyan) for leading and trailing edge deflection (a), and a snapshot of a deformed wing (b) with  $\beta_{LE}=\beta_{TE}=10^\circ$  and a twist of  $10^\circ$ ,  $5^\circ$ , and  $0^\circ$  at the three spanwise stations, from tip inboard. Root section twist is fixed.

An intuitive snapshot of the complete parametrization grid around the baseline wing is exemplified in Fig. 3.7, showing the framework manipulation capabilities extent for this study. Remarks for single design variables are reported in the following paragraphs.

### 3.2.1. Local shape variables

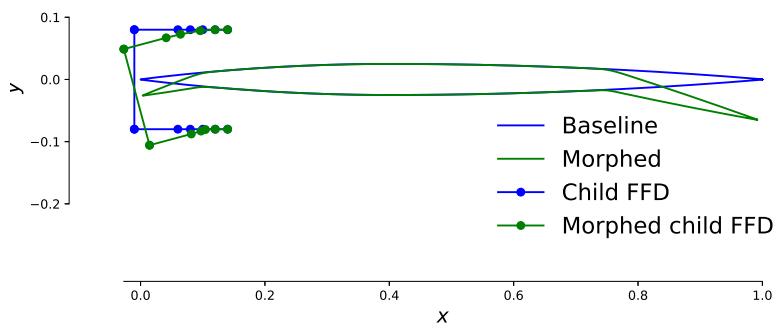
Wing section shape manipulation and optimization is the backbone of this study: the optimizer has direct control on the local geometry deformation. The airfoil is embedded in a  $n \times 2 \times 2$  (chordwise, vertical and spanwise direction respectively) FFD grid, while the wing is parametrized by a  $m \times 2 \times 4$ , with equally spaced spanwise stations.  $n$  and  $m$  are arbitrary chosen numbers, with the chordwise distribution being tuned to maximise geometry deformation capabilities, as later investigated in Chap. 4- 5. Control points are solely displaced along the vertical direction. For airfoil optimization, spanwise symmetry is imposed to avoid deformations in the third dimension and thus introducing unrealistic crossflow effects. Conversely, the wing control sections are independent, given that optimization constraints are satisfied.

It is expected that for supersonic regimes, leading and trailing edges shapes play a key role in drag reduction. Having a higher control density in these areas has beneficial effects on final performance, increasing manipulation accuracy. However, FFD control points effectiveness is related to local CFD grid refinement. Having an excessive number different CP displacing few mesh cells leads to inaccurate sensitivity analysis and, ultimately, to a wavy layout - given that the optimizer converges. As a rule of thumb, there should be at least 4 (25 most conservatively) grid elements between each FFD control point.

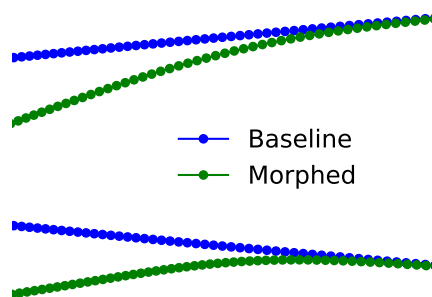
### 3.2.2. Morphing Capabilities Implementation

The introduction of morphing capabilities adds two geometric variables to the problem, namely the two deflection angles  $\beta_{LE}$  and  $\beta_{TE}$ . To model these deflections, two child FFD frames are attached to the main frame and are allowed to rotate around a fixed virtual hinge, as schematically illustrated in Fig. 3.8(a). For both airfoil and wing, the virtual hinge locations are fixed to 10% and 75% of the chord for leading and trailing edge respectively. The rigid rotation of these sub-grids drive the deflections, while local shape perturbation and

wing twist remain under control of the main frame variables. The distribution of control points around the virtual hinge is arranged so to limit the propagation of shape deformations along the airfoil surface [35], as highlighted in Fig. 3.8(b).



(a)



(b)

Figure 3.8: Example of morphing leading and trailing edge for NACA 2S-(40)(015)-(40)(015) (a) and detail of airfoil deformation around the front virtual hinge (b). Deflection is  $\beta_{LE}=\beta_{TE}=15^\circ$

$\beta_{LE}$  and  $\beta_{TE}$  vary independently for each flight condition, thereby defining an ideal case to run the different flight condition cases in parallel on the computer and cutting down the overall optimization time.

### 3.2.3. Twist

The independent spanwise stations implemented to alter airfoil shapes wing optimization cases, when rotated around a spanwise axis, are used to locally alter the wing geometrical angle of attack. I add an additional global variable for twist to each of these stations, excluded the root section, allowing a rigid rotation of local control points around a virtual hinge, located at 25% of the chord. This is a standard implementation in *PyGeo* and do not present additional challenges. The designer however must enforce a constraint on vertical translation of these control sections, that would otherwise introduce a dihedral angle as design variable. Fig. 3.7(b) shows an example of twist of the initial geometry, including edges deformation as introduced in the previous paragraph.

### 3.3. Flight Envelope

An intuitive description of an SST flight envelope is provided in Sec. 1.2.4. The multipoint optimization strategy described in Sec. 1.3.1 is effectively used to improve the performance of the aircraft over a discrete set of flight conditions, resembling a realistic SST commercial mission. A higher number of flight regimes would imply a higher number of flow solution that, at this stage, are considered of secondary relevance.

I use both literature [19, 41], Concorde historical data [81] - as presented in Chap. 1, and predicted performance of Aerion AS2 [17], to establish a realistic flight envelope for a SBBJ. From a physical standpoint, every flight condition is defined by a specific Mach number, altitude (Reynolds number and temperature are calculated according to ISO standard atmosphere), and a fixed lift coefficient.

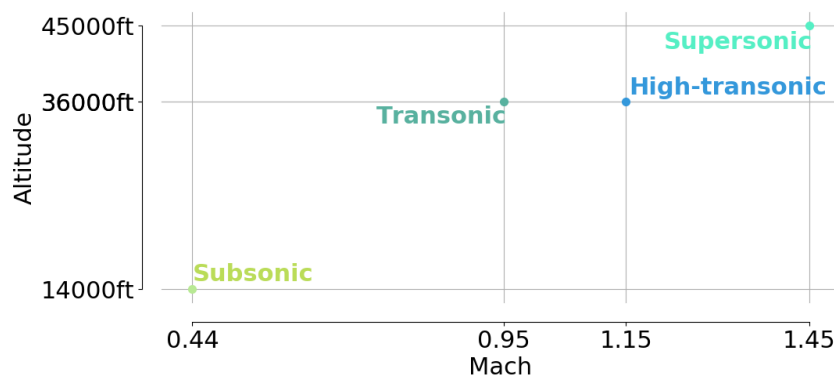


Figure 3.9: Visualization of the four target flight regimes identified for an SST ideal mission, reported on an altitude vs. Mach plot.

As reported in Fig. 3.9, I identify four different flight conditions: a supersonic flight regime at high altitude ( $M=1.45$ ), a high-transonic ( $M=1.15$ , theoretically suitable for “boomless cruise”) and “conventional” transonic ( $M=0.95$ ) regimes, and finally a subsonic case for holding and descent ( $M=0.44$  at 14000 ft, to observe FAA regulations on holding speed and altitude). Lift coefficients are estimated from Aerion AS2 predicted MTOW and wing area, considering a full fuel load for cruise cases and an approximately 15% fuel reserve for low-speed holding. For an ideal flight path from Paris-“*Charles de Gaulle*” to New York-“*JFK*” I estimate an 85% of the route at unrestricted speed, 10% overland (thus at  $M \leq 1.15$ ) and 5% at subsonic speed.

### 3.4. Constraints

As discussed in Sec. 1, constraint definition has a crucial role as it defines the design space and directly affects the optimal shape. A well-posed problem ensures that the final design is feasible and consistent with mission requirements and objectives. A compromise has to be made to guarantee that an optimal solution is reached without excessively biasing the numerical search, limiting the tool explorative capabilities. Moreover, a careful tuning of some of the design constraints, as presented later, has beneficial effects on computational cost. By

forbidding the optimizer to evaluate odd and clearly unreasonable layouts, the number of unsuccessful line searches and costly CFD evaluations of complex geometries is consistently limited. In this sense, constraint definition is one of the aspects of ASO and MDO problem where user experience mostly plays a crucial role for a successful design investigation.

For sake of clarity, constraints are split into two main categories: geometrical, strictly looking at the target shape, and performance, related to the aerodynamic coefficients obtained from flow analysis. Their combination guarantees the robustness of the final layouts and, ultimately, the optimization framework reliability.

### **3.4.1. Geometry Constraints**

Aiming primarily at guaranteeing structural feasibility, both volume and thickness constraints are imposed on the geometry. The reference biconvex airfoil and wing section presented in the previous section provide the minimum cross-sectional area and internal volume values for 2D and 3D optimization cases respectively. Minimum thickness constraints are set to be in the order of magnitude of 1 mm from 10% to 90% of the chord and 0.1 mm closer to the edges. This is to increase optimization robustness and prevent the optimizer from crossing the upper and lower surfaces (as discussed in [5]), but at the same time allow the tool to design sharp leading and trailing edges, as it is expected for typical supersonic airfoils.

#### **Volume and cross-sectional area constraint**

Imposing a volume - or cross-sectional area in the airfoil optimization case - constraint on the problem is crucial to ensure feasibility of the final shape. This is true for both a consistent aerodynamic analysis and comparison and for broader design considerations. Having a fixed, absolute value for minimum internal volume is necessary to perform a multi-start ASO approach as presented in Sec. 3.1. All the different initial shapes have to (ideally) converge to the same layout, thus constraints have to be unrelated to initial shape. In the study, the reference value is usually extrapolated from the “thinnest” shape among those chosen for the study, namely the biconvex wing section. Volume constraint also serves as a pseudo-structural constraint: although the stresses on the wingbox are outside the scope of this analysis, preserving a minimum volume at least ensures that the baseline structure fits the final layout. Moreover, if fuel tanks are located in the wings, their capacity would not be affected by the optimizer (with trickle-down effects on mission range, subsystems design, etc.)

Considering supersonic optimization in particular, as illustrated in Sec. 1.1, the object volume AND its chordwise variations have a direct impact on the overall drag, thus the optimizer is not expected to dramatically shrink the edges as reported in previous unconstrained optimization studies [5]. For this reason, volume constraint is considered the driving geometrical constraint in this study.

#### **Thickness constraint**

As just mentioned, minimum thickness limitations have a merely “safety” role in this study. Given the predominant role of supersonic flight regime in any optimization, the risk of gen-

erating unrealistically thin leading edges is minimized.

### 3.4.2. Performance constraints

Geometrical limitations are essential to ensure optimal layout feasibility, but are not sufficient to provide a robust optimal shape. To ensure a sound design that reflects engineers intentions, configuration performance in addition to the mere objective function has to be quantified.

From a purely aerodynamic perspective, lift and pitching moment constraints are necessary to guarantee optimal layout consistency with aircraft design requirements, in terms of take-off and cruise weight, and (longitudinal) flight stability. To further take into account structural considerations, bending moment has to be quantified to verify that a sufficiently strong wingbox can be coupled with the OML at a later design stage.

#### Lift constraint

Enforcing a lift constraint on the optimization problem is a necessary condition to obtain any meaningful design from the design framework. It is fair to assume that otherwise the  $C_{l/L}$  would tend to zero so to minimize lift-induced drag. Target values are obtained by estimating a realistic flight envelope, as discussed earlier in this section.

To maintain consistency between airfoil and wing lift constraints, I apply the formula proposed by H. B. Helmbold for finite wing correction for low aspect ratio wings, considering compressibility effects:

$$a_{\text{comp}} = \frac{a_0}{\sqrt{1 - M_\infty^2 + [a_0/(\pi AR)]^2 + a_0/(\pi AR)}} \quad (3.1)$$

valid at subsonic speeds, while for supersonic regime the following is used:

$$a_{\text{comp}} = \frac{4}{\sqrt{M_\infty^2 - 1}} \left( 1 - \frac{1}{2AR\sqrt{M_\infty^2 - 1}} \right) \quad (3.2)$$

with  $a_{\text{comp}}$  and  $a_0$  the lift slope ( $\partial C_{l,L}/\partial\alpha$ ), assumed constant at cruise regime, for wing and airfoil respectively, AR the wing aspect ratio and  $M_\infty$  the freestream correction

#### Pitching moment constraint

Well-posed, full-configuration aircraft optimization include a force and moment balance in the problem formulation, considering the force distribution of lifting and non-lifting surfaces with respect to the center of gravity. In the search for minimum drag or minimum fuel consumption, the optimizer could explore unconventional or odd wing shapes, whose flight attitude would have to be compensated by horizontal tail trim. Tail deflection implies additional drag: thus, full-configuration studies implicitly limit pitching moment for performance purposes, even regardless of safety or manoeuvrability concerns.

Trim requirements are indirectly enforced in the form of a minimum  $C_{m_z}$  (pitching moment coefficient) value. For airfoil cases, I refer to ADODG case 2 [87] minimum value, while for planar wings I impose the pitching down attitude to not increase over the initial values. It is important to remember from Sec. 1.1 that the aerodynamic center location shifts from 25% of the chord to 50% when the aircraft flies through the sound barrier. The reference axis for  $C_{m_z}$  is set accordingly for different flight regimes.

As a side note, it is worth to consider that designers usually minimize supersonic aircraft aerodynamic shift with a design gimmick. The fuel, located in different tanks inside the fuselage and wings, is relocated during flight (especially when breaking the sound barrier) to shift the center of gravity and thus neutralize the aircraft pitching attitude. This could be also applied with a more systematic approach as a trim device throughout the entire flight, relegating tail deflection to manoeuvring purposes or trimming during the last phases of the flight. This is however outside the scope of the analysis; thus the optimization takes into account pitching issues in the conventional fashion presented above.

### **Bending moment constraints**

The nature of ASO studies implies that any kind of consideration involving disciplines other than aerodynamics are outside the analysis framework capabilities. To roughly ensure structural feasibility of the wing without embedding a structural model in the analysis, I limit the bending moment maximum values to not exceed baseline wing values. For the current study, this is considered sufficient to provide robust wing designs. Adding a stress analysis module is recommended in case more complex planform geometries are allowed, as a first step of a broader MDO investigation.

## **3.5. Optimization Problem Definition**

The coalescence of objective function(s), design variables, and constraints set the base for a well-posed formulation, both from a mathematical and engineering point of view. The optimization problem, as described in this section, is summarized in Tab. 3.2. The four flight conditions are characterized by two different lift constraints, depending on if a 2D or 3D problem is investigated. Design variables span from a minimum of 25 (24 FFD + 1  $\alpha$ ) for a clean airfoil case up to 70 for a morphing wing optimization run. The small number of performance constraints (coming from flow evaluations) once more supports the claim that adjoint-based sensitivity analysis (Appx. D) is the best approach for this kind of engineering optimization problems. The objective function is defined as the weighted average of different flight conditions (when present) as discussed in Sec. 3.3, using the same strategy already applied in [11, 35, 36]. Exploiting *MACH* MPI features, the flow and sensitivity analyses for single flight regimes are carried out in parallel on different cores or processors, before the optimizer collects the information and calculates the following optimization step.

Table 3.2: Optimization problem definition. Parameters in blue on the table apply to wing optimization, while the additional design variables for morphing edges are highlighted in green.

| Objective: minimize $C_d$ |                   |  |                    |
|---------------------------|-------------------|--|--------------------|
| Boundary conditions       |                   |  |                    |
| Case name                 | Mach              | $C_L/C_l$  | Altitude [m]([ft]) |
| <b>Supersonic</b>         | 1.45              | 0.195/0.236  | 13700 (45000)      |
| <b>High-Transonic</b>     | 1.15              | 0.2/0.3  | 11000 (33000)      |
| <b>Transonic</b>          | 0.95              | 0.295/0.4  | 11000 (33000)      |
| <b>Subsonic</b>           | 0.44              | 0.324/0.62   | 4280 (14000)       |
| Design Variable           | Qty               | Constraints  | Qty                |
| <i>Shape</i>              | 24/40 for airfoil | Volume $\geq$ Volume <sub>ref</sub>                                  | 1                  |
|                           | 64 for wing       | Thickness $\geq$ Thickness <sub>min</sub> 40 chordwise + 20 spanwise | 1                  |
| $\alpha$                  | 1                 | $C_{l_{cruise}} = C_{l_{ref}}$                                       | 1                  |
| $\beta_{LE}, \beta_{TE}$  | 2                 | $C_m \geq C_{m_{min}}$   | 1                  |
| <i>Twist</i>              | 3(/7)             | $C_x \leq C_{x_{init}}$  | 1                  |

I stress again that the objective of this work is to minimize the drag of airfoils and wings for supersonic regime while taking into account the performance at lower speed flight. Rather than a design exercise, the project investigates different sub-problems involving both pure supersonic and multipoint optimization. The goal is to gain better insight on the design space characteristics and the influence of different physical and numerical parameters on the optimal layouts. A limited but consistent set of cases presented in Chap. 4- 5 explores different “combinations” of the conditions and variables sets presented in the table below.

An optimization run is considered converged when the residual of first order optimality conditions drops below a tolerance of  $10^{-6}$ , while tolerance for the flow solver is set at  $10^{-12}$ .



# 4

## 2D Optimization Results

The results of our study for airfoil drag minimization cases are discussed in this section. I initially optimize an airfoil for supersonic regime at both lifting and non-lifting conditions. The influence of both Mach,  $C_l$  and FFD control point distribution is investigated. Following that, the problem is extended to simultaneously take into account multiple flight conditions, using the multipoint strategy discussed in Sec. 3.5. I compare the optimal “clean” designs, obtained with local shape deformation alone, with the configurations that allow gap-less leading and trailing edges deflection. Relative weight influence of the different flight conditions is briefly discussed as I optimize the airfoil for an ideal transatlantic route.

### 4.1. Single-Point Supersonic Optimization

The first set of optimization test cases is carried out for the solely supersonic regime. This has been done to familiarize with both the tool features and especially with the characteristics of low-drag, high-speed airfoils. The optimization pipeline is validated with a simple and well-known case in Sec. 4.1.1, before tackling “unexplored” design cases. The effect of Mach and  $C_l$  constraint is investigated in Sec. 4.1.2, together with an assessment of the impact and effectiveness of different FFD grids, the design space topology and ultimately generate a reference optimal supersonic layout in Sec. 4.1.3.

#### 4.1.1. 2D non-lifting minimum drag shape

To initially assess optimization routine accuracy I run a simplified case, the drag minimization of a non-lifting airfoil in supersonic flow (Fig. 4.1), and I compare the final shape with the 2D Sears–Haack body as theoretical minimum-drag shape. Airfoil cross-sectional area is fixed (1% tolerance on baseline value), while no thickness constraints are enforced. I use two different control point sets with 12 and 16 points respectively as I enforce symmetry between upper and lower surfaces, so to avoid inconsistent shape modifications induced by machine-level numerical errors on  $C_l$  prediction.

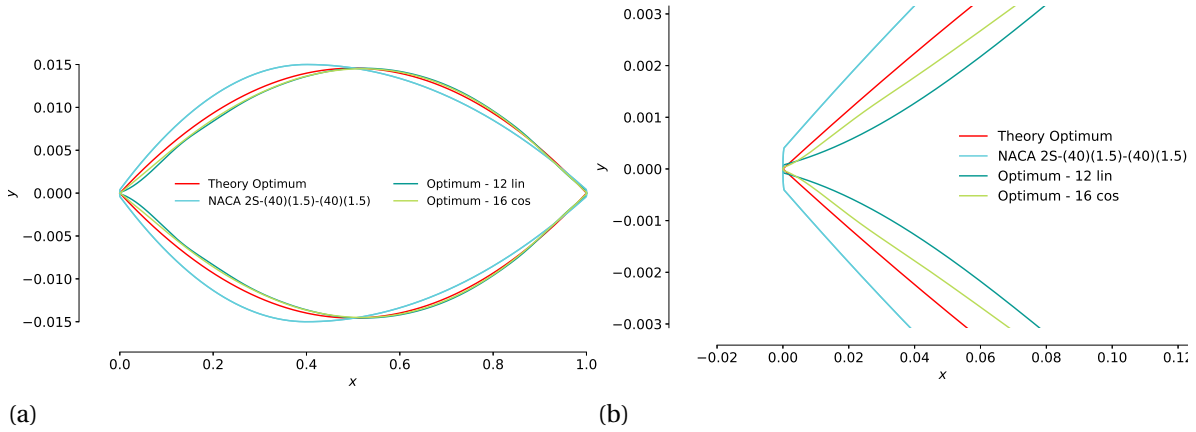


Figure 4.1: Comparison between optimal shape for non-lifting viscous optimization and theoretical minimum drag 2D section, derived from Sears–Haack body. Figure highlights both the discrepancy from analytical reference due to non-linear effects (a), and the influence of shape parametrization at the leading edge on the final layout (b).

I observe a mismatch in maximum thickness position along the longitudinal axis, being it shifted rearward with respect to theoretical optimum. This result is in accordance with the work made by Palaniappan and Jameson [45] on nonlinear inviscid supersonic optimization for minimum shape drag. As discussed by the just mentioned authors, the difference from theoretical optimum is explained by the presence of a shockwave on the leading edge that is not predicted by the analytical model.

The optimizer minimizes shockwave intensity by reducing the slope in the airfoil fore part, as illustrated in Fig. 4.2. The optimal shape shows a drag reduction of 10.6% and 11.5% for 12-DV and 16-DV cases respectively. The more refined parametrization guarantees an additional drag reduction thanks to a further reduction in nose radius minimization and, concurrently, a more limited chordwise propagation of the local deformation at the leading edge (Fig. 4.1(b)). Although part of the overall drag reduction is given by a small reduction in cross-sectional area, I consider the reduction in leading edge radius and thickness in the airfoil foremost part as main factors that improve airfoil performance.

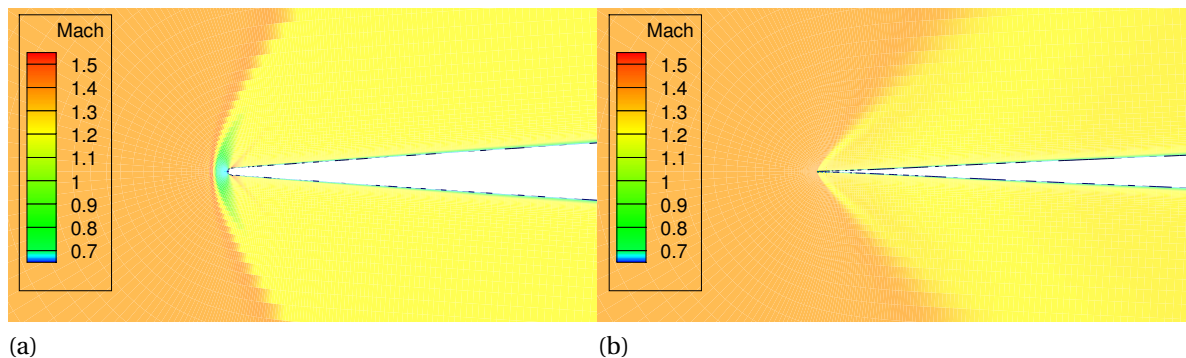


Figure 4.2: Snapshots of Mach contours for baseline (a) and optimal shape (b) for drag minimization at  $C_l=0$ . The different intensity of leading edge shock is highlighted. 16 chordwise design variables are used in the optimization. Scaling is identical for both figures.

### 4.1.2. Influence of Physical Factors

After having assessed the optimizer accuracy for a supersonic, non-lifting case, I extend my investigation to the influence of  $C_l$  constraint and freestream Mach on the optimized layout.

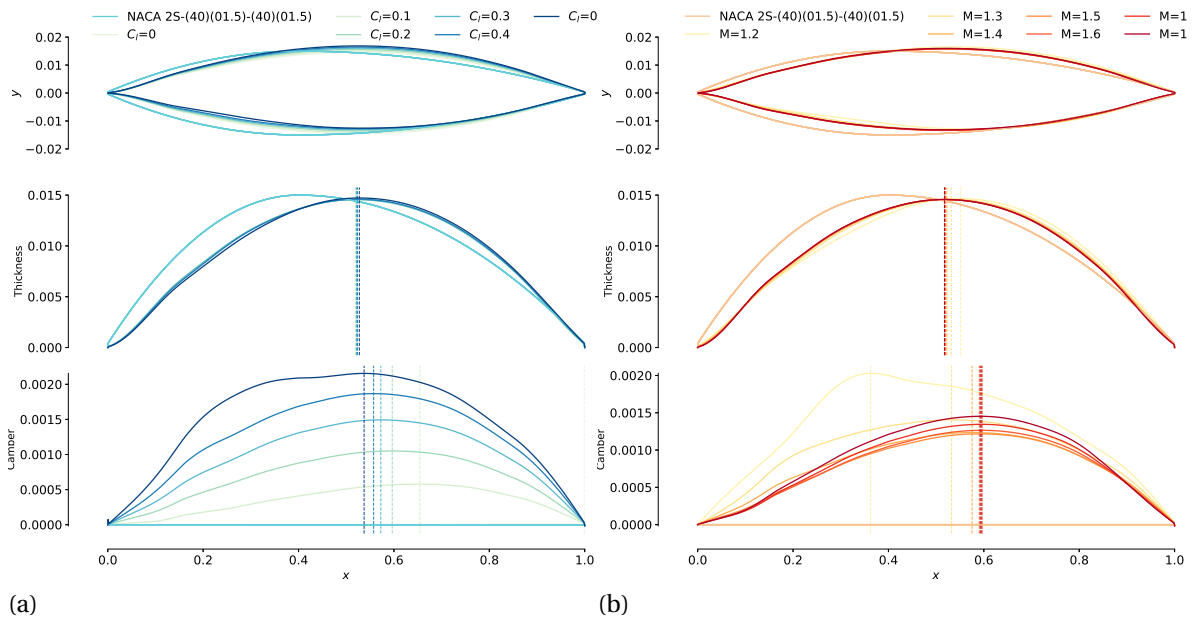


Figure 4.3: Set of optimization results for (a) fixed flow conditions ( $M=1.45$  @ 45000ft) and variable  $C_l$  constraint and (b) fixed  $C_l=0.236$  and altitude (45000ft), and variable freestream Mach. While thickness distribution is mostly unaffected, increase in  $C_l$  tends to shift the maximum camber position closer to the leading edge, while an increase in freestream Mach has the opposite effect. Lift constraint has the biggest impact on camber magnitude.

Fig. 4.3(a) refers to a set of optimization results where flow conditions are kept fixed to reference supersonic case (Tab. 3.2) and the target lift coefficient is varied from 0 to 0.5 with 0.1 steps. Thickness distribution for different layouts is identical, with a slight shift in the maximum thickness position between 52-53% of the chord - the same value obtained for non-lifting case. On the other hand, airfoil camber becomes noticeably more pronounced as  $C_l$  increases, with a shift in maximum height position from 65% to 54% of the chord and the appearance of a “bump” between 15% and 40% of the chord. The optimizer appears thus to deal with the increasing  $C_l$  by diverging from theoretical symmetrical shape and reducing the final angle of attack if compared to theoretical results, as shown in Tab. 4.1.

In Fig. 4.3(b) conversely I keep the same constant target  $C_l$  and vary inflow speed for  $M=1.1-1.6$  range with 0.1 steps. In this case, I observe a maximum thickness position shift with increasing freestream Mach, from 55% to 52% of the chord, and at the same time a change in camber of the airfoil foremost section as speed decreases, almost matching the values obtained for  $C_l=0.5$  at  $M=1.45$ . In this case however, such modification is justified by the minimization of subsonic flow regions close to the front lower surface, thus reducing wave drag.

This brief analysis shows how, although shape shows small discrepancy from analytical re-

sults, the use of a high-fidelity tool improves the performance of a well-known and theoretically-investigated shape such as the 2D minimum-drag section.

Table 4.1: Angle of attack variation for optimal layouts with varying design  $C_l$ , and comparison with linearized supersonic theory prediction. Analytical results become less accurate with higher  $\alpha$ , as expected from model assumptions.

|                           | $C_l=0$     | $C_l=0.1$    | $C_l=0.2$    | $C_l=0.3$    | $C_l=0.4$    | $C_l=0.5$    |
|---------------------------|-------------|--------------|--------------|--------------|--------------|--------------|
| $\alpha_{\text{optimal}}$ | $0.0^\circ$ | $1.49^\circ$ | $2.97^\circ$ | $4.43^\circ$ | $5.84^\circ$ | $7.17^\circ$ |
| $\alpha_{\text{theory}}$  | $0.0^\circ$ | $1.51^\circ$ | $3.01^\circ$ | $4.52^\circ$ | $6.02^\circ$ | $7.52^\circ$ |

Data in Tab. 4.1 reports the difference in angle of attack between analytical formulation presented in Sec. 1.1 (Eq. (1.2)) and the results of the optimization runs. As expected, at low  $C_l$  and  $\alpha$  there is a good match between the approaches. At higher - but still relevant from a design point of view - lift coefficients, the linear theory no longer holds and the discrepancy raises more than linearly with  $\alpha$ . This once more underlines the benefits of using high-fidelity tools even for such simple and well-known cases.

### 4.1.3. Parametrization Study and Unimodality Assessment

Having obtained insight on the physical factors that affect supersonic airfoil optimization, I then shift the focus on shape parametrization impact on the minimum-drag layout. As discussed in Sec. 3.5, I want to ensure that the initial airfoil choice, although relevant for flow solver performance and computational time, has a minimum impact on the final shape. I thus compare a set of FFD grids with different design variables number, from 12 to 20 stations (each station includes the two control points for upper and lower surface respectively), with both a uniform and cosine spanwise distribution. Results in terms of final drag discrepancy and computational time for two reference geometries, the biconvex NACA2S-(40)(1.5)-(40)(1.5) airfoil a NACA0012 profile, are reported in Fig. 4.4:

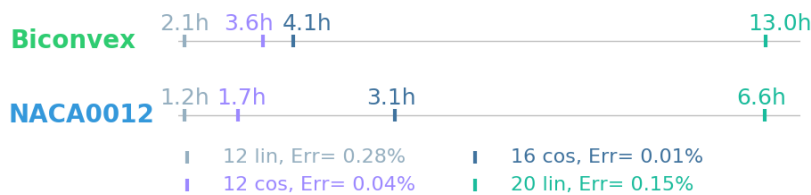
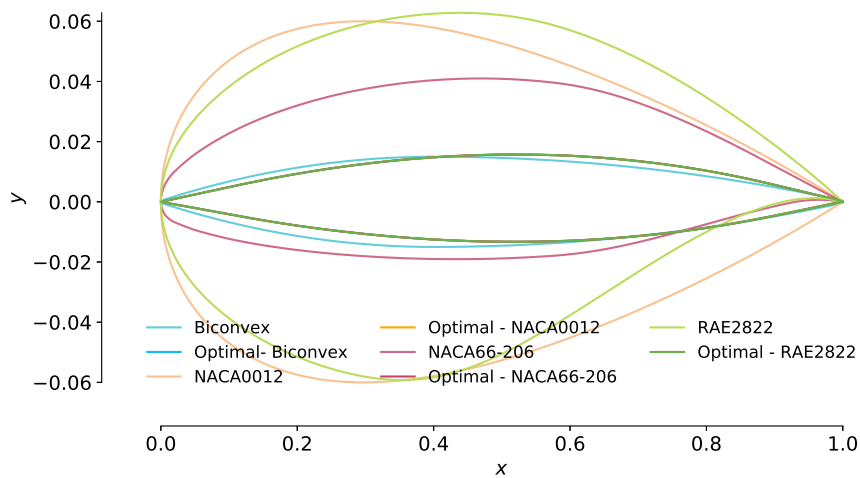


Figure 4.4: Computational time and discrepancy for a single-point supersonic optimization, starting from different baseline airfoils and using different FFD grids. Optimization runs are performed on University of Michigan’s HPC cluster (FLUX) using 12 processors for each case.

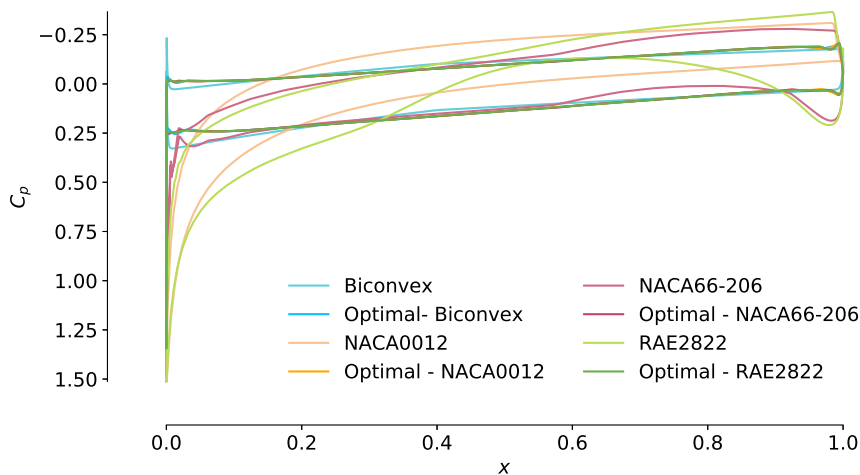
It turns out that the 16-cosine distribution offers the best accuracy with a relatively small computational time penalty, if compared to FFD grids with a higher number of control points. It is also highlighted how starting the optimization from a shape that is “distant” from the optimal layout leads to a faster, even though slightly less accurate, optimization case. This is most likely due to the higher sensitivities and, consequently, deformations

when starting from a bad-performing shape. In this way most of the improvement originates in the first optimization steps; close to the optimum there is less manipulation flexibility and thus less optimization steps to converge to the optimum.

I ultimately prove the accuracy of our selected 16-cosine parametrization scheme by performing two additional optimization runs starting from different airfoils, the RAE2822 and NACA66-206 sections. Shape, pressure distribution and drag coefficient, shown respectively in Fig. 4.5(a), Fig. 4.5(b) and Tab. 4.2, highlight an excellent match between the different cases. Final results differ by a maximum of 0.06 drag counts (0.025%) and minimum discrepancy (up to  $0.8^\circ$ ) in the optimal angle of attack due to mesh distortion. This comparison further support the assumption of unimodality for the supersonic optimization problem.



(a) Shape comparison



(b) Pressure distribution comparison

Figure 4.5: Drag minimization of an airfoil for  $M=1.45$  at 14500m,  $C_l=0.236$ , starting from NACA2S-(40)(1.5)-(40)(1.5), NACA0012, NACA66-206, and RAE2822.

Fig. 4.5(b) highlights how, for single-point supersonic optimization, the framework ultimately tends to linearize the chordwise  $C_p$  distribution, as expected from linear theory. This

indicates that the flow is uniformly accelerated around the airfoil upper and lower surfaces, thus minimizing wave drag. The small results discrepancy between runs also demonstrates the effective meshing work illustrated in Sec. 3.1.1, showing the minimal impact of different meshes on final shape and numerical solver.

Table 4.2: Results for single-point, supersonic optimization starting from different initial airfoils reported in Fig. 4.5.  $C_d$  is provided in drag counts ( $C_d \times 10^4$ )

| Base airfoil               | Initial $C_d$ | Final $C_d$ | $\Delta C_d$ | $\alpha$ |
|----------------------------|---------------|-------------|--------------|----------|
| NACA2S-(40)(1.5)-(40)(1.5) | 253.80        | 240.74      | -5.14%       | 3.53°    |
| NACA 0012                  | 1173.94       | 240.76      | -79.49%      | 3.54°    |
| NACA 66-206                | 485.15        | 240.70      | -50.38%      | 3.45°    |
| RAE2822                    | 1100.56       | 240.72      | -78.12%      | 3.46°    |

## 4.2. Multipoint Optimization

After I investigate the features of 2D supersonic optimization, I move on to multipoint airfoil optimization so to minimize the drag penalty of a high-speed airfoil when used at both transonic and subsonic speeds. This section is particularly critical because it implies a simultaneous optimization for three (only one between *transonic* and *high-transonic* flight conditions is selected for each optimization) flight regimes. The design features of clean, non-morphing airfoils are investigated in and benchmarked with equivalent morphing layouts for different mission profiles.

### 4.2.1. Equal-weights testcase

As first test case, I choose to simultaneously optimize a baseline wing section for supersonic, transonic and subsonic reference conditions while enforcing the same relative weight on the objective function. Although this problem formulation is hardly applicable on a real engineering design problem, it is an extreme test case useful to prove optimization robustness, highlight the features required to minimize the drag for the single design cases and ultimately extremize the benefits of the airfoil morphing capabilities. In Fig. 4.6 I compare the results of this “equal-weights” optimization problem both without and with the addition of edges deflection variables. The selected baseline shape is a NACA 66-206 wing section.

When leading and trailing edge deflection is not allowed, as expected, the optimizer converges to a shape that is characterized by a strong trade-off between typical features of supersonic and subsonic airfoils. The optimal layout features a thick and rounded leading edge. This is due the necessity to match subsonic lift constraint while minimizing boundary layer separation, which would most likely occur on a sharp-edged airfoil. Camber curvature is higher in proximity of the edges. If, on the one hand, the leading edge shape is associated again to subsonic drag reduction, on the other hand the trailing edge shows a kink and pitching-down tail of typical supercritical transonic airfoils. Thickness distribution, except for the bigger nose section, is conversely comparable to the typical parabolic distribution for efficient supersonic shape I discussed earlier.

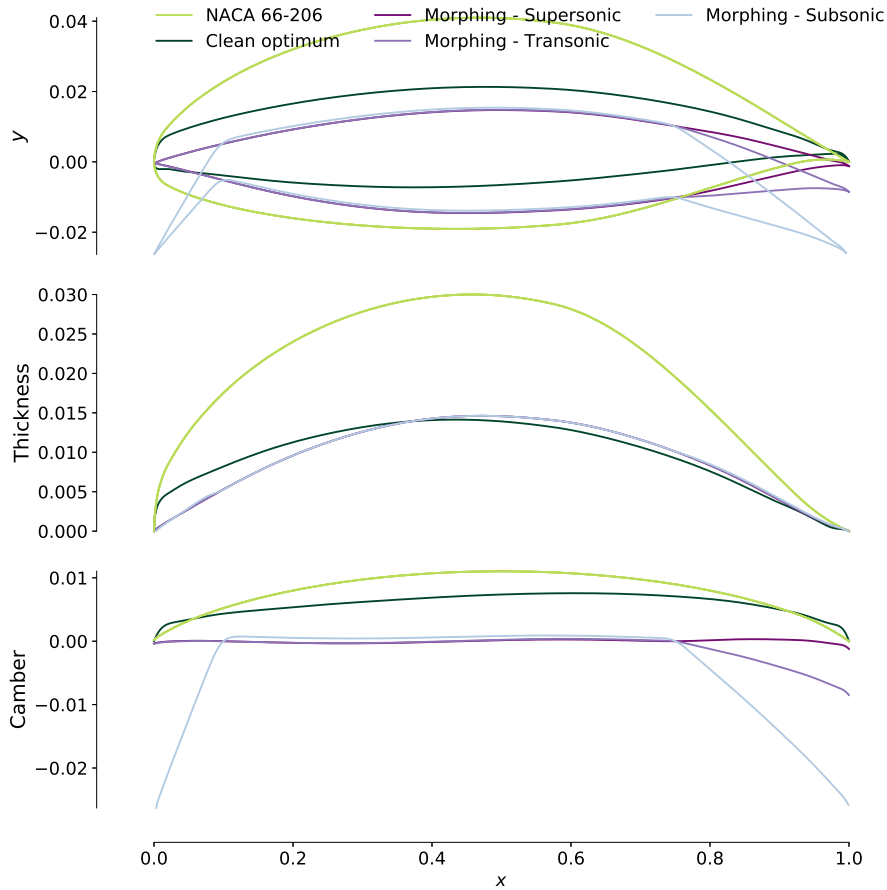


Figure 4.6: Shape comparison between clean, fixed-edges and morphing airfoil multi-point optimization. Supersonic, transonic and subsonic flight regimes from Tab. 3.2 are taken into account with same weight in the objective function.

The performance trade-off is reported in Tab. 4.3. Although drag reduction varies from a minimum of 0.2%, for subsonic speed, up to 57.2% for transonic regime (cross-sectional area reduction from the initial NACA66-206 geometry is certainly contributing to this), supersonic performance is more than 77 drag counts (32%) higher than single-point optimization results.

Table 4.3: Baseline and optimized shape drag for multi-point optimization, comparing clean and morphing airfoil cases. Flow conditions refer to Tab. 3.2 and have the same weight in the objective function. Drag coefficient is provided in drag counts ( $C_d \times 10^4$ ).

| $C_d$            | Supersonic | Transonic | Subsonic |
|------------------|------------|-----------|----------|
| NACA 66-206      | 485.15     | 618.55    | 81.82    |
| Clean optimum    | 307.54     | 264.76    | 81.65    |
| Morphing optimum | 243.23     | 263.80    | 73.74    |

The introduction of morphing capabilities, which advantages are underlined by both Fig. 4.6 and Tab. 4.3, apparently allows to relax the trade-off between different design conditions by

decoupling the main optimization problem into three, almost-independent, drag minimization problems. Supersonic performance benefits the most from the edges deflection, with final  $C_d$  only 1% higher than pure supersonic optimization results. I consider this improvement to be given by the reduction of leading edge radius, thus virtually eliminating the bow-shock in front of the airfoil. At the same time, thanks to the deflection of both leading and trailing edges ( $15.4^\circ$  and  $-5.7^\circ$  respectively), subsonic drag is reduced by 9.7% with respect to the clean-airfoil results. Surface curvature increase at the virtual hinges location, together with the reduction of local angle of attack at the leading edge, minimize the disadvantages of using a sharp airfoil at low speeds. As for the transonic case, it is observed, despite the different layout, a difference of just one drag count between the clean and the morphing case. This suggests that at this specific flight regime, leading edge radius has a minor influence on performance. Once again, camber distribution, with the kink at the rear virtual hinge, is associated with typical supercritical airfoils, although local curvature is smaller than the previous case.

#### 4.2.2. Transatlantic path testcase

Given the insight provided by this first multipoint optimization example, I then assess the potential of our optimization strategy when applied to a more realistic optimization problem. Data in Tab. 4.4 and Fig. 4.7 refer to a drag minimization case where flight conditions relative weight on objective function is related to an ideal Paris–New York route with high-transonic ( $M=1.15$ ) overland segment, as presented in Sec. 3.5. I additionally verify the unimodality of the problem by showing how two different initial airfoils, NACA2S-(40)(1.5)-(40)(1.5) and NACA66-206 converge with minimal discrepancy ( $\max \Delta C_d=0.54\%$ ) to the same results. I consider the relative mismatch between angle of attack and edges deflection respectively as a result of different FFD grid distortion when starting from different geometries. These  $\alpha$  and  $\beta$  discrepancies compensate each other to eventually return identical pressure distributions, as shown in Fig. 4.7.

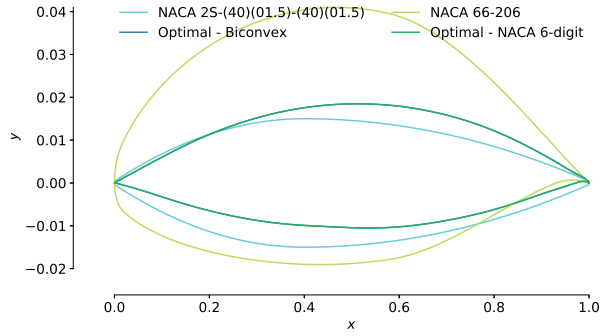
Shape and pressure distribution for single cases are compared in Fig. 4.7. As expected, clean optimum is much closer to a typical supersonic shape than what shown in Sec. 4.2.1, as the relative weight of this flight segment is increased up to 85%. However, some of the features discussed for previous case are still present. In particular, clean shape in Fig. 4.7(a) appears to have a positive camber if compared to the quasi-symmetrical, morphing airfoil in Fig. 4.7(b); it moreover presents the twisted-down trailing edge already observed in Fig. 4.6. Morphing-shape optimum has once again a superior performance at all the different flight conditions, with supersonic drag matching with good approximation single-point optimization values, as summarized in Tab. 4.5. Highest performance improvement, 86.9% drag reduction, is obtained at subsonic regime, where clean, sharp-edged optimum has a much higher drag penalty.

Table 4.4: Results relative discrepancy for multi-point optimization, starting from NACA2S-(40)(1.5)-(40)(1.5) and NACA66-206. Both clean and morphing airfoil results are taken into account: supersonic, high-transonic and subsonic conditions refer to Tab. 3.2 and are weighted for CDG-JFK flight route. In  $\beta$  rows, leading and trailing edge deflections are reported ( $\beta_{LE}/\beta_{TE}$  respectively), with counter-clockwise positive deflection. \* high relative deflection discrepancies highlighted with the asterisks do not undermine the overall excellent match of the results, as the absolute difference in deflection is in the order of  $1^\circ$ . Final shapes consistently overlap, as illustrated in Fig. 4.7.

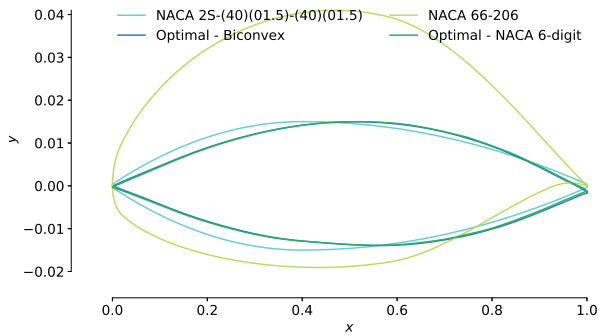
| Results discrepancy |                |          |              |
|---------------------|----------------|----------|--------------|
| Clean               | Supersonic     | $C_d$    | <b>0.02%</b> |
|                     |                | $\alpha$ | 1.12%        |
|                     | High-Transonic | $C_d$    | <b>0.04%</b> |
|                     |                | $\alpha$ | 1.67%        |
|                     | Subsonic       | $C_d$    | <b>1.29%</b> |
|                     |                | $\alpha$ | 2.04%        |
| Morphing            | Supersonic     | $C_d$    | <b>0.03%</b> |
|                     |                | $\alpha$ | 10.18%       |
|                     |                | $\beta$  | 20.00%/428%* |
|                     | High-Transonic | $C_d$    | <b>0.07%</b> |
|                     |                | $\alpha$ | 14.83%       |
|                     |                | $\beta$  | 53.3%/764%*  |
|                     | Subsonic       | $C_d$    | <b>0.54%</b> |
|                     |                | $\alpha$ | 16.85%       |
|                     |                | $\beta$  | 2.23%/16.54% |

Table 4.5: Performance comparison between clean and morphing airfoil optimization along the reference CGD-JFK route, for cases reported in Fig. 4.7. Reference initial drag refers to NACA2S-(40)(1.5)-(40)(1.5).

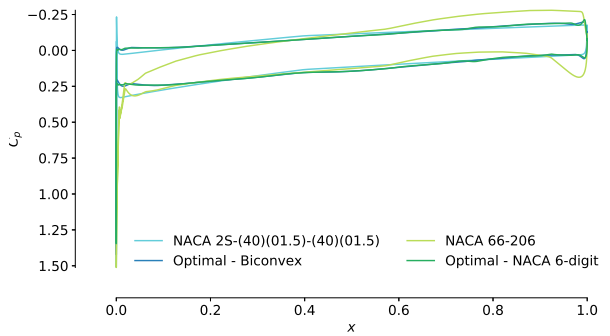
| $\Delta C_d$ | Supersonic | Transonic | Subsonic |
|--------------|------------|-----------|----------|
| Clean        | -4.1%      | -5.9%     | -21.4%   |
| Morphing     | -5.1%      | -6.7%     | -86.9%   |



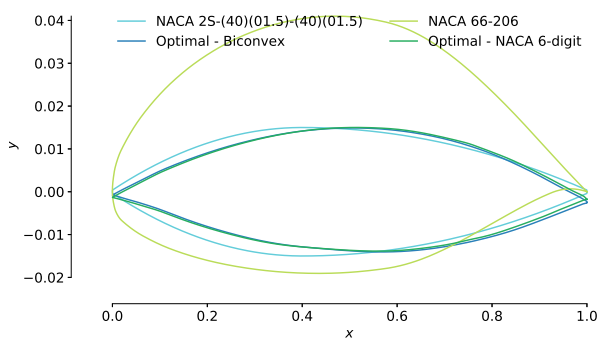
(a) Clean, optimized shape



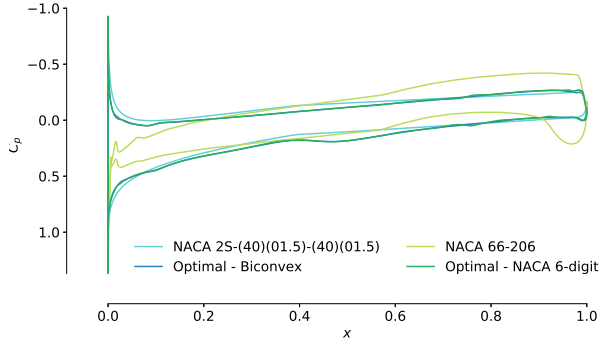
(b) Morphing - Supersonic



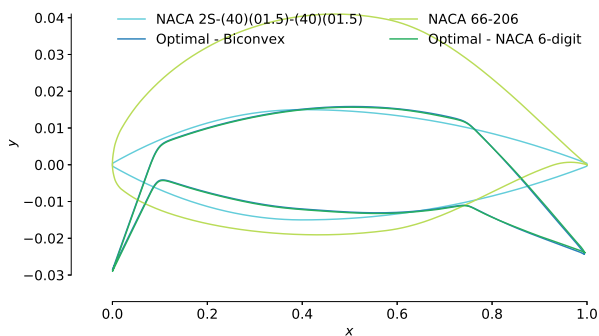
(c) Pressure distribution at supersonic regime



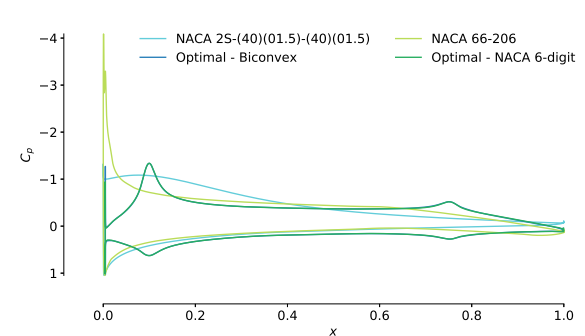
(d) Morphing - Transonic



(e) Pressure distribution at transonic regime



(f) Morphing - Subsonic



(g) Pressure distribution at subsonic regime

Figure 4.7: Shape comparison for both clean and morphing airfoil multi-point optimization starting from NACA2S-(40)(1.5)-(40)(1.5) and NACA66-206 respectively. Morphing results refer to the same optimization case and are reported in different plots for clarity purposes. Supersonic, high-transonic and subsonic conditions from Tab. 3.2 are weighted for CDG-JFK flight route.

### 4.2.3. Boom-less vs conventional transonic flight

As last 2D case study, I compare the clean shape, multi-point optimal airfoils considering high-transonic and transonic flight regime for the 10% overland flight segment respectively. Despite the minor relative weight in the optimization case, final layouts show a slight but measurable difference in shape, as reported in Fig. 4.8. While upper surfaces are overlapping, the forward shift in maximum thickness position and the rearward shift of maximum camber location lead to a different lower surface curvature. For the “conventional” ( $M_{\text{overland flight}}=0.95$ ) optimization case, the algorithm tends to minimize the supercritical flow regions over the pressure side, minimizing the wave drag. The higher freestream speed for the “boomless” ( $M_{\text{overland flight}}=1.15$ ) case implies a different optimal pressure distribution and consequently a higher curvature in the rearmost part of the lower surface.

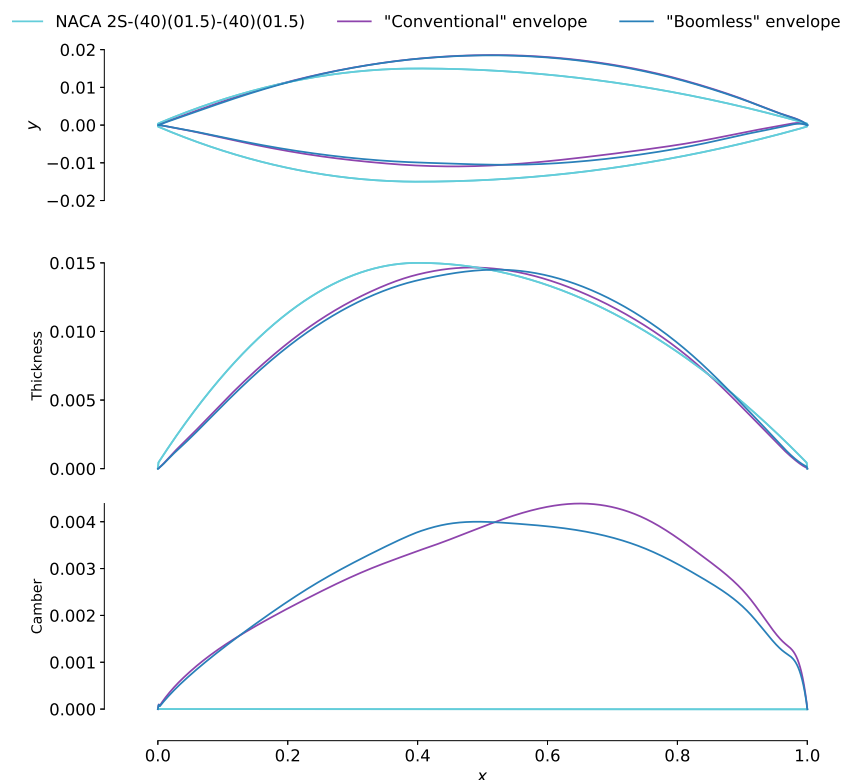


Figure 4.8: Shape comparison for two clean airfoils optimized for CDG-JFK route, considering transonic (conventional) and high-transonic (boomless) overland cruise speed respectively.

The above-mentioned shape discrepancies lead to quantifiable drag benefits, as highlighted in Tab. 4.6. I observe a better performance of the “boomless” optimal wing at supersonic and high-transonic regime, as the 95% of the objective function is related to flight regimes with  $M \geq 1$ . However, this layout has a higher drag at lower speed, with a net drag increase of 5.5% at transonic ( $M=0.95$ ) regime. Thus, the high-fidelity optimization tool demonstrates the capability to capture the complex phenomena of transonic and supersonic flows and maximize the performance with minor but essential shape adjustments.

Table 4.6: Results comparison for airfoils reported in Fig. 4.8. Optimization for CDG-JFK route, considering transonic (conventional) and high-transonic (boomless) overland cruise speed respectively. Case names refer to Tab. 3.2. Results highlighted in gray refer to flight conditions outside the specific optimization case. Drag coefficients are provided in drag counts ( $C_d \times 10^4$ ).

| $C_d$                      | Supersonic | High-Transonic | Transonic | Subsonic |
|----------------------------|------------|----------------|-----------|----------|
| NACA2S-(40)(1.5)-(40)(1.5) | 253.80     | 273.66         | 310.82    | 569.25   |
| “Conventional” optimum     | 244.23     | 260.79         | 277.57    | 434.87   |
| “Boomless” optimum         | 243.31     | 257.52         | 292.95    | 447.13   |

The performance of clean-shape optimized layouts is compared in Fig. 4.9, where I report the lift/drag polars at the different design flight conditions. Single-point optimized and both “conventional” and “boomless” multi-point, optimized shapes show comparable lift/drag profiles at supersonic regime, Fig. 4.9(a).

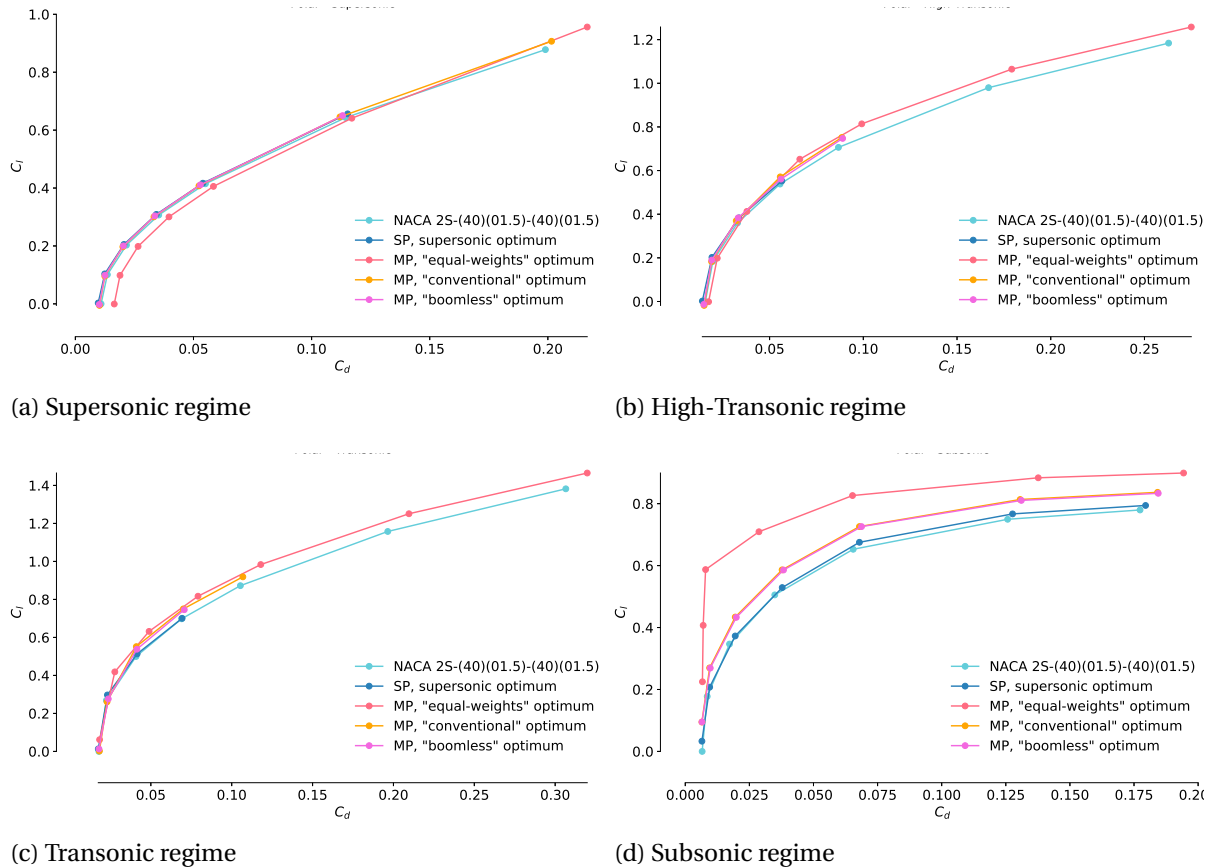


Figure 4.9:  $C_l$  vs.  $C_d$  polars for clean, optimal airfoils reported in this section. Case names refer to Tab. 3.2. Note that in the legend *SP* stays for single-point and *MP* stays for multi-point.

The airfoil optimized with equal relative weights for different flight regimes, shown in Fig. 4.6, is tagged on the legend as *MP, “equal-weights” optimum*. Its high-speed drag penalty, if compared to other optimized airfoils, is up to 34% at low angles of attack and tends to decrease

as  $\alpha$  increases, Fig. 4.9(a). The sharp leading-edge radius benefits are more relevant at low angles of attack. At  $M=1.15$ , Fig. 4.9(b), the performance discrepancy is minimal at low-lift conditions, with the “conventional” and “boomless” optimized shapes showing lower drag between  $C_l=0.2-0.4$ , in proximity of their design lift. The thick-nosed airfoil disadvantage is again minimized at high-lift conditions. In this case, other sharp-edged shapes are more likely affected by early boundary-layer separation issues due to interactions shocks interactions. At transonic and especially subsonic regime, the “equal-weights” optimized airfoil has a higher lift efficiency, as expected from optimization problem formulation. The other multi-point optimized shapes show a smaller but still consistent advantage with respect to both baseline and single-point optimized airfoil, with a maximum increase in  $C_l$  of 30% with the same  $C_d$  at  $\alpha=1.5^\circ$ .

The plots in Fig. 4.9 confirm the expected performance for the optimal airfoils that have been designed. The effectiveness of multi-point optimization strategies to capture non-intuitive design trade-offs for such unconventional optimization problems is thus further proven. The insights provided by high-fidelity optimization, of which I have hereby discussed a selection of cases, offer an unmatched advantage with respect to low-fidelity strategies in terms of design accuracy and information availability for the designer. RANS-based, CFD analysis is necessary to capture the non-linear fluid dynamics phenomena at both supersonic, transonic and subsonic regimes.



# 5

## 3D Optimization Results

Following the investigation on 2D shape optimization, I shift the focus to full-wing drag minimization problem. The additional challenges and problem formulation for this design problem have been discussed in Chap. 3. As done for the airfoil, I first investigate the performance improvements obtainable for supersonic regime-only and then extend the problem to transonic and subsonic regime. I start from a simple planar wing designed along the lines of the Aerion AS2, with a biconvex wing section and imposing the same constraints (plus an additional one on bending moment). Single-point shape and twist optimization results are illustrated and I offer a physical explanation of the optimal supersonic layout. The investigation is then extended to clean, multipoint optimization, to generate a benchmark configuration. Finally, a multi-point, morphing optimization case is presented and the performance of such configuration is compared to the clean layout. Particular emphasis is put on the analysis of spanwise lift, drag and twist profiles to better understand the fluid dynamic interactions over the wing surface.

### 5.1. Supersonic Optimization

As first design case, I perform a single-point supersonic optimization with solely twist design variables, in addition to the angle of attack. This gives the opportunity to investigate the new design variables effect and identify the best control points distribution for the optimization problem. Following that, shape variables - at the same twist control sections - are introduced to investigate the benefits of coupling local deformations and twist manipulation. Both planform and wing section pressure distributions are reported to justify a sound physical explanation of the optimal layout.

#### 5.1.1. Twist Optimization

As a rough but effective parametrization study, three different FFD grids with 4, 6, and 8 spanwise stations are investigated. Root station rotation is fixed and it is only used to fully embed the wing geometry and manipulate root airfoil geometry at a later stage. This analysis also provides the first opportunity to investigate the baseline configuration performance.

The reference wing indeed presents a lift distribution close to elliptical, given by the spanwise chord distribution of the trapezoid planform. Despite it being the ideal force distribution for minimum induced drag, the final layout presents an unexpected lift trend that diverges from baseline. Fig. 5.1(a) shows that, regardless of the selected parametrization, the optimizer increases the sectional lift close to the root section and then non-linearly decreases it along the outboard direction. Local lift values flatten in proximity of the wing tip: this behaviour, less evident on the baseline wing, is explained by the flow vorticity at the straight, large tip. A possible explanation for such unconventional lift distribution could be traced back to non-linear viscosity and compressibility effects that affect the 3-dimensional flow over the wing, urging for a more detailed investigation at a later stage.

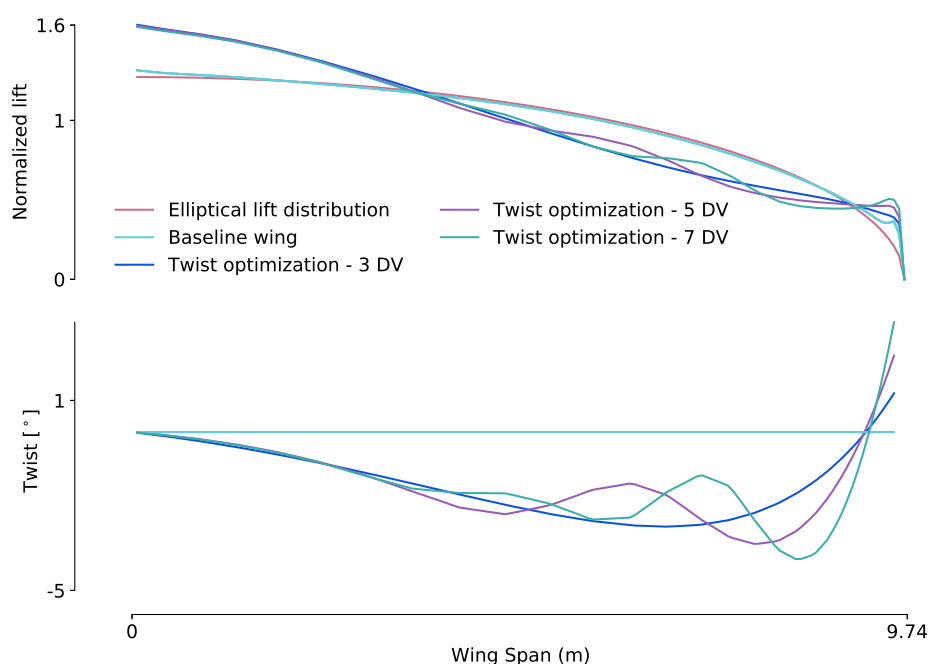


Figure 5.1: Spanwise lift and twist profiles for twist-only, supersonic optimization of a planar wing, using 3,5, and 7 twist design variables respectively. Twist sections are linearly spaced along the span.

Fig. 5.1(b) provides insights on the final wing shape, as planform and wing sections are fixed. In first place, note how the general trend is to linearly decrease the twist on the 30% innermost wing section and, conversely, to pitch up the wing in the tip proximity. This, coupled with an increase in the angle of attack, allows to match the  $C_L$  constraint while minimizing the local  $\alpha$  in the wing central section, with benefits on wave and lift-induced drag. It is also evident how an increase in uniformly-spaced twist variables reduces the wing profile smoothness, introducing an unwanted twist oscillation between 50% and 85% of the wing span. Given this concern and the minimal advantages in terms of drag when using a higher number of twist variables (Tab. 5.1), I opt to use 3 spanwise twist sections for the following optimization studies.

Table 5.1: Results for twist-only optimization of a planar wing for supersonic regime. Twist sections are linearly spaced along the span. Pitching moment constraint is active for this design problem.

| Initial $C_d$ : 207.05 |               |              |
|------------------------|---------------|--------------|
| Twist variables        | Optimum $C_d$ | $\Delta C_d$ |
| 3                      | 194.72        | -6.0%        |
| 5                      | 194.25        | -6.2%        |
| 7                      | 193.66        | -6.5%        |

It has been observed that, if unconstrained, the optimizer would increase the pitching down attitude with detrimental effects on trim drag looking at the overall aircraft design. For this reason, the imposed pitching moment constraint is active and essential for this optimization case, so to provide a feasible final layout. As reported in Tab. 5.1, despite these constraints the optimal layout shows a 6% drag decrease thanks to the sole manipulation of three twist variables.

### 5.1.2. Twist and Shape Optimization

I then increase the design case complexity by including local shape variables in the problem, increasing the DV count from 4 (3 twist +  $\alpha$ ) to 68. After a short parametrization study (omitted in this report), an 8-chordwise-stations conical distribution for each section has proven to be the most effective. The lower number of chordwise grid elements, if compared to the most refined airfoil meshes, makes any more refined parametrization counterproductive for this specific design case.

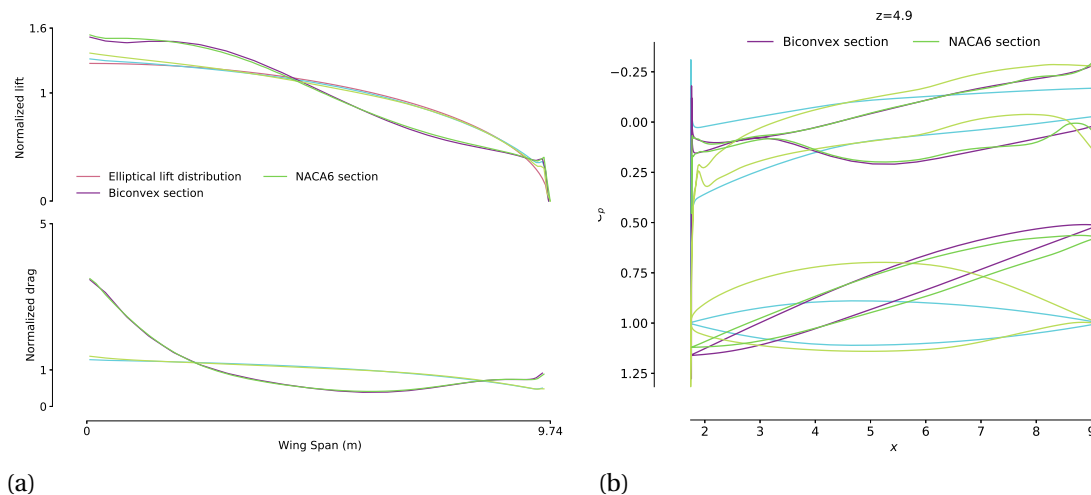


Figure 5.2: (a) Lift and drag spanwise distribution for the biconvex and NACA 66-206 testcases and (b) comparison of wing shape and pressure distribution at mid span. Despite a small geometry difference due to manipulation issues, the fluid over the wing has the same behaviour in both cases. This supports the confidence of the final design as a global optimum.

To ensure the quality of the parametrization and assess the convexity of the design space, I compare two test runs in Fig. 5.2, one with the baseline geometry and a benchmark case with the same planform, but with a NACA 66-206 section. In Fig. 5.4(a) it is highlighted how the two different cases converge to the same physical solution, with spanwise lift and drag curves consistently overlapping. As expected, also the local pressure distributions in Fig. 5.4(b) are matching. This last figure however also shows a discrepancy in the local geometry, with a small relative rotation between the two, otherwise identical, wing sections. This discrepancy appears to be compensated by a different optimal  $\alpha$ , as shown in Tab. 5.2. The  $0.7^\circ$  discrepancy apparently accounts for the different geometry; an effect that, with a smaller magnitude, has been noted in 2D cases. It is fair to assume that the limiting factor in this case is the parametrization, which could be perfected at the cost of a more refined mesh and consequent higher computational cost. However, a 0.6% difference in the final drag starting from such different layouts confirms the reliability of the optimization tool and rules out the presence of local minima in this specific design case.

Table 5.2: Drag and optimal angle of attack for two identical supersonic shape-and-twist optimization of the reference wing, one with a biconvex wing section (same case presented in Tab. 5.3) and a NACA 66-206 wing section. Results highlight how, despite parametrization-induced discrepancies compensated by a different  $\alpha_{\text{optimal}}$ , the two cases converge to approximately the same optimal design. Multimodality does not affect this specific optimization case.

| Design variables    | Initial $C_d$ | Optimum $C_d$   | $\alpha_{\text{optimal}}$ |
|---------------------|---------------|-----------------|---------------------------|
| Biconvex section    | 207.05        | 154.74 (-25.2%) | $4.75^\circ$              |
| NACA 66-206 section | 411.66        | 155.60 (-62.2%) | $4.07^\circ$              |

Engineering-relevant results for the twist and shape optimization case, focusing on the biconvex-section initial geometry, are highlighted in Fig. 5.3. Compared to the twist-only case, lift distribution shows a similar non-linear trend, with higher sectional lift between 15% and 60% of the span and, conversely, lower lift close to the root and the tip. Twist distribution has a parabolic trend, with a minimum of  $5^\circ$  close to the 50% of the wing span. Fig. 5.3(b) provides better insight on how the optimizer minimizes the overall drag. The algorithm accepts a higher drag penalty at the tip and especially root section, where the combination of local twist and angle of attack is likely to increase the drag due to shock-waves. At the same time, the central, twisted-down section of the wing presents a local drag reduction with respect to both baseline and twist-optimized wing.

The performance of the this central wing section outcores the drag increase at root and tip spanwise and ultimately lead to a more efficient wing. The benefits of simultaneous manipulation of shape and twist are evident from results in Tab. 5.3. Compared to the reference planar wing, our novel supersonic wing layout shows a 25% drag decrease. Such a high drag reduction, if compared to more conventional optimization studies, is definitely magnified by the sub-optimal performance of the simple wing geometry I chose as reference. Nevertheless, the optimal layout sets an upper limit in drag reduction for further full-configuration or aerostructural studies. Possible concerns are given by the reduced optimized wing off-design performance, addressed later in this section, and design feasibility in terms of structure and manufacturing. Although the optimal wing lift distribution reduces

the bending moment at the root, the structural feasibility of such a twisted wing needs to be addressed by further investigations. However, the constraints I impose demonstrated their effectiveness and marginal effect on computational cost. If necessary, the robust and flexible optimization tool can be efficiently used to investigate more tightly constrained design problems.

Table 5.3: Results comparison between twist-only optimization and twist-and-shape single point, supersonic wing optimization case. As for previous case, pitching moment constraint is active.

| Initial $C_d$ : 207.05 |               |              |          |
|------------------------|---------------|--------------|----------|
| Design variables       | Optimum $C_d$ | $\Delta C_d$ | $\alpha$ |
| Twist-only             | 194.72        | -6.0%        | 4.42°    |
| Twist + Shape          | 154.74        | -25.2%       | 4.75°    |

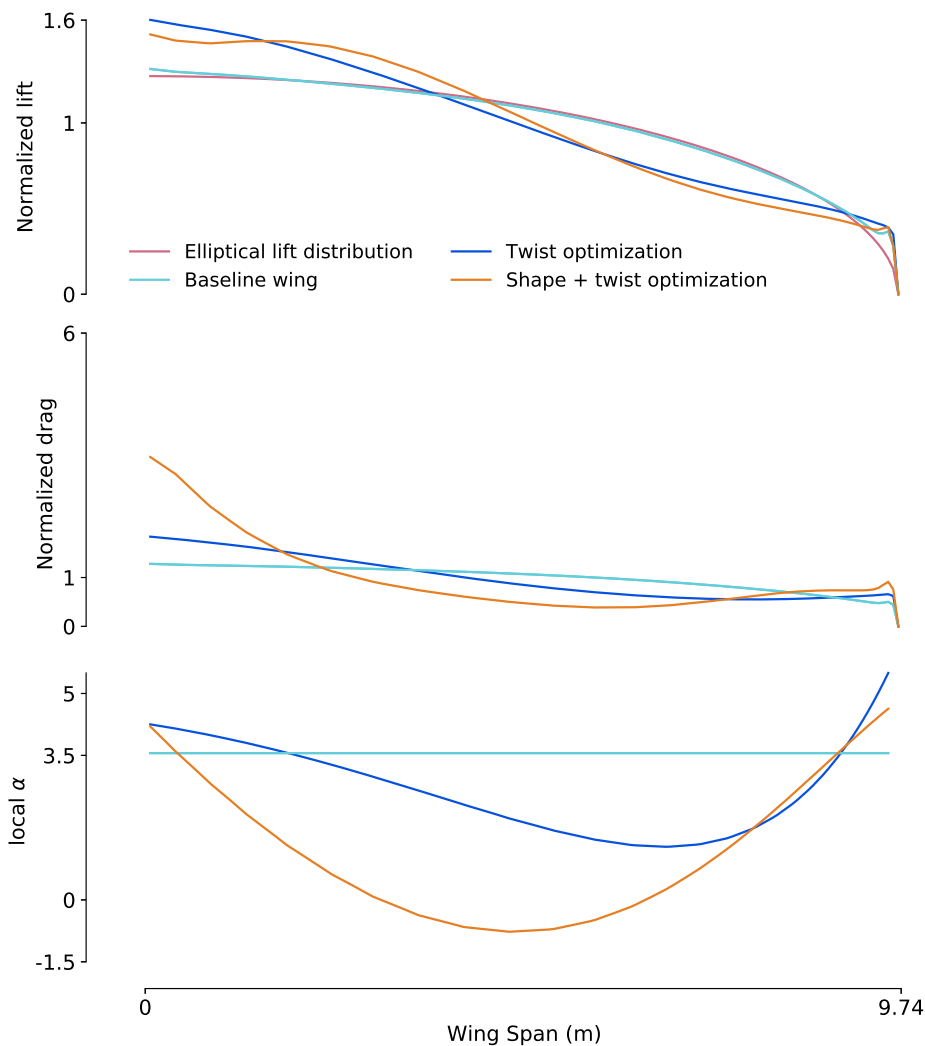


Figure 5.3: Spanwise lift, drag and twist distributions for twist-only and twist+shape single point, supersonic wing optimization case.

Looking at the optimal configurations more in detail, some hints offer an interpretation for such high drag reduction for the shape and twist optimization case. In Fig. 5.4, four different wing sections are compared. It emerges how, while the twist-only optimization case shows a pretty uniform and well-known linear  $C_p$  distribution over the entire wingspan, as typical for biconvex sections. When the optimizer is allowed to manipulate the shape however, pressures substantially vary at different span locations. Close to the root, a flat-top, negatively cambered airfoil induces a strong lift force in the fore section of the wing. Conversely, at approximately mid span, Fig. 5.4(c), the front part of the wing generates virtually no lift as there is no pressure difference, while the rear section has a higher pressure difference than on the baseline shape. This suggests that at mid-span the leading edge shockwave is much weaker than baseline as the airfoil is locally aligned with the flow (as highlighted by the small acceleration due to the curvature).

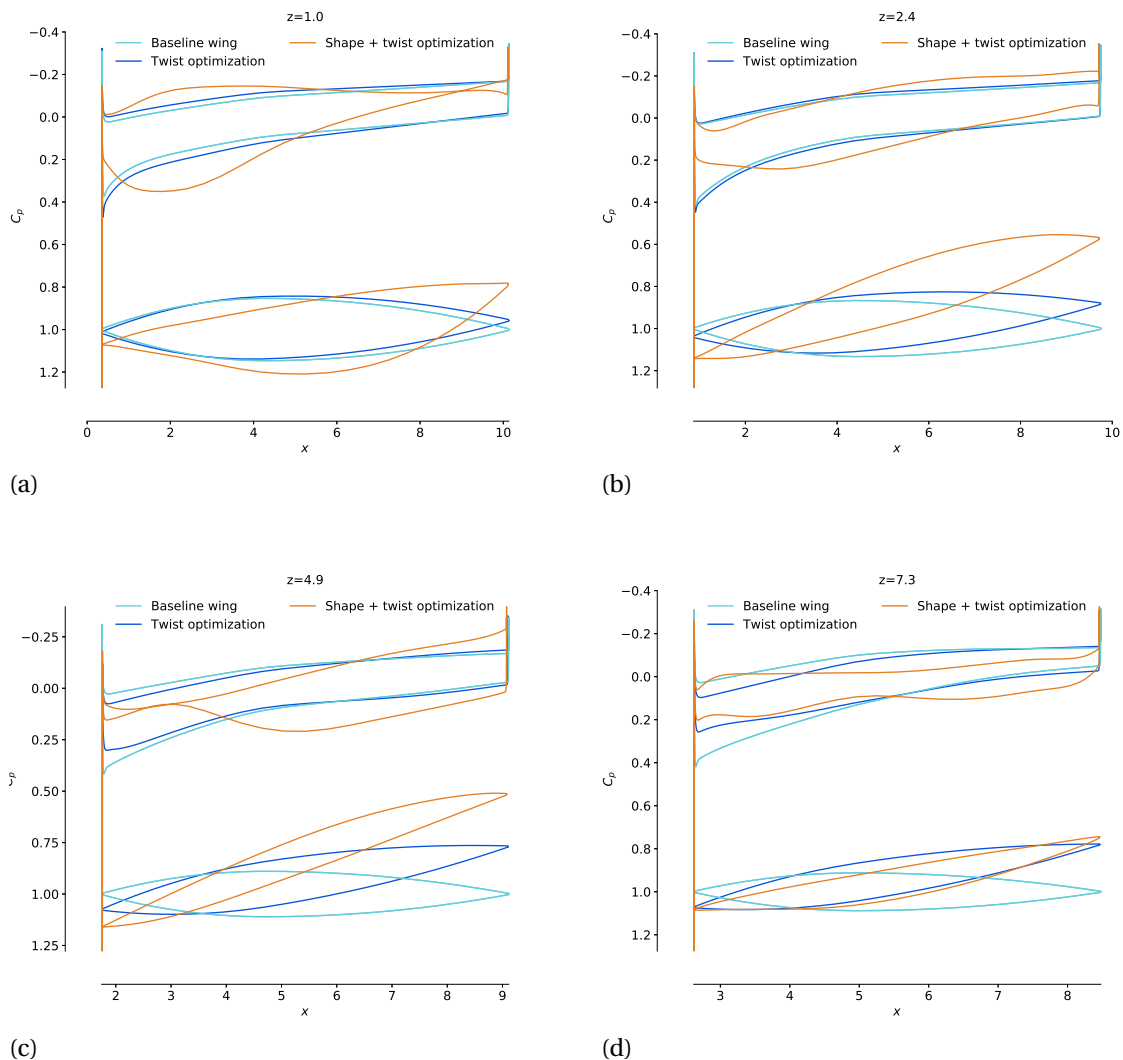


Figure 5.4: Local wing section and supersonic pressure distribution comparison between baseline, twist-only, and twist+shape optimized wing. Sections reported are highlighted in Fig. 5.5

Also, despite the higher twist,  $C_p$  magnitude is comparable with biconvex airfoils from twist-only case. At wing tip, the flat-top section has a virtually circular-arc pressure side and the twist is close to the twist-only benchmark, suggesting that airfoil shape itself has a minimal influence on tip vortex.

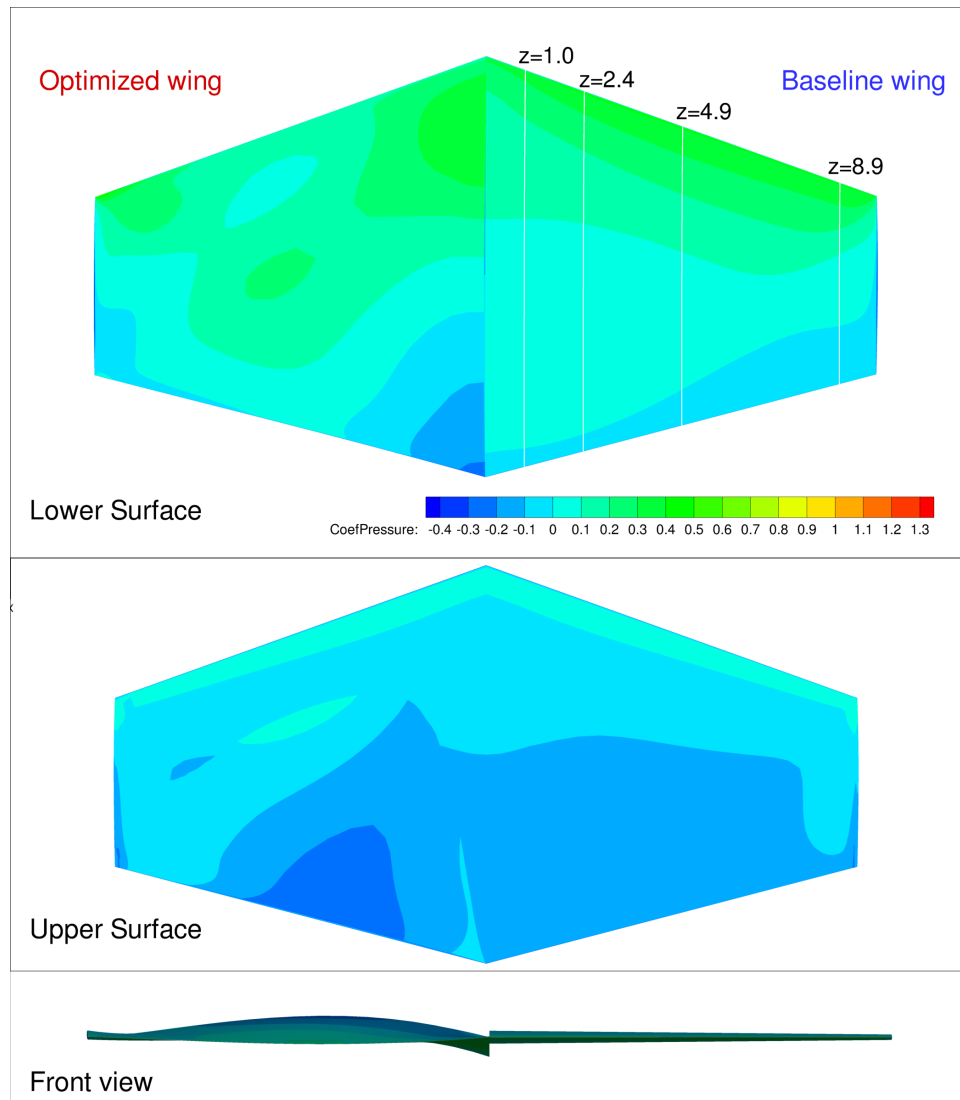


Figure 5.5: Pressure distribution comparison between baseline and twist+shape optimized wing at reference supersonic regime.

Ultimately, a glimpse at the pressure distribution over the entire wing surface as shown in Fig. 5.5 suggest a physical explanation for the unconventional supersonic lift distribution observed so far. Thanks to the experience of Prof. Philip Roe, who kindly offered his help to interpret these results, I noted how the rise in pressure generated at the wing root has a predominant influence on the rest of the wing. As summarized in Sec. 1.1, at supersonic regime the influence of pressure disturbances propagates only inside the so-called Mach cone. As the reference planform has a low aspect ratio, the cone of influence stemming from wing root - which has a nose Mach angle of 43.5% according to  $\beta = \sin^{-1}(1/M)$  - hits most of the wing lower surface. Top plot in Fig. 5.5 confirms this phenomena, looking at the “diagonal”

high pressure area on the optimal wing on the top left. This phenomena has been defined by Prof. Roe himself and other sources [189] as interference lift, as equivalent to the more commonly observed interference drag. The high pressure zone induced by the root, which is magnified by local shape and high angle of attack, despite the local drag penalty has beneficial effects on the overall performance: the central sections of the wing receive some kind of “drag-free lift” as a consequence of the overpressure coming from the root. The sections are locally aligned with the flow because they do not need to generate additional pressure difference, minimizing both wave and lift-induced drag. This concept has been also explored on full-configuration scale, taking advantage of the engine nacelles position and shape, by the so called “*waverider*” aircraft such as the XB-70 Valkyrie and, less markedly, by the Concorde itself.

## 5.2. Multipoint Optimization

Finally, I present the last and most complex optimization problems of this study. I perform a multi-point wing optimization for supersonic, transonic and subsonic regime, first on the clean layout and then including the morphing capabilities of which we highlighted the benefits for 2D optimization cases. Geometry constraints are the same we enforced for the single-point case; for lower-speed regimes, pitching and bending moment constraints lower and upper value respectively are set to match baseline wing values. The relative weights of flight conditions in the optimization refer to the previously discussed CDG-JFK route, with “conventional” overland transonic flight.

### 5.2.1. Clean wing

The clean layout section in this context is principally used as a benchmark, as 2D studies suggest the strong benefits of morphing capabilities for this aircraft configuration. Given the weight of supersonic flight segment, the supersonic performance of this multi-point optimized layout is just 5 drag counts (3.2%) higher than the single-point optimum, as highlighted in Tab. 5.4. Transonic performance, probably due to the twist distribution previously discussed, has the higher improvement, with a 32% drag decrease. Subsonic performance however, as expected from 2D studies, has minimum benefits in this optimization case.

Table 5.4: Performance improvement of a multi-point optimized reference wing, highlighting drag reduction and final angle of attack for supersonic, transonic, and subsonic regime.

| Design variables | Initial $C_d$ | Optimum $C_d$ | $\Delta C_d$ | $\alpha_{\text{optimal}}$ |
|------------------|---------------|---------------|--------------|---------------------------|
| Supersonic       | 207.05        | 159.67        | -22.9%       | 5.31°                     |
| Transonic        | 207.44        | 141.04        | -32.0%       | 6.04°                     |
| Subsonic         | 305.09        | 290.39        | -4.8%        | 8.97°                     |

Fig. 5.6 highlights how the supersonic lift distribution is close to the “bell-shaped” trend reported and discussed in Sec. 5.1.2, while both transonic and subsonic lift distributions are

very close to the elliptical distribution reference. A strong tip vortex is indicated by the sharp lift and drag increase in that span section.

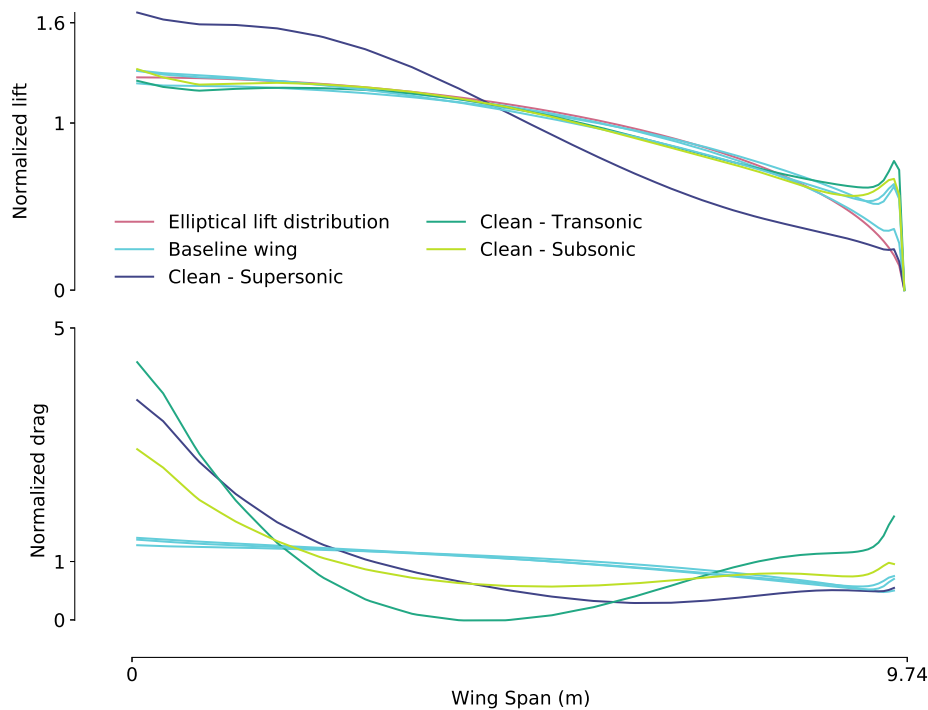


Figure 5.6: Spanwise, lift and drag distribution for clean, optimized wing at supersonic, transonic, and subsonic regime; objective function is weighted according to the reference Paris-New York route. Elliptical lift distribution is reported as a reference.

The drag reduction at mid span already observed at supersonic regimes in Sec. 5.1.2 is present in this layout as well: moreover, this trend is even more relevant at transonic regime, coherently with the data reported in Tab. 5.4. The combination of twist and shape modifications for supersonic speed are apparently highly beneficial (remember that transonic regime has a 10% weight in this optimization runs) for this flight conditions although the physical explanation provided in previous section is no longer valid, as the flow under the wing is subsonic. The higher-than-usual and non-linear twist, combined with the wing section curvature, apparently minimizes both pressure drag ( $\alpha$  is similar in the two cases, so the the airfoil nose is aligned to the incoming flow) and lift-induced drag - considering the forward pitching resultant vectors over the aft section. It is expected that the introduction of morphing capabilities extremises this behaviour while consistently improving subsonic performance, as for the airfoil test cases.

### 5.2.2. Morphing wing

Finally, the 6 additional  $\beta$  variables are included in the problem and the optimization is run again with the same objective function and boundary conditions. Lift, drag and twist distribution for multi-point optimized wing are compared to single-point supersonic drag-minimization results in Fig. 5.7. For supersonic regime, lift and drag distributions of the

two optimization cases have comparable trend: however, morphing optimum show a 5% force increase at the inboard section and an average 14% decrease at the tip. As for twist, which is fixed for the different design cases (the vertical displacement in Fig. 5.7 bottom plot is given by edges deflection), it appears to be more negative by 0.5–0.8% in the wing outboard half. At lower speed regimes, the optimizer maintains the lift distribution close to the elliptical reference, with the exception of the already mentioned tip vortex influence on the outermost 10% of the span.

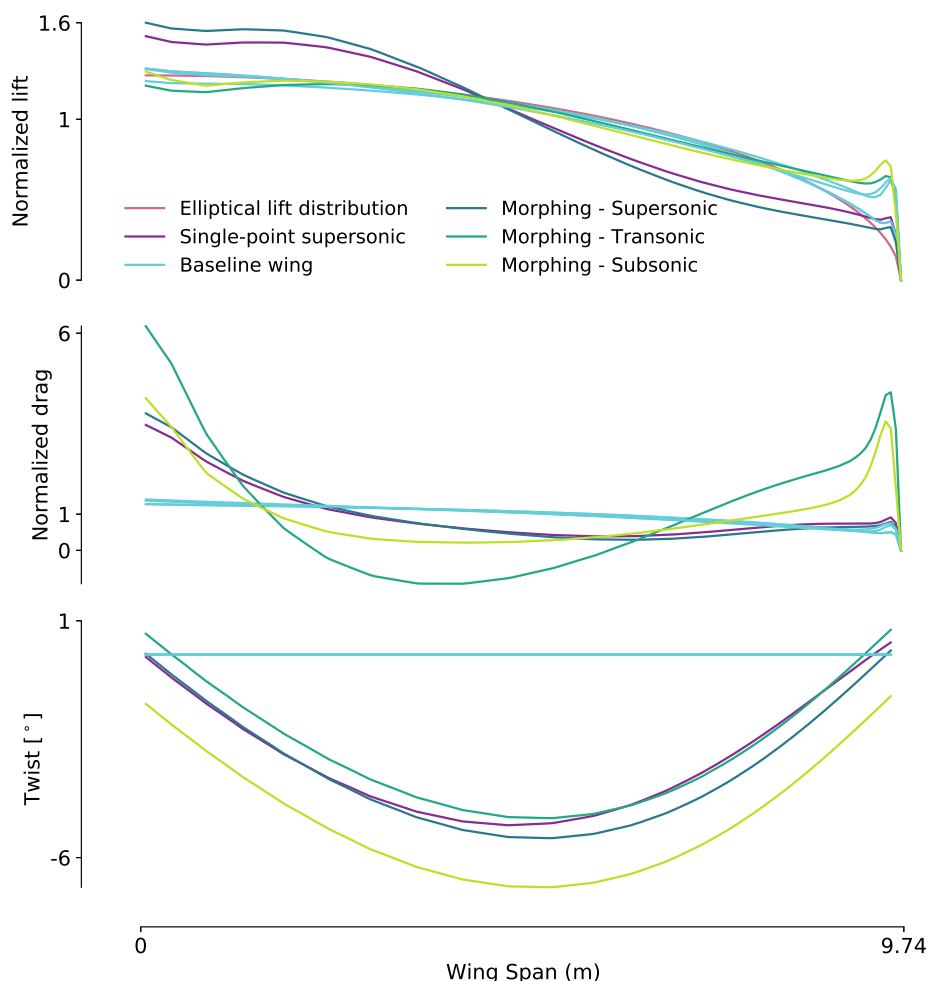


Figure 5.7: Spanwise lift, drag and twist distributions for multi-point morphing wing optimization. Objective function is weighted according to the reference Paris–New York flight route, with conventional transonic overland flight.

Drag, following a similar pattern to the one observed for both single-point and clean multi-point optimization, is higher at the wing root and the tip, with the tip vortex having an influence on the outboard wing area at subsonic and especially transonic regime. The drag distribution observed at transonic speed is highly non-linear, with a 4.4-times higher than reference drag at root-section compensated by a drag reduction in the central section. The performance of this particular configuration, characterized by the combination of high local downward twist and trailing edge downward deflection, is consistent with clean optimal layout but requires further investigation and should be evaluated into a broader optimization

study. However, for the specific wing planform and cruise conditions I am investigating, the drag minimization at supersonic regime is outscored by the improvements at subsonic and transonic speed when morphing capabilities are enabled, as reported in Tab. 5.5. This, considering the biconvex wing section I selected for the baseline airfoil, is in line with NACA2S-(40)(1.5)-(40)(1.5) 2D morphing optimization cases I discussed earlier in this section.

Table 5.5: Drag, angle of attack and edge deflection for multi-point wing optimization with morphing capabilities - same test case reported in Fig. 5.7.

| Flight condition | Initial $C_d$ | Optimum $C_d$ | $\Delta C_d$ | $\alpha$ | $\beta_{LE}$ | $\beta_{TE}$ |
|------------------|---------------|---------------|--------------|----------|--------------|--------------|
| Supersonic       | 207.05        | 156.29        | -24.5%       | 4.89°    | -0.65°       | -0.04°       |
| Transonic        | 207.45        | 53.30         | -74.3%       | 4.30°    | 1.18°        | -3.11°       |
| Subsonic         | 305.09        | 87.97         | -71.2%       | 8.37°    | 16.12°       | -0.56°       |

As it is illustrated in Fig. 5.8, while the drag reduction at supersonic speed is increased by 1.6%, the benefits at lower speed are much higher, with a 42.3% additional improvement at supersonic speed and a shift from the relatively small 4.8% drag benefit on the clean wing up to a 71.2% drag reduction when the leading and trailing edge are allowed to deflect. Comparisons in Fig. 5.9- 5.10 offer additional insights on the optimal layout performance.



Figure 5.8: Comparison between clean and morphing wing drag improvement at different flight conditions for the test cases reported in Fig. 5.6 and Fig. 5.7.

As expected from the overall performance data and the previous airfoil optimization studies, the lift and drag distribution at supersonic regime are not revolutionised by the introduction of edges deflection. Morphing wing shows a 3% lower lift at the root and a 34% higher at the tip (but still small and almost negligible in absolute values). This most likely affects drag distribution by consistently reducing inboard drag and locally increasing the drag at the tip by 44%. Transonic performance is characterized by a even higher drag reduction, by almost 99% for clean wing and 180% for morphing layout at 40% of the span. Indeed drag is negative in this section, a peculiar phenomena that however is consistent with physics and wing design considering the entire configuration analysed. With deflected edges however, the drag at the root and tip is increased by 40% and 146% respectively if compared to clean optimum. Subsonic drag distribution has an even more marked increase at root and tip with respect to benchmark, with an U-shaped profile that however compensates this poorer local performance with much more extensive drag reduction from approximately 15% to 75% of the wing.

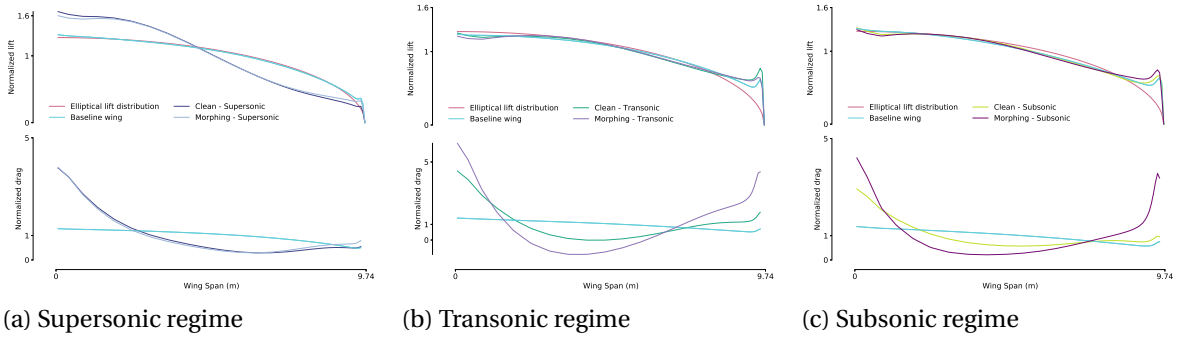


Figure 5.9: Spanwise, lift and drag distribution comparison between clean, optimized wing and morphing optimized wing at reference supersonic, transonic, and subsonic cruise conditions.

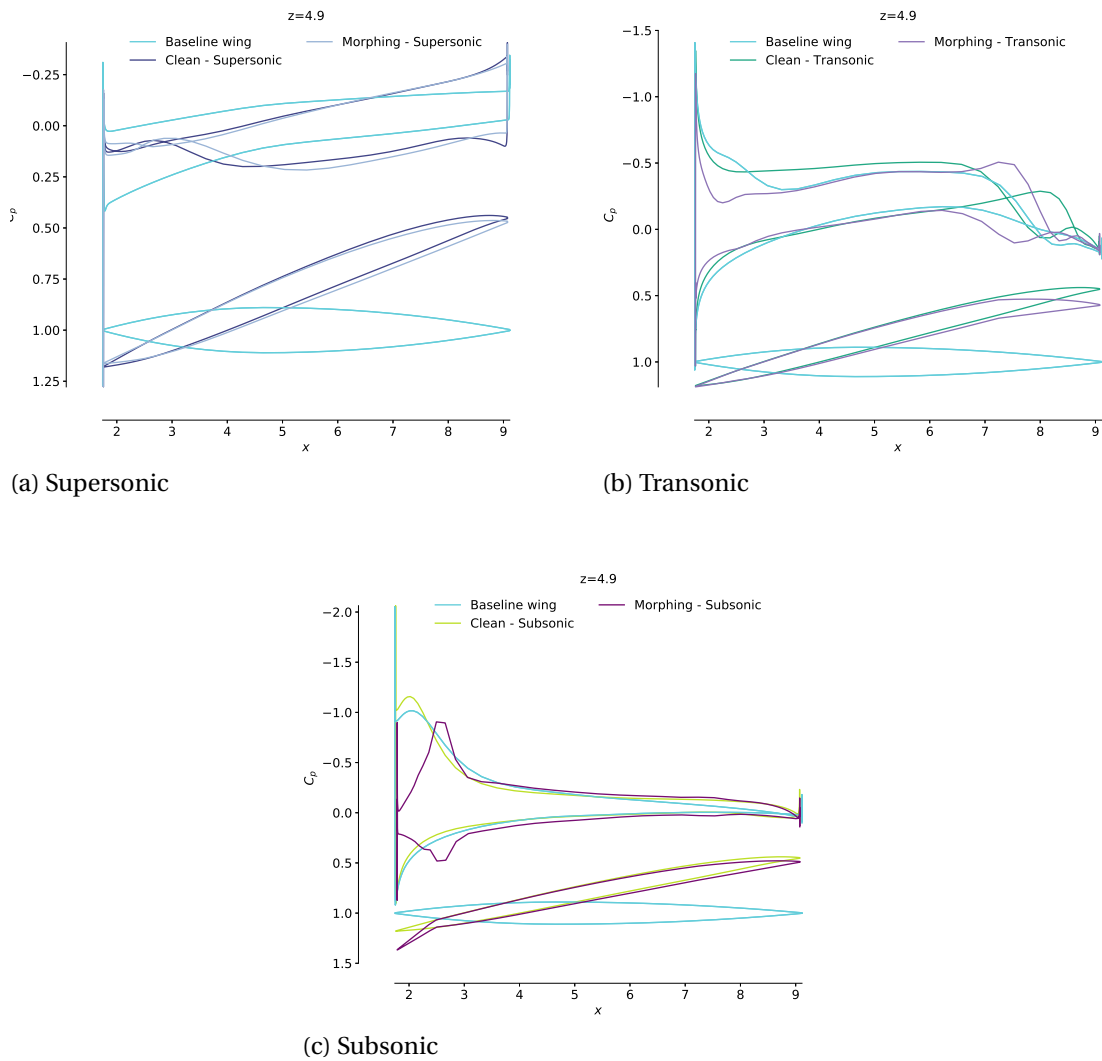


Figure 5.10: Local, mid-span wing section and pressure distribution comparison between clean optimized wing and morphing optimized wing at reference cruise conditions.

A snapshot of the wing section and corresponding pressure distribution at mid span, as reported in Fig. 5.10, further help to understand the design choices made by the optimizer. While at supersonic speed there are not any measurable differences, at transonic regime it is observed how the crucial difference is given by the trailing edge deflection. Conversely, at subsonic speed (and higher angle of attack, as Tab. 5.5), the drag reduction is obtained with the downward deflection of the leading edge. As initial result suggested, wing sections shape does not markedly differ between clean and morphing optimal shapes: the better performance is given in greatest part by the solely morphing capabilities in this specific design problem.

The advantages that come from using morphing edges are further illustrated in Fig. 5.11. At supersonic regime, single-point and multi-point optimized wing lift vs. drag polar are well-matching. At transonic regime however, Fig. 5.11(b), the morphing design shows drag advantage up to 70% at  $C_L=0.17$ . Such an efficiency increase confirms the expectations for this study, as we aim to minimize the drag penalty of a supersonic aircraft when flying at lower design speeds. At subsonic regime, the high edge deflection (see Tab. 5.5) provides an odd  $C_L/C_D$  curve. However, wing clearly benefits from edges deflection at positive lift conditions.

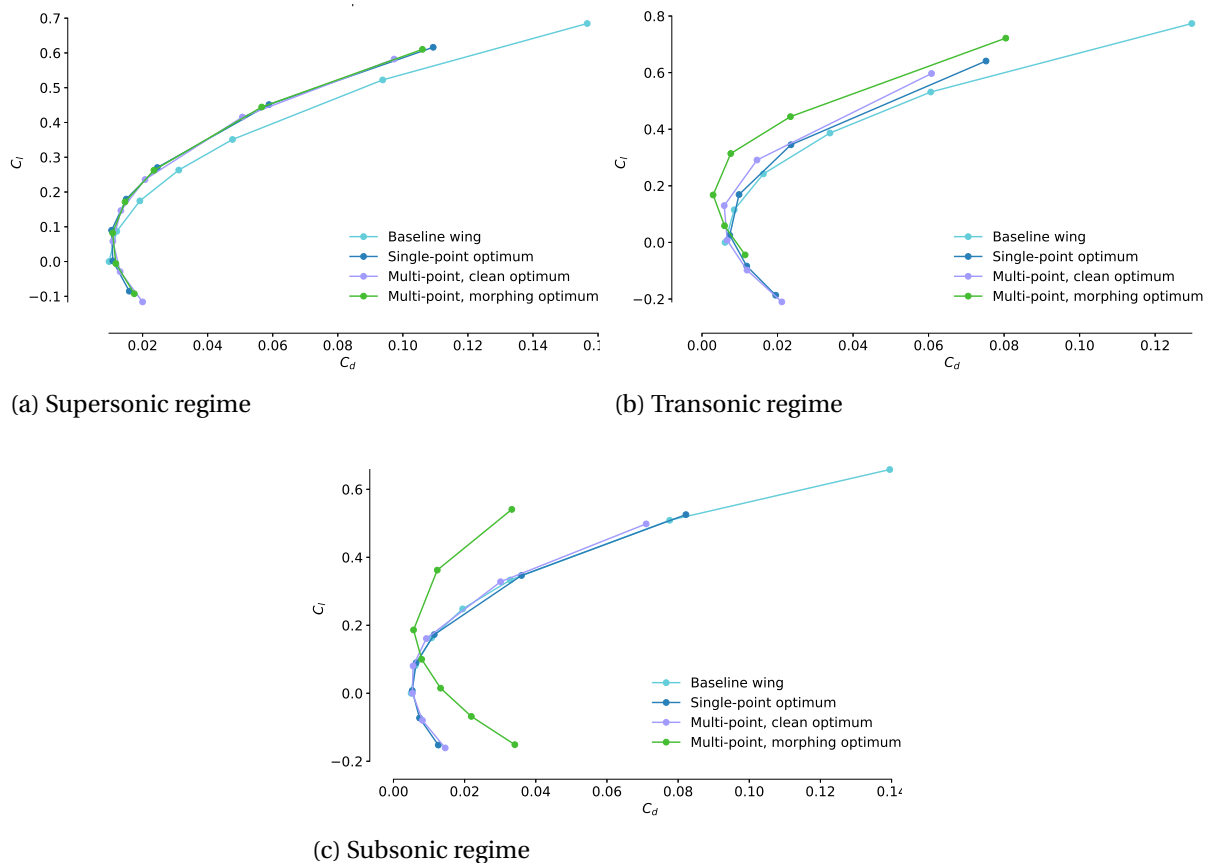


Figure 5.11:  $C_l$  vs.  $C_d$  polars for single-point and multi-point optimized wings. Edges deflection for multi-point, morphing layout is kept fixed to cruise-optimized values reported in Tab. 5.3. Flight conditions refer to Tab. 3.2.

I observe that the negative twist and edges deflection of both wing design induces a negative  $C_L$  at low angles of attack. Such issue could be however overcome by assuming a positive wing mounting angle on the fuselage. This would further ensure that design lift is achieved at a smaller angle of attack (considering the fuselage system of reference) with respect to the wing-only values, minimizing lift-induced fuselage drag. In last instance, I restate that  $\beta_{LE}$  and  $\beta_{TE}$  have been kept constant during the  $\alpha$  sweep report in Fig. 5.11. Allowing the edges to adapt to specific angles of attack by performing an optimization sub-routine could bring further benefits to wing performance.

Results hereby presented prove that the observations and trends discussed for the airfoil optimization studies reported in Chap. 4 are consistent with 3D optimization results; moreover, additional fluid dynamics effect such as the *interference lift* at supersonic speed and local negative drag areas at subsonic regimes further magnify the benefits showed by 2D cases. Although there is room for improvement in terms of results analysis, more specific case study comparison and ultimately a broader (and possibly multidisciplinary) design optimization problem, the effectiveness and flexibility of the optimization framework, together with the unprecedented insight in such novel optimized layouts, ultimately prove the necessity of high-fidelity, gradient-based optimization strategies for ASO and MDO of SST configurations.

# 6

## Conclusions

In this report I present a selection of aerodynamic shape optimization studies for supersonic aircraft, considering both supersonic, transonic and subsonic conditions. The overview on historical background highlights a gap in literature on state-of-the-art gradient-based, high-fidelity optimization for this design case. To address this issue, I use University of Michigan's *MACH* framework to minimize the drag of airfoil and wings at a range of high and low speed flight conditions, while subject to lift, pitching and bending moment, and geometry constraints.

Concerning airfoil optimization, I investigate the influence of both control points distribution, freestream conditions, and design lift coefficient on the final shape for supersonic optimization. I improve the performance of a typical biconvex airfoil by 5.5%, enforcing both geometry, lift and pitching moment constraints. I then present a selection of multi-point optimization studies aimed at minimizing the drag penalty at lower speeds without compromising supersonic performance. I am able to improve the same reference airfoil performance at supersonic, transonic, and subsonic speed by 5.1%, 6.7% and 86.9% respectively. It is also demonstrated how deflecting edges allow to relax the trade-offs between different flight conditions, with higher benefits at all flight regimes. Results moreover support the unimodality hypothesis for this optimization problem.

Shifting the focus on full-wing optimization, I take as reference a planar, trapezoid-planform wing and investigate how twist and shape modifications affect drag at supersonic regime. The solely twist manipulation allows a drag reduction by 6%, which raises to 25% when shape variables are included. Lift distribution follows an unconventional, non-elliptical trend that, for this specific case, is beneficial to wave and lift-induced drag reduction. Finally, I perform a multi-point shape optimization on the same wing, also including leading and trailing edge deflections among the design variables. It is shown how supersonic performance matches with good approximation the results for single-point cases, while the  $C_D$  for subsonic and supersonic speed is reduced by 74.3% and 71.2% respectively. The designed morphing wing matches or outperforms the reference and optimal supersonic wing at design flight conditions over a  $\alpha=0^\circ-12^\circ$  interval, without even optimizing the edges deflection over the angle of attack sweep.

The case studies hereby illustrated mark a step forward in terms of accuracy and manipula-

tion capabilities of the optimization framework, with respect to what has been made publicly available in recent years. The results I discuss provide a qualitative and quantitative insight on the numerical and physical factors that affect the optimization routine. Ultimately, the outcome of this work supports the necessity to use high-fidelity, RANS-based frameworks to perform supersonic and subsonic multi-point optimization, so efficiently capture trade-offs for different flight regimes while taking into account non-linear effects due viscosity and compressibility.

## Answering the Research Questions

To wrap up the key points of this broad investigation, the fundamental research questions presented in Sec. 1.4 are shortly answered below:

1. *What are the main bottlenecks in the optimization workflow? What are the potential weaknesses of the different modules and how can they be addressed?*

This specific question has been tackled mostly behind the scenes, tuning and fixing the framework streamline while troubleshooting the test runs. Collecting the sparse observations reported in previous chapters, the main issues came from CFD solver convergence and optimizer set-up. The tool is intuitive and well-documented, so the base cases run smoothly. However, the specific design case presented by SST mission profile forced to extensive testing for the best settings in terms of robustness and computational cost. A more specific scheme to capture shockwaves and shockwave-boundary layer interaction could be useful, but not necessary, as this work proves. In terms of optimizer settings, SNOPT has proven to be effective and efficient. However, a trade-off between robustness and explorative capabilities (at least in the first optimization steps) has to be made to avoid to get *MACH* stuck in some odd shapes evaluations. The geometry and mesh manipulation modules work fine with minor adjustments. On a personal note, the necessity of generating high-quality 3D meshes on ICEM rapidly becomes an excessively time consuming task: this is not however directly related to optimization framework performance. More detailed notes are reported in Appx. D.4.

2. *How can Free-Form Deformation scheme be tailored to the specific problem, to improve the optimizer manipulation capabilities and at the same time ensure the optimization framework robustness?*

The effect of parametrization on the optimization routine has been addressed at different stages of this study, with specific observations in Sec. 4.1.3 and Sec. 5.1.1. A wider number of testcases has been evaluated during the setting and tuning of the optimization framework. It turns out that FFD scheme is consistently flexible and efficient for the cases investigated, as discussed in Sec. 2.1. For wing section manipulation, a compromise has been found in terms of accuracy and computational cost, as an excessively high number of design variables may lead the optimizer itself to stall. For the meshes used in this study, 16 chordwise stations have the best performance for airfoil optimization, while for wings 8 stations are sufficient to address any multimodality issue and minimize numerical discrepancies. Using non-uniform chordwise point distribution improves the tool manipulation capabilities, specifically at leading and trailing edges, without the increase in computational cost typical for

denser parametrization grids. Along the span, 4 uniformly-spaced stations (including the root) are enough for the selected low-aspect ratio planform.

3. *How do different boundary conditions, constraints and morphing capabilities affect the optimized airfoil and wing, and what is the justification from a physical and numerical perspective?*

This question is the core of the result analysis in both Chap. 4 and 5. To sum up, different flight conditions influence the layout inducing some specific airfoil traits for supersonic, transonic, and subsonic conditions (Sec. 4.2.1). It has been shown that even if theoretical models for supersonic aerodynamics are relatively accurate, RANS CFD is crucial to capture non-linear effects (ex.Sec. 4.1.2) at higher speeds and minimize optimal shape drag. This is also valid when subsonic regimes are considered (Sec. 4.2.3). For wing design, the optimizer explorative capabilities are fundamental to fill the gaps in the designer intuition for such an unconventional case study. Since the early, twist-only optimization cases, it is evident how the algorithm takes advantage of compressible-flow, three-dimensional phenomena to minimize wave and lift-induced drag at supersonic regime - Sec. 5.1.1- 5.1.2. The role of *interference lift* is predominant on such a low-aspect ratio wing at high speed. Twist and shape combined effect is key to exploit this feature. At lower speeds, although the smaller relative weights in the objective functions, lift distributions show a more conventional, elliptical behaviour, with the presence of a stronger tip vortex. For both 2D and 3D cases, the implementation of morphing capabilities leads to drastic drag reduction. Edges deflection apparently allow to decouple the different design cases. The predominant and more “sensitive” to flow disruptions supersonic case rules the clean shape manipulation. Leading and trailing edge deflection, used to align the nose to the incoming wing or altering pressure distributions on the wing aft section, can decrease drag by more than 70% in the presented cases. The capability to modify part of the wing section camber at different flight regimes thus offers substantial benefits for SST wing design. Constraints, as expected, play a key role in design space definition. From a geometrical point of view, the volume (and cross-sectional area, for airfoils) constraint is dominant, while thickness constraint only minimize the risk of incurring into odd, unfeasible shapes during the optimization run. While the effect of lift constraint has been specifically investigated, pitching moment constraint has a less evident impact. For airfoil optimization, it only activates for some of the most extremely deflected morphing case, while clean and high-speed airfoils show small  $C_{m_z}$  variations. For 3D wing cases, as discussed in Sec. 5.1.1, the constraint is always active and limits the downward twist of the mid-wing sections. Finally, bending moment constraint has a marginal role in the cases investigated, as at supersonic speed the lift is shifted inboard while there are minimum lift distribution variations at lower speed regimes. Ultimately, there are no evident numerical or algorithmic issues that limit the design space or prevent the optimizer to obtain further performance increases for the cases I investigated.

4. *What design-specific conclusions can be drawn from this study, in particular for the full wing case?*

Design observations are partially addressed in the previous question. To give few hints for future SST design, the work shows that a compromise for high and low speed performance for airfoils and wings by manipulating the baseline shape is possible.

Adding morphing edges to the design, in the form of gap-less flaps, allows to minimize drag at higher and especially lower speeds, with final layouts outperforming clean benchmark cases throughout the entire flight envelope. The current study does not take into account the added weight or complexity of the mechanism; however, results suggest that this specific design solution should be carefully considered even at conceptual design stage due to the radical effect on aircraft performance. Considering the sole airfoil optimization, RANS-based tools show how the conventional biconvex shape can be improved for specific flight speed and design lift coefficient. This becomes more evident for 3D cases where more complex non-linear effects can be exploited: results shown in Chap. 5 show how the optimal wing section can differ from standard design choices for SST wing. Looking at wing optimization for low-aspect-ratio planforms in particular, *interference lift* has strong beneficial effects on the layout performance and should be exploited when such low-aspect-ratio wings are selected. It is expected that full-configuration optimization could take advantage of fuselage and engine nacelles to further benefit of this phenomenon at supersonic speed.

## 6.1. Limitations and Recommendations for Future Research

Observations on the limitations of the specific tool modules and case studies have been discussed throughout the report and partially summed up in the first research question (Sec. 6). Considering first the scope of this research, the fundamental engineering limitation is given by the focus on the solely aerodynamic performance. The analysis hereby presented has indeed to be considered as a first step of a broader multidisciplinary investigation that (hopefully) will be carried out in the future. Narrowing the focus down to a single discipline, however, has allowed to focus on specific details that would have been otherwise overlooked in a more complex system optimization. The absence of a structural analysis module has been compensated by tuning the geometry and performance constraints. However, for more robust and realistic layouts, a FEM module should be included to address structural issues and wing box analysis. Such MDO problem could also shift the objective function from the current drag minimization to more industry-relevant objectives, such as fuel consumption minimization or mission range maximization.

Considering the state-of-the-art ASO tool, the efficient implementation of CFD software into a gradient-based optimization framework has provided unprecedented insight on the optimal design. However, some intrinsic limitation of RANS tool, including lift and drag prediction at high angles of attack and the limitation of the adjoint method to a single turbulence model, partially limit the physical accuracy of the investigation. The FFD framework has proven to be flexible and efficient, but however is not able to alter the initial topology. The optimization, for example, of multiple-element wing sections requires an additional effort and it has not recently been applied to full-wing cases with *MACH*. Finally, more efficient optimization strategies including multiple sources of information and different level of fidelity, if efficiently implemented, could further reduce computational cost without compromising the accuracy provided by high-fidelity tools.

With the same approach applied for this research, and with the possible inclusion of struc-

tural models and other sub-systems in the loop, an extension of the study could be implemented relatively straight-forward. Including different wing planforms, additional design variables, and a wider range of flight regimes could further extend the breadth of the observations discussed in this report. A full-configuration optimization is the ultimate goal of this design approach and the fundamental reason why *MACH* framework has been developed in the last years. In this case, some of the “pseudo” constraints (bending moment, pitching moment, fixed internal volume) could be replaced or eliminated as the entire aircraft performance, and not just a component, is taken into account. As a side note, for specific SST design, it would be also interesting to implement a sonic-boom analysis module in the gradient-based optimization tool, to simultaneously tackle the noise and performance challenges for the second generation of supersonic transport, as discussed in Chap. 1.

I am confident that this work, although specifically focused on the selected design cases, can foster further investigation on SST and other novel configurations using this type of state-of-the-art tools. The literature presented in Chap. Sec. 1 partially identifies the research direction of the industry in this sense. A glance at market trends, research efforts and company investments suggest that we are potentially on the verge of a new era of aviation, as the industry starts to capitalize on decades of experience coupled with modern manufacturing and design technologies. A greener, smarter and more design efficient air transportation will most likely take-off in the next few decades. Even going beyond the configuration investigated in this project, the search for more efficient and possibly faster aircraft has necessarily to include advanced simulation and optimization tools earlier in the design process. Although the long road ahead to adapt the current MDO tools to industry practice and requirements, it is strongly desirable and recommended to push for a wider and standardised application of high (and low) fidelity optimization framework by aircraft manufacturers and other heavy industry players.

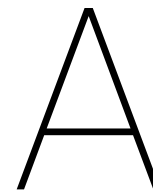
## Research Acknowledgments

The high-fidelity optimization tool used to perform this research, *MACH*, has been developed in the last decade at University of Michigan’s MDO Lab. *MACH* aerodynamic shape optimization toolbox used for the present research has been recently released in an open-source format on the MDO Lab [Git Hub page](#). Check [MDO Lab website](#) for updates and other MDO and ASO publications.

The computations were performed on the Flux HPC cluster at the University of Michigan Center of Advanced Computing. This research has been partially funded by TU Delft’s Justus and Louise van Effen research grant.



# **Appendices**



## Brief review of parametrization methods for ASO

The definition of design variables - as discussed in Sec. 3.5 - has a crucial role in every analytical or numerical problem, due to their strong influence on design space topology. Methods are classified between constructive approaches (such as splines or PDE definitions), which functions define basic shapes from scratch, or deformative approaches such as FFD, where baseline geometries are modified acting directly on (appropriately mapped) grid points [85, 86]. Considering OML parametrization of a wing, most of its global design variables such as span, dihedral angle, twist, sweep angle, nacelle position, are intuitively implemented in the geometry manipulator by reciprocally constraining sets of design variables. Global modifications are coupled with local ones, which refer to single control points, to give the designer (and the optimizer) total and direct control on the external shape. Defining an efficient approach to define and manipulate complex curves and surfaces is however a complex task.

Multiple approaches have been implemented for wing section manipulations. Set of equations such as those defining NACA airfoils are widely used in aircraft design, but their limitations to single airfoil families make them less than ideal for optimization problems. The polynomial-based approach for airfoil parametrization introduced by Hicks and Henne [95] is still particularly effective, even though limited to 2D definition and low curvatures [85]. Airfoil baseline shape is directly modified by acting on the coefficients of the polynomial functions that, linearly combined, are superimposed to the base function. A comparable polynomial scheme named parametric section (PARSEC) has been introduced by Sobieczky [190]. Functions coefficients are based on physical parameters to provide more meaningful insight: again, the approach is limited to the solely airfoil problem, but however its intuitive definition has been extended to more advanced schemes such as CST [191], presented later in this section.

Spline-based methods consist in a more advanced application of polynomial functions that are extended to surface definition. They have a large application in computer graphics due to the robustness of the defining algorithms and are highly appreciated for industrial applications. Bezier-curves, based on Bernstein polynomials, are particularly efficient due to the

small number of parameters required to define an airfoil, but however offer poor local control [86]. B-spline approach tackle this issue by splitting the curve into a series of piecewise lower-order base spline functions connected at a number of fixed “knots”. Low-order functions, which weight is again related to a single control point, provide better local control due to the smaller propagation through adjacent knots. Mathematical considerations for both B-splines and NURBS (Non-uniform rational B-splines), a generalization of the above mentioned methods, are extensively addressed in [192].

CST parametrization, developed by Brenda Kulfan at Boeing [193], is based on a well-behaved class function and shape function interaction to define smooth geometries. One of its main advantages is the intuitive extension to non-lifting surfaces such as complex fuselage and nacelle shapes, thanks to the direct control on main engineering parameters (radiuses, angles, thickness) [194]. Straathof [195, 196] proposed a CST approach with improved local shape manipulation by coupling additional B-splines functions, nevertheless increasing the number of design variables. For specific SST design, Morris at Al. [53] developed an effective scheme for tailless configuration, with however low chances to extend this approach to broader studies. Despite its robustness and flexibility indeed, CST is reportedly “built from, but limited to, human imagination” [99]. Ceze et al. [194] have moreover shown how this scheme can potentially compromise the optimization path, slowing down the convergence rate for specific design space regions and presenting an ill-conditioned problem when high-order shape functions (not used for airfoil though) are considered.

In comparison to these constructive methods, FFD parametrization [158, 197] used for this thesis project (see Sec. 2.1 for more detailed description) allows a much higher design freedom and application flexibility, at the cost of a more careful definition of geometric constraints to avoid unfeasible layouts or critical errors in mesh manipulation routine. Being it strictly related to the input baseline geometry, its application is based on the assumption that the problem has a constant topology [86]. Studies such as [162, 163] prove that its performance is comparable to other approaches specifically designed for airfoil applications. Its advantages emerge when ASO is extended to 3D and complex geometries; furthermore, it can simultaneously handle different grids without additional effort, making it the ideal candidate for aerostructural optimization.

More recently, separate ASO studies by Allen et al. [198] and the already presented Li et al. [118] and Poole et al. [116, 117] successfully implemented the so-called “airfoil modes” [199]. With this methodology a set of orthogonal modal design variables is derived from a set of training airfoils by singular-value-decomposition approach. The novel feature of this approach is the strict mathematical derivation of common shape traits that does not rely on user-experience or a-priori defined shapes, such as CST. At the same time, it provides a more compact set of design variables rather than the simple interpolation of a set of reference airfoils. Such approach turns out to be particularly efficient even when considering local shape deformations [198]. The main challenge for an extensive applications lays in the proper extraction of the modes for specific optimization problems.

What emerges from the works presented in this short overview is that once again there is not a perfect parametrization choice that suits all ASO problems [85, 162]. For 2D problems, advanced constructive methods such as B-spline, CST and modes are particularly effective. In case the initial shape is relatively close to the optimal shape (as the case for most common

high-fidelity ASO studies), the final layout is unconventional or is locally non-smooth (e.g. sharp edges), deformative methods such as FFD are as efficient. For 3D problems, this last approach appear to currently be the most mature and consistent. More detailed comparison between FFD and other approaches to support our choice is reported in Sec. 2.1. As future work, it may be interesting to extrapolate and use a set of airfoil and wing modes specifically designed for supersonic optimization, and to further couple them with subsonic and transonic modes to assess their effectiveness when complex multipoint trade-offs are taken into account.

# B

## Discretization Error Estimation for CFD Meshes

Ensuring that the CFD solutions consistently match with the real-physics fluid dynamics is a fundamental issue for any numerical flow simulation. Assessing both algorithm and mesh quality by benchmarking with experimental data is generally possible for a restricted number of shapes and flow regimes; it can moreover be applied to the solely initial shape in ASO problems.

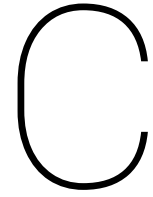
Using a RANS-equation model implies a number of assumptions on viscosity and turbulence model, which account as *physical approximation error* [200]. On the other hand, mesh quality plays an important role in the overall accuracy of the result, as the discretization of a continuous space domain (and time, for non-steady analyses) leads to an intrinsic *Discretization error*. According to Roache [201], among the techniques for quantification of numerical uncertainties: “*systematic grid refinement studies are the most common, most straightforward and arguably the most reliable*”. Such convergence studies have to be critically assessed and used to iteratively improve mesh quality for specific case. Vassberg and Jameson [202] highlight how the order of convergence for a grid family (Eq. (B.1)) also depends on solver and flow conditions, often leading to results “*worse than we would like to see*”.

For what concerns the optimization problems, a trade-off between accuracy and computational cost must be achieved. For the this project the reference approach (documented in Sec. 3.1.1 is provided by [201], as further summed up in [203]. This milestone work provides the guidelines to assess the mesh quality based on Richardson’s extrapolation and an estimation of the order of grid convergence. As first step, an initial reference refined mesh is uniformly coarsened in each direction. Given a relevant functional  $f$ , as for example  $C_d$ , the order of convergence  $p$  of a mesh family is obtained with Eq. (B.1):

$$p = \ln\left(\frac{f_3 - f_2}{f_2 - f_1}\right) / \ln(r) \quad (\text{B.1})$$

$$f_{h=0} \cong f_1 - \frac{f_1 - f_2}{r^p - 1} \quad (\text{B.2})$$

with the subscript indicating the mesh coarsening level (0 is most refined) and  $r = \frac{h_3}{h_2} = \frac{h_2}{h_1}$ . To solve  $p$ , the functional has to be a monotonic behaviour and if the argument of the logarithm at the denominator is  $<1$ ,  $p$  is negative. This approximated formula holds only if the ratio  $r$  is constant for each mesh coarsening step. It is also assumed here that flow solutions are sufficiently converged to provide a meaningful functional value. Order of convergence  $p$  is then used in Eq. (B.2) to extrapolate from finest and second finest meshes the asymptotic value of the functional as mesh spacing  $h \rightarrow 0$ . The so-called Richardson's extrapolation is indeed defined as “*a method for obtaining a higher-order estimate of the continuum value*” [203], with  $f_{h=0}$  value generally assumed to have an accuracy of  $p + 1$  order.



## Notes on Gradient-Free Optimization

The lack of dependence on sensitivity information of gradient-free methods make them particularly robust and capable to handle “*nonconvexities or disjointness*” [204], as well as being able to identify multiple local minima with negligible sensitivity to numerical noise. However, their convergence to global optimum, as for gradient-based methods, cannot be mathematically proved. There are different approaches that fall within this definition.

Genetic algorithms (GA), first introduced by Holland [205], are “*population-based optimisation technique based on the Darwinian theory of survival of the fittest*” [86]. Initial population is randomly generated and individuals are mapped and evaluated (with discipline solvers) for “survivability”; best candidates are then selected and a new generation of design points is generated by genetic “reproduction” operations - as crossover and mutation - until the stop conditions are met. All these intermediate steps present different challenges that have been extensively addressed with a vast number of approaches in the last decades. Again, Skinner and Zare-Behtash [86] provide an extensive review on relevant research.

Another nature-based effective methodology is Particle Swarm Optimization [206], which is again based on an initial population of candidates that, conversely to GA, are assigned with “velocity” vectors in addition to “position” vectors in the design space (i.e. design vectors). The velocity vector, after function evaluation, is updated taking into account current, local best and global best position of the particles. After each iteration, these particles “*fly through hyperspace*” [206] as a swarm of insects towards the global minimum. This methodology has very small memory requirements and it is particularly easy to implement, but the number of evaluations is often too high to be tolerated on high-fidelity ASO [86].

One of the main advantages of gradient-free algorithms, besides their reduced tendency to get stuck into local minima due to a huge number of layouts evaluations throughout the design space, it is given by the lack of required previous knowledge of design space topology and the absence of fundamental assumptions on its properties. For this reason, their implementation (and parallelization) is much simpler than gradient-based approaches such as the adjoint method presented in Appx. D. However, this comes at the cost of a increase of computational time up to orders of magnitude, which rapidly becomes unacceptable when high-fidelity discipline analyses are included in the framework. Evolutionary algorithms are particularly useful to analyse Pareto fronts for multi-objective optimization and give the de-

signer a better insight of the complex trade-offs [24]. Such approaches have been successfully applied to SST studies (Sec. 1.3.5), while Peigin and Epstein [109] used a GA approach coupled with a database-based reduced order model to reduce the cost of high-fidelity transonic ASO, showing promising results.

In this sense, surrogate models, i.e continuous “trained” approximated functions that relate design variables to outputs (out of the scope of this review) have recently demonstrated great improvements in accuracy [118] and the possibility to be coupled with both gradient-free and gradient-based methods [207]. Their implementation is not new to aerospace research; however there is a well-identified margin of improvement to be exploited by future works to compete with high-fidelity studies. Reference sources for this approach are listed in [86].



## The adjoint method and applications to gradient-based optimization

Among the sensitivity analysis methods briefly introduced in Sec. 2.4, the so-called adjoint method is currently one of the most successfully implemented approaches in ASO and MDO [1, 86]. First introduced in fluid dynamics by Pironneau [208], who estimated the disturbance given by a bump on an aerodynamic surface, and later applied by Jameson [3, 92] to ASO (Sec. 1.3.2), its efficiency and accuracy have been demonstrated in a number of publications in the last decade (see Sec. 2.4). Reuther et al. [6, 7] in their seminal work claimed how the adjoint method was particularly suitable to ASO due to the overall smoothness of the design space and the reduced number of flow solutions required with respect to finite-step approaches, together with the lower level of convergence necessary to obtain consistent sensitivity information.

Scheme implementation is demanding and time-consuming, as it requires deep insight on the physical model and substantial modifications of the discipline source code. Algorithmic differentiation approach presented in Appx. D.3 is a powerful methodology to tackle this issue reducing the burden on the software developer. Two different approaches are possible for adjoint derivation applied to PDE-based systems, namely continuous and discrete, depending on if equations are differentiated before or after system discretization. The latest is preferred in high-fidelity ASO due to its consistency with the actual discrete numerical problem - namely solving Navier–Stokes equations on a discretized flow field. In the following paragraphs the discrete adjoint approach, as implemented in *MACH*, is presented.

### D.1. Mathematical formulation

The objective of the method is to calculate the sensitivity of a function  $I$  (which can be both the objective function of the problem or one of its constraints) with respect to both design variables  $x_j$  and state variables  $y_k$  defined as:  $I = I(x_j, y_k)$  [209]. State variables dependence on the design variables, according to the governing equations of the system, are written in an implicit general form as:  $R_k(x_j, y_k(x_j)) = 0$  - with the residual that could explicitly depend on  $x_j$ . For CFD-based ASO,  $R$  is the residual matrix of the Navier–Stokes equations solved at

each mesh node. The total variation of an objective function  $I$  and governing equations  $R$  are derived with chain rule in Eq. D.1 and Eq. D.2 respectively. As  $x_j$  and  $y_k$  are dependent and the perturbed system has to satisfy  $R$ , i.e. the residual must always be zero, it follows that  $\delta R_{k'} = 0$  [1].

$$\delta I = \frac{\partial I}{\partial x_j} \delta x_j + \frac{\partial I}{\partial y_k} \delta y_k \quad (\text{D.1})$$

$$\delta R_{k'} = \frac{\partial R_{k'}}{\partial x_j} \delta x_j + \frac{\partial R_{k'}}{\partial y_k} \delta y_k = 0 \quad (\text{D.2})$$

Eq. D.2 could be solved directly for  $\frac{\partial y_k}{\partial x_j}$  by rearranging it into  $\frac{\partial y_k}{\partial x_j} = - \left[ \frac{\partial R_{k'}}{\partial y_k} \right]^{-1} \frac{\partial R_{k'}}{\partial x_j}$ . However, this formulation implies solving  $x_j$  linear systems, one for each design variable, thus presenting the sole advantage of linearity with respect to finite difference approach [101]. Conversely, a set of adjoint equations is developed introducing as much arbitrary scalar *adjoint variables*  $\varphi_{k'}$  when linearly combining Eq. D.1 and Eq. D.2. This mathematical step is comparable to control theory approach to constrained optimization, where equality constraints are added to the objective function by means of *Lagrange multipliers* to turn the problem into an unconstrained one [1].

$$\delta I = \frac{\partial I}{\partial x_j} \delta x_j + \frac{\partial I}{\partial y_k} \delta y_k + \varphi_{k'} \left( \frac{\partial R_{k'}}{\partial x_j} \delta x_j + \frac{\partial R_{k'}}{\partial y_k} \delta y_k \right) = \quad (\text{D.3})$$

$$= \left( \frac{\partial I}{\partial x_j} + \varphi_{k'} \frac{\partial R_{k'}}{\partial x_j} \right) \delta x_j + \left( \frac{\partial I}{\partial y_k} + \varphi_{k'} \frac{\partial R_{k'}}{\partial y_k} \right) \delta y_k \quad (\text{D.4})$$

As  $\varphi_{k'}$  are arbitrary, we can impose the second term of Eq. D.4 to be zero, leading to Eq. D.5. Note that this system has to be solved once for each objective function  $I$ , thus resulting particularly efficient for ASO problems that typically have a large amount of design variables but a limited amount of functions to be evaluated and optimized.

$$\varphi_{k'} = - \frac{\partial I}{\partial y_k} \left[ \frac{\partial R_{k'}}{\partial y_k} \right]^{-1} \quad (\text{D.5})$$

Finally, having calculated  $\varphi_{k'}$ , Eq. D.4 is manipulated into Eq. D.6 and sensitivity information  $\frac{dI}{dx_j}$  is obtained.

$$\frac{dI}{dx_j} = \frac{\partial I}{\partial x_j} + \varphi_{k'} \frac{\partial R_{k'}}{\partial x_j} \quad (\text{D.6})$$

This brief mathematical explanation proves how, as already discussed in this survey, the adjoint method cost is virtually independent from the number of design variables scaling with the sole objective functions. The bottleneck related to partial derivatives calculation, assembled into a large sparse matrix, is effectively tackled with automatic differentiation, as shown in the following section.

## D.2. Implementation through Automatic Differentiation

As briefly introduced in Sec. 1.3.3, the hybrid adjoint-based framework developed at *MDOLab* is based on the fundamental work by Mader et al. [101]. A detailed assembly description of the adjoint solver for RANS equations currently implemented in *MACH* is provided by Lyu et al. [102]. While the backbone of the process is the same presented in previous Appx. D.1 and following paragraph, the actual calculation of  $\partial R/\partial y$ ,  $\partial I/\partial y$ ,  $\partial R/\partial x$  and  $\partial I/\partial x$  required a specific gimmick. Partial derivatives with respect to state variables  $y$  (including a turbulence variable for SA model), which involve inviscid and artificial dissipation together and viscous fluxes calculation, require information from a stencil around each cell to obtain both residuals and single-cell forces and moments. Design variables partials are indirectly obtained in a modular fashion by first calculating sensitivities for mesh points displacements and then extending it to grid displacement sensitivity to FFD scheme deformations, analytically derived as discussed in Sec. 2.1. A coloring acceleration technique is implemented to numerically rearrange the highly sparse Jacobian matrix and to populate it with lower number of evaluations. Kenway et al. [104] extended this adjoint method to coupled aerostructural systems including structural design variables and solver equations, as initially proposed by Martins [209].

## D.3. Automatic Differentiation

Differentiating mathematical expressions by hand becomes an extremely complex task when dealing with huge multivariate non-linear systems such as those involved in aircraft MDO, even if the underlying method, the chain rule, is substantially straight-forward. Symbolic differentiation consists in a set of logic steps on elementary operations that allow the computer to generate derivatives with respect to a selected variable, directly from source code. Extending this approach to an entire solver script (or selected sections), automatic differentiation (AD) consists in the “[...] *systematic symbolic differentiation of each line of a computer program, and the accumulation of total derivatives using the chain rule. The method relies on tools that automatically produce a program that computes user-specified derivatives based on the original program*” [1]. This approach guarantees the same numerical precision of the original algorithm. Dependent variables are generated to decompose the original function into a set of hierarchically ordered (or child-parent related, using graph theory) simpler sub-functions [82]. Given a set of variables allocated for a computer script  $t = [t_1, t_2, \dots, t_m]$ , including both independent variables  $t_1, t_2, \dots, t_n$  and dependent variables  $t_{n+1}, t_{n+2}, \dots, t_m$ , chain rule is applied in the following form:

$$\frac{dt_i}{dt_j} = \delta_{ij} + \sum_{k=j}^{i-1} \frac{\partial T_i}{\partial t_k} \frac{\partial t_k}{\partial t_j} \quad (\text{D.7})$$

with  $i = n+1, n+2, \dots, m$  the index of dependent variables and  $t_i = T_i(t_1, t_2, \dots, t_{i-1})$ . Forward mode AD consists in fixing an independent design variable  $t_j$  and move on for  $i = n+1, n+2, \dots, m$  indices until the desired derivative  $\frac{dT_i}{dt_j}$  is obtained. With reverse mode conversely, the derivative index  $i$  is fixed and differentiation goes backwards until the function derivative is broken down into single components  $j$  [1]. This latest approach is implemented in *MACH*

due to its substantial equivalency with adjoint method, depending only on the number of output functions [102].

At machine-level, implementation is done in two different ways, operator overloading and source code transformation [1]. In the first case, a new variable type, that includes both function and derivative value, replaces floating point real numbers. This approach implies minimum changes to the source code, but shows low efficiency due to the necessity to re-define (i.e. *overload*) basic operations and functions. On the other hand, source code transformation adds additional instances to the initial script, calculating derivatives without altering fundamental functions. *MACH* adjoint solver has been developed with this latest approach. Nocedal [82] discusses theory and computational requirements more in detail. At development stage only, the differentiated code is tested against derivative values calculated with complex-step approximation [1] introduced in Sec. 2.4 to ensure the correct implementation of the AD algorithm.

## D.4. Observations on flow solver and optimizer settings

The extensive optimization campaign carried out on both airfoils and wings, in addition to the “background” case set-up and design approach, has implied the troubleshooting of a number of issues. Even if most of them are tool-specific, I briefly note down some general observations that could be relevant for future studies. Main bottlenecks involved convergence issues for the CFD solver and for the optimizer itself.

In terms of basic flow solver settings, without going too much into details, most conventional implicit methods such as DADI have been dropped (except for high  $\alpha$  cases) in favour of faster and more robust Newton–Krylov and approximate Newton–Krylov schemes, since the first iterations of the flow solver. A multiple-algorithm approach, involving the introduction of a second order scheme and the simultaneous coupling with the turbulence solver have helped to increase the algorithm robustness. Concurrently, the combination of sharp edges and supersonic flight conditions has generated complex fluid dynamics couplings that represented a challenge for the CFD tool. A crucial settings modification has involved the increase in tolerance for fluid properties values change from one iteration to another. This is due to the numerical “shockwave oscillations” while the solver is trying to converge the flow properties. If the oscillation in value is upper limited, the solver would impose an excessively small step between iterations to respect such a constraint, and consequently tend to stall the residual convergence. In these terms, the concurrent setting of CFL limit values and algorithm switch tolerances have been the main coding tweak during most troubled runs. The adjoint solver has proven to be robust and efficient, with solutions times consistently lower than the flow solutions. In the few cases where the algorithm “stalled”, an increase of the solution subspace (for GMRES scheme) has solved the issues without compromising the computational performance.

As for the optimizer, some cases required a more tailored definition of the search settings to avoid inconsistent optimization steps or a genuine interruption of the run. The main tweaks for SNOPT issues focused on the maximum step size of the line search and the tolerance on constraint violations. Especially for the first optimization steps, the algorithm explores the design space according to sensitivity information: if the “design direction” is given, the

magnitude of shape modifications has to be investigated with line search strategies (outside the scope of this discussion and research). An excessively generous limit could lead the optimizer to explore odd shapes as minor iteration steps that, given the complex boundary conditions, could be not solved by the CFD software. Playing with these parameters, thus limiting the exploration of the optimizer in the very first steps of the run, leads to a more robust routine with small or null increase of optimization steps. The optimizer still has the capability to explore odd and wobbly shapes as reported in Fig. D.1.

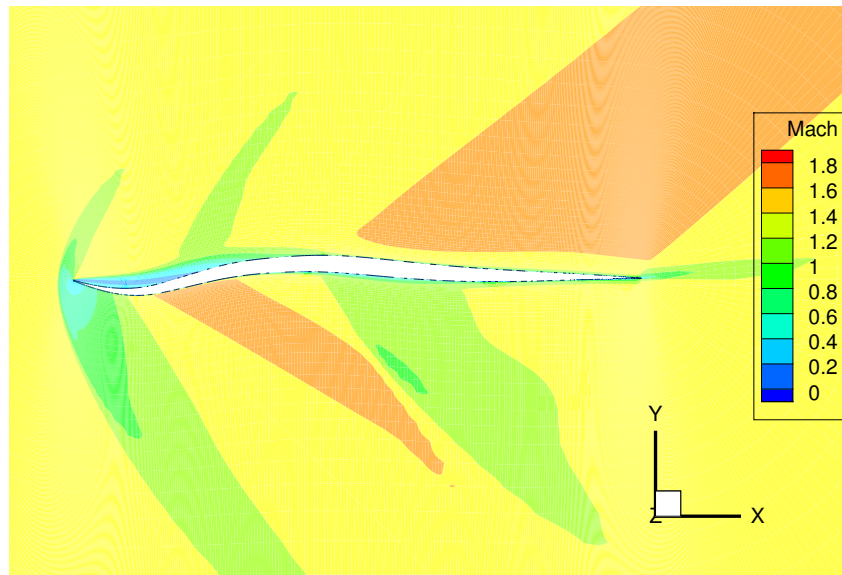


Figure D.1: Example of odd airfoil shape evaluated during early optimization steps. ADflow fully converged for this supersonic simulation.

As a side note, the tolerance of the grid deformation module has to be decreased for most refined meshes, to avoid corrupted grids and consequent “false steps”. Overall, the ultimate goal has been to ensure that the process is completely automatic. Human intervention in terms of optimization restarts or adjustments on the run is allowable by *MACH* and recommended for debugging issues. However, final runs reported in this work have been completed in one shot, with time varying from few hours to a maximum of four days, for most complex and conservatively-set 3D multipoint cases.

All the observations hereby discussed for 2D optimization hold for wing optimization as well. In particular, probably due to a less dense chordwise elements distribution, ADflow has generally shown higher robustness than what experienced for airfoil cases and, despite the higher number of cell elements and the presence of more complex fluid dynamics phenomena (cross-flow effects, tip vortices), a relatively small increase in computational time, as further discussed in Chap. 5.

# Bibliography

- [1] Joaquim R. R. A. Martins and John T. Hwang. *Multidisciplinary Design Optimization of Aircraft Configurations—Part 1: A modular coupled adjoint approach*. Lecture Series. ISSN0377-8312. Rode Saint Genèse, Belgium: Von Karman Institute for Fluid Dynamics, 2016.
- [2] Joaquim R. R. A. Martins and Andrew B. Lambe. “Multidisciplinary Design Optimization: A Survey of Architectures”. In: *AIAA Journal* 51.9 (2013), pp. 2049–2075. DOI: [10.2514/1.J051895](https://doi.org/10.2514/1.J051895).
- [3] A. Jameson. “Aerodynamic Design via Control Theory”. In: *Journal of Scientific Computing* 3.3 (Sept. 1988), pp. 233–260.
- [4] Mark Drela. “Design and Optimization Method for Multi-Element Airfoils Aerospace Design Conference”. In: *Proceedings of the AIAA/AHS/ASCE Aerospace Design Conference*. AIAA 1993-0969. Irvine, CA, 1993. DOI: [10.2514/6.1993-969](https://doi.org/10.2514/6.1993-969).
- [5] Mark Drela. “Frontiers of Computational Fluid Dynamics”. In: ed. by D. A. Caughey and M. M. Hafez. World Scientific, 1998. Chap. Pros and Cons of Airfoil Optimization, pp. 363–381. ISBN: 978-981-02-3707-3. DOI: [10.1142/9789812815774\\_0019](https://doi.org/10.1142/9789812815774_0019).
- [6] James J. Reuther et al. “Constrained Multipoint Aerodynamic Shape Optimization Using an Adjoint Formulation and Parallel Computers, Part 1”. In: *Journal of Aircraft* 36.1 (1999), pp. 51–60.
- [7] James J. Reuther et al. “Constrained Multipoint Aerodynamic Shape Optimization Using an Adjoint Formulation and Parallel Computers, Part 2”. In: *Journal of Aircraft* 36.1 (1999), pp. 61–74.
- [8] Marian Nemec, David W. Zingg, and Thomas H. Pulliam. “Multipoint and Multi-Objective Aerodynamic Shape Optimization”. In: *AIAA Journal* 42.6 (June 2004), pp. 1057–1065.
- [9] Charles Alexander Mader. “Stability-Constrained Aerodynamic Shape Optimization with Applications to Flying Wings”. PhD thesis. University of Toronto, 2012.
- [10] Zhoujie Lyu, Gaetan K. W. Kenway, and Joaquim R. R. A. Martins. “Aerodynamic Shape Optimization Investigations of the Common Research Model Wing Benchmark”. In: *AIAA Journal* 53.4 (2015), pp. 968–985. DOI: [10.2514/1.J053318](https://doi.org/10.2514/1.J053318).
- [11] Gaetan K. W. Kenway and Joaquim R. R. A. Martins. “Multipoint Aerodynamic Shape Optimization Investigations of the Common Research Model Wing”. In: *AIAA Journal* 54.1 (2016), pp. 113–128. DOI: [10.2514/1.J054154](https://doi.org/10.2514/1.J054154).
- [12] Gaetan K. W. Kenway and Joaquim R. R. A. Martins. “Multipoint High-Fidelity Aerostructural Optimization of a Transport Aircraft Configuration”. In: *Journal of Aircraft* 51.1 (2014), pp. 144–160. DOI: [10.2514/1.C032150](https://doi.org/10.2514/1.C032150).
- [13] Timothy R. Brooks, Graeme J. Kennedy, and Joaquim R. R. A. Martins. “High-fidelity Multipoint Aerostructural Optimization of a High Aspect Ratio Tow-steered Composite Wing”. In: *Proceedings of the 58th AIAA/ASCE/AHS/ASC Structures, Structural Dynamics, and Materials Conference, AIAA SciTech Forum*. Grapevine, TX, 2017. DOI: [10.2514/6.2017-1350](https://doi.org/10.2514/6.2017-1350).

- [14] Charles A. Mader et al. “Aerostructural Optimization of the D8 Wing with Varying Cruise Mach Numbers”. In: *18th AIAA/ISSMO Multidisciplinary Analysis and Optimization Conference*. American Institute of Aeronautics and Astronautics, 2017. DOI: [10.2514/6.2017-4436](https://doi.org/10.2514/6.2017-4436).
- [15] *airliners.net*, “The only picture ever taken of Concorde flying at Mach 2”. <http://www.airliners.net/forum/viewtopic.php?t=1389585>. Accessed: 2018-04-14.
- [16] Lockheed Advanced Development Company. *Lockheed SR-71 researcher’s handbook: Supersonic/hypersonic research facility*. Lockheed Advanced Development Co, 1990.
- [17] *Aerion Supersonic website*. <https://www.aerionsupersonic.com>. Accessed: 2018-04-14.
- [18] *Lockheed Martin’s Quiet Supersonic X-plane*. <https://www.lockheedmartin.com/en-us/products/quesst.html>. Accessed: 2018-08-29.
- [19] Yicheng Sun and Howard Smith. “Review and prospect of supersonic business jet design”. In: *Progress in Aerospace Sciences* 90 (2017), pp. 12–38. DOI: [10.1016/j.paerosci.2016.12.003](https://doi.org/10.1016/j.paerosci.2016.12.003).
- [20] H Robert Welge, Chester Nelson, and John Bonet. “Supersonic vehicle systems for the 2020 to 2035 timeframe”. In: *28th AIAA Applied Aerodynamics Conference*. Chicago, Illinois, 2010. DOI: [10.2514/6.2010-4930](https://doi.org/10.2514/6.2010-4930).
- [21] Ilan Kroo et al. *Multifidelity analysis and optimization for supersonic design*. Tech. rep. NASA/CR-2010-216874, Dec. 2010.
- [22] James Reuther and Antony Jameson. *Supersonic wing and wing-body shape optimization using an adjoint formulation*. Tech. rep. NASA, 1995.
- [23] A Van der Velden. “Supersonic Aircraft Shape Optimization”. In: *New Design Concepts for High Speed Air Transport*. Springer, 1997, pp. 237–250. DOI: [10.1007/978-3-7091-2658-5\\_16](https://doi.org/10.1007/978-3-7091-2658-5_16).
- [24] Shigeru Obayashi and Daisuke Sasaki. *Self-organizing map of Pareto solutions obtained from multiobjective supersonic wing design*. *AIAA Paper* 2002-0991. 2002.
- [25] Joaquim R. R. A. Martins, Juan J. Alonso, and James J. Reuther. “High-Fidelity Aerostructural Design Optimization of a Supersonic Business Jet”. In: *Journal of Aircraft* 41.3 (2004), pp. 523–530. DOI: [10.2514/1.11478](https://doi.org/10.2514/1.11478).
- [26] Seongim Choi, Juan J Alonso, and Ilan M Kroo. “Two-level multifidelity design optimization studies for supersonic jets”. In: *Journal of Aircraft* 46.3 (2009), p. 776. DOI: [10.2514/1.34362](https://doi.org/10.2514/1.34362).
- [27] Valerio Lattarulo, Pranay Seshadri, and Geoffrey T Parks. “Optimization of a supersonic airfoil using the multi-objective alliance algorithm”. In: *Proceedings of the 15th annual conference on Genetic and evolutionary computation*. ACM. 2013, pp. 1333–1340. DOI: [10.1145/2463372.2463531](https://doi.org/10.1145/2463372.2463531).
- [28] Firat Kiyici and Selin Aradag. “Design and Optimization of a Supersonic Business Jet”. In: *22nd AIAA Computational Fluid Dynamics Conference*. 2015, p. 3064. DOI: [10.2514/6.2015-3064](https://doi.org/10.2514/6.2015-3064).
- [29] Darcy Allison et al. “A multidisciplinary design optimization framework for design studies of an efficient supersonic air vehicle”. In: *12th AIAA Aviation Technology, Integration, and Operations (ATIO) Conference and 14th AIAA/ISSMO Multidisciplinary Analysis and Optimization Conference*. 2012, p. 5492. DOI: [10.2514/6.2012-5492](https://doi.org/10.2514/6.2012-5492).
- [30] Karl Geiselhart et al. “Integration of multifidelity multidisciplinary computer codes for design and analysis of supersonic aircraft”. In: *49th AIAA Aerospace Sciences Meet-*

- ing Including the New Horizons Forum and Aerospace Exposition. 2011, p. 465. DOI: [10.2514/6.2011-465](https://doi.org/10.2514/6.2011-465).
- [31] Xiaoqiang Feng, Zhanke Li, and Bifeng Song. “Research of low boom and low drag supersonic aircraft design”. In: *Chinese Journal of Aeronautics* 27.3 (2014), pp. 531–541. DOI: [10.1016/j.cja.2014.04.004](https://doi.org/10.1016/j.cja.2014.04.004).
- [32] Irian Ordaz, Karl A Geiselhart, and James W Fenbert. “Conceptual Design of Low-Boom Aircraft with Flight Trim Requirement”. In: *Journal of Aircraft* 52.3 (2015), pp. 932–939. DOI: [10.2514/1.C033160](https://doi.org/10.2514/1.C033160).
- [33] Yicheng Sun and Howard Smith. “Supersonic Business Jet Conceptual Design in a Multidisciplinary Design Analysis Optimization Environment”. In: *2018 AIAA/ASCE/AH-S/ASC Structures, Structural Dynamics, and Materials Conference*. 2018, p. 1651. DOI: [10.2514/6.2018-1651](https://doi.org/10.2514/6.2018-1651).
- [34] Gaetan K. W. Kenway. “A Scalable, Parallel Approach for Multi-Point, High-Fidelity Aerostructural Optimization of Aircraft Configurations”. PhD thesis. University of Toronto, 2013.
- [35] David A. Burdette and Joaquim R. R. A. Martins. “Impact of Morphing Trailing Edge on Mission Performance for the Common Research Model”. In: *Journal of Aircraft* 56.1 (2019), pp. 369–384. DOI: [10.2514/1.C034967](https://doi.org/10.2514/1.C034967).
- [36] David A. Burdette and Joaquim R. R. A. Martins. “Design of a Transonic Wing with an Adaptive Morphing Trailing Edge via Aerostructural Optimization”. In: *Aerospace Science and Technology* 81 (2018), pp. 192–203. DOI: [10.1016/j.ast.2018.08.004](https://doi.org/10.1016/j.ast.2018.08.004).
- [37] Nicolas Bons et al. “Multimodality in Aerodynamic Wing Design Optimization”. In: *AIAA Journal* 57.3 (2019), pp. 1004–1018. DOI: [10.2514/1.J057294](https://doi.org/10.2514/1.J057294).
- [38] Marco Mangano and Joaquim R. R. A. Martins. “Multipoint Aerodynamic Shape Optimization for Subsonic and Supersonic Regimes”. In: *57th AIAA Aerospace Sciences Meeting, AIAA SciTech Forum, 2019*. San Diego, CA, 2019. DOI: [10.2514/6.2019-0696](https://doi.org/10.2514/6.2019-0696).
- [39] Theodore Von Karman. “Supersonic aerodynamics - principles and applications”. In: *Journal of the Aeronautical Sciences* 14.7 (1947), pp. 373–409. DOI: [10.2514/8.1394](https://doi.org/10.2514/8.1394).
- [40] John D Anderson Jr. *Fundamentals of aerodynamics*. McGraw-Hill, 2011. ISBN: 978-0073398105.
- [41] William H Mason. *Configuration aerodynamics*. Virginia Tech, 2006, pp. 3–41.
- [42] Ilan Kroo. *Applied Aerodynamics: a digital textbook*. <http://docs.desktop.aero/appliedaero/preface/welcome.html>. 1997.
- [43] William R Sears. “On projectiles of minimum wave drag”. In: *Quarterly of Applied Mathematics* 4.4 (1947), pp. 361–366. DOI: [10.1016/0021-8928\(59\)90004-8](https://doi.org/10.1016/0021-8928(59)90004-8).
- [44] W Haack. “Geschossformen kleinsten wellenwiderstandes”. In: *Bericht der Lilienthal-Gesellschaft* 136.1 (1941), pp. 14–28.
- [45] Karthik Palaniappan and Antony Jameson. “An analysis of bodies having minimum pressure drag in supersonic flow: Exploring the nonlinear domain”. In: *Computational Fluid Dynamics 2004*. Springer, 2006, pp. 675–680. DOI: [10.1007/3-540-31801-1\\_98](https://doi.org/10.1007/3-540-31801-1_98).
- [46] Richard T Whitcomb and Thomas L Fiscetti. *Development of a supersonic area rule and an application to the design of a wing-body combination having high lift-to-drag ratios*. Tech. rep. NASA, 1953.

- [47] Richard T Whitcomb. *A study of the zero-lift drag-rise characteristics of wing-body combinations near the speed of sound*. Tech. rep. NASA, 1956.
- [48] Dietrich Kuchemann. *The Aerodynamic Design of Aircraft: A Detailed Introduction to the Current Aerodynamic Knowledge and Practical Guide to the Solution of Aircraft Design Problems*. Pergamon Press, 1978.
- [49] Robert T. Jones. “Theoretical determination of the minimum drag of airfoils at supersonic speeds”. In: *Journal of the Aeronautical Sciences* 19.12 (1952), pp. 813–822. DOI: [10.2514/8.2493](https://doi.org/10.2514/8.2493).
- [50] Robert T Jones. *Theory of wing-body drag at supersonic speeds*. Tech. rep. NASA, 1956.
- [51] *Public Domain Aeronautical Software*. <http://www.pdas.com/index.html>. Accessed: 2018-08-20.
- [52] Beryl A Erickson. “Flight Characteristics of the B58 Mach 2 Bomber”. In: *The Aeronautical Journal* 66.623 (1962), pp. 665–671.
- [53] Craig C Morris et al. “Parametric geometry model for design studies of tailless supersonic aircraft”. In: *Journal of Aircraft* (2014). DOI: [10.2514/1.C032340](https://doi.org/10.2514/1.C032340).
- [54] John W Boyd, Eugene Migotsky, and Benton E Wetzell. *A study of conical camber for triangular and sweptback wings*. Tech. rep. NASA, 1955.
- [55] G. G. Brebner. *Some simple conical camber shapes to produce low lift-dependent drag on a slender delta wing*. Tech. rep. 1959.
- [56] Jeremy HB Smith and KW Mangler. *The Use of Conical Camber to Produce Flow Attachment at the Leading Edge of a Delta Wing and to Minimize Life-dependent Drag at Sonic and Supersonic Speeds*. Tech. rep. 1963.
- [57] Gene P Menees. *Lift, Drag, and Pitching Moment of an Aspect-Ratio-2 Triangular Wing with Leading-Edge Flaps Designed to Simulate Conical Camber*. Tech. rep. NASA, 1958.
- [58] *Lockheed Martin website, F-22 capabilities*. <https://www.lockheedmartin.com/en-us/products/f-22/f-22-capabilities.html>. Accessed: 2018-08-03.
- [59] H Smith. “A review of supersonic business jet design Issues”. In: *The Aeronautical Journal* 111.1126 (2007), pp. 761–776. DOI: [10.1017/S0001924000001883](https://doi.org/10.1017/S0001924000001883).
- [60] Robert T Jones. “The oblique wing—aircraft design for transonic and low supersonic speeds”. In: *Acta Astronautica* 4.1-2 (1977), pp. 99–109. DOI: [10.1016/0094-5765\(77\)90035-2](https://doi.org/10.1016/0094-5765(77)90035-2).
- [61] John E Lamar et al. “Leading-Edge Vortex-System Details Obtained on F-106B Aircraft Using a Rotating Vapor Screen and Surface Techniques”. In: (1993).
- [62] Ben R Rich. “F-12 series aircraft aerodynamic and thermodynamic design in retrospect”. In: *Journal of Aircraft* 11.7 (1974), pp. 401–406. DOI: [10.2514/3.60356](https://doi.org/10.2514/3.60356).
- [63] Sherman N Mullin. “The evolution of the F-22 advanced tactical fighter”. In: *1992 AIAA Aircraft Design Systems Meeting*. 1992. DOI: [10.2514/6.1992-4188](https://doi.org/10.2514/6.1992-4188).
- [64] Albert Piccirillo. “Origins of the F-22 Raptor”. In: *AIAA and SAE, 1998 World Aviation Conference*. 1998, p. 5566. DOI: [10.2514/6.1998-5566](https://doi.org/10.2514/6.1998-5566).
- [65] CS Leyman. “A review of the technical development of Concorde”. In: *Progress in Aerospace Sciences* 23.3 (1986), pp. 185–238. DOI: [10.2514/4.868122](https://doi.org/10.2514/4.868122).
- [66] *Spike Aerospace website*. <http://www.spikeaerospace.com/>. Accessed: 2018-08-20.

- [67] Brenda Kulfan. “New supersonic wing far-field composite-element wave-drag optimization method”. In: *Journal of Aircraft* 46.5 (2009), pp. 1740–1758. DOI: [10.2514/1.42823](https://doi.org/10.2514/1.42823).
- [68] DA Lovell. “European research to reduce drag for supersonic transport aircraft”. In: *Aerodynamic Drag Reduction Technologies*. Springer, 2001, pp. 117–132. DOI: [10.1007/978-3-540-45359-8\\_14](https://doi.org/10.1007/978-3-540-45359-8_14).
- [69] Akira Murakami. “Silent supersonic technology demonstration program”. In: *Proceedings on 25th International Council of the Aeronautical Sciences*. 2006.
- [70] Peter Sturdza. “An Aerodynamic Design Method for Supersonic Natural Laminar Flow Aircraft”. PhD thesis. Stanford, CA: Stanford University, Dec. 2003.
- [71] Kenji Yoshida. “Supersonic drag reduction technology in the scaled supersonic experimental airplane project by JAXA”. In: *Progress in Aerospace Sciences* 45.4 (2009), pp. 124–146. DOI: [10.1016/j.paerosci.2009.05.002](https://doi.org/10.1016/j.paerosci.2009.05.002).
- [72] Olivier Vermeersch et al. “Natural laminar flow wing for supersonic conditions - Wind tunnel experiments, flight test and stability computations”. In: *Progress in Aerospace Sciences* (2015), pp. 64–91. DOI: [10.1016/j.paerosci.2015.07.003](https://doi.org/10.1016/j.paerosci.2015.07.003).
- [73] Michael A. Frederick et al. “Flight tests of a supersonic natural laminar flow airfoil”. In: *Measurement Science and Technology* 26.6 (2015).
- [74] Andres Garzon and Jason Matisheck. “Supersonic Testing of Natural Laminar Flow on Sharp Leading Edge Airfoils. Recent Experiments by Aerion Corporation”. In: *42nd AIAA Fluid Dynamics Conf. and Exhibit*. 2012.
- [75] Richard R Tracy. *High efficiency, supersonic aircraft*. US Patent 5,322,242. 1994.
- [76] Richard Tracy et al. *Exploiting Natural Laminar Flow for Economical Supersonic Transport*. SAE Paper 952040. 1995.
- [77] Peter Sturdza. “Extensive Supersonic Natural Laminar Flow on the Aerion Business Jet”. In: *Proceedings of the 45th AIAA Aerospace Sciences Meeting and Exhibit*. AIAA 2007–0685. Reno, NV, Jan. 2007.
- [78] *Boom Supersonic website*. <https://boomsupersonic.com/>. Accessed: 2018-04-14.
- [79] Mathias Wintzer, Peter Sturdza, and Ilan Kroo. “Conceptual design of conventional and oblique wing configurations for small supersonic aircraft”. In: *44th AIAA Aerospace Sciences Meeting and Exhibit*. 2006, p. 930. DOI: [10.2514/6.2006-930](https://doi.org/10.2514/6.2006-930).
- [80] M Wintzer et al. “Conceptual design of low sonic boom aircraft using adjoint-based CFD”. In: *Seventh International Conference on Computational Fluid Dynamics (IC-CFD7) Big Island, Hawaii*. 2012.
- [81] *Concorde transatlantic navigation map*. <http://smartsync.me/concorde-flight-map/>. Accessed: 2018-07-31.
- [82] Jorge Nocedal and Stephen J. Wright. *Numerical Optimization*. 2nd. Springer-Verlag, 2006.
- [83] Gaetan K. W. Kenway and Joaquim R. R. A. Martins. “Buffet Onset Constraint Formulation for Aerodynamic Shape Optimization”. In: *AIAA Journal* 55.6 (2017), pp. 1930–1947. DOI: [10.2514/1.J055172](https://doi.org/10.2514/1.J055172).
- [84] David H Wolpert, William G Macready, et al. *No free lunch theorems for search*. Tech. rep. Technical Report SFI-TR-95-02-010, Santa Fe Institute, 1995.
- [85] Tian-tian Zhang et al. “A review of parametric approaches specific to aerodynamic design process”. In: *Acta Astronautica* (2018).

- [86] SN Skinner and H Zare-Behtash. “State-of-the-art in aerodynamic shape optimization methods”. In: *Applied Soft Computing* (2017). DOI: [10.1016/j.asoc.2017.09.030](https://doi.org/10.1016/j.asoc.2017.09.030).
- [87] *Aerodynamic Design Optimization DG Website*. <https://info.aiaa.org/tac/ASG/APATC/AeroDesignOpt-DG/default.aspx>. Accessed: 2018-03-28.
- [88] Garret N Vanderplaats. *Numerical optimization techniques for engineering design: with applications*. Vol. 1. McGraw-Hill New York, 1984.
- [89] William Karush. “Minima of functions of several variables with inequalities as side constraints”. In: *M. Sc. Dissertation. Dept. of Mathematics, Univ. of Chicago* (1939).
- [90] HW Kuhn and AW Tucker. “Proceedings of 2nd berkeley symposium”. In: Berkeley: University of California Press, 1951.
- [91] Philip E. Gill, Walter Murray, and Michael A. Saunders. “SNOPT: An SQP algorithm for large-scale constrained optimization”. In: *SIAM Journal of Optimization* 12.4 (2002), pp. 979–1006. DOI: [10.1137/S1052623499350013](https://doi.org/10.1137/S1052623499350013).
- [92] A. Jameson, L. Martinelli, and N. A. Pierce. “Optimum Aerodynamic Design Using the Navier–Stokes Equations”. In: *Theoretical and Computational Fluid Dynamics* 10.1–4 (1998), pp. 213–237. DOI: [10.1007/s001620050060](https://doi.org/10.1007/s001620050060).
- [93] Joaquim R. R. A. Martins, Gaetan K. W. Kenway, and Timothy R. Brooks. *Multidisciplinary Design Optimization of Aircraft Configurations—Part 2: High-fidelity aerostuctural optimization*. Lecture Series. ISSN0377-8312. Rode Saint Genèse, Belgium: Von Karman Institute for Fluid Dynamics, 2016.
- [94] R. M. Hicks, E. M. Murman, and G. N. Vanderplaats. *An assessment of airfoil design by numerical optimization*. Tech. rep. NASA TM X-3092, July 1974.
- [95] R. M. Hicks and P. A. Henne. “Wing Design by Numerical Optimization”. In: *Journal of Aircraft* 15 (1978), pp. 407–412.
- [96] Clive Irving. *Wide-Body—The Triumph of the 747*. New York: William Morrow and Company, 1993.
- [97] J. E. Hicken and D. W. Zingg. “Aerodynamic Optimization Algorithm with Integrated Geometry Parameterization and Mesh Movement”. In: *AIAA Journal* 48.2 (Feb. 2010), pp. 400–413. DOI: [10.2514/1.44033](https://doi.org/10.2514/1.44033).
- [98] Jason E. Hicken and David W. Zingg. “Induced-Drag Minimization of Nonplanar Geometries Based on the Euler Equations”. In: *AIAA Journal* 48.11 (2010), pp. 2564–2575. DOI: [10.2514/1.52436](https://doi.org/10.2514/1.52436).
- [99] Hugo Gagnon and David W Zingg. “Two-level free-form deformation for high-fidelity aerodynamic shape optimization”. In: *12th AIAA Aviation Technology, Integration, and Operations (ATIO) Conference and 14th AIAA/ISSMO Multidisciplinary Analysis and Optimization Conference*. 2012, p. 5447.
- [100] Siva K Nadarajah and Charles Tatossian. “Multi-objective aerodynamic shape optimization for unsteady viscous flows”. In: *Optimization and Engineering* 11.1 (2010), pp. 67–106.
- [101] Charles A. Mader et al. “ADjoint: An Approach for the Rapid Development of Discrete Adjoint Solvers”. In: *AIAA Journal* 46.4 (Apr. 2008), pp. 863–873. DOI: [10.2514/1.29123](https://doi.org/10.2514/1.29123).
- [102] Zhoujie Lyu et al. “Automatic Differentiation Adjoint of the Reynolds-Averaged Navier–Stokes Equations with a Turbulence Model”. In: *21st AIAA Computational Fluid Dynamics Conference*. San Diego, CA, 2013. DOI: [10.2514/6.2013-2581](https://doi.org/10.2514/6.2013-2581).

- [103] L. Hascoët. “TAPENADE: A tool for Automatic Differentiation of programs”. In: *Proceedings of 4<sup>th</sup> European Congress on Computational Methods, ECCOMAS’2004, Jyväskylä, Finland*. 2004.
- [104] Gaetan K. W. Kenway, Graeme J. Kennedy, and Joaquim R. R. A. Martins. “Scalable Parallel Approach for High-Fidelity Steady-State Aeroelastic Analysis and Derivative Computations”. In: *AIAA Journal* 52.5 (2014), pp. 935–951. DOI: [10.2514/1.J052255](https://doi.org/10.2514/1.J052255).
- [105] Charles A. Mader and Joaquim R. R. A. Martins. “Stability-Constrained Aerodynamic Shape Optimization of Flying Wings”. In: *Journal of Aircraft* 50.5 (2013), pp. 1431–1449. DOI: [10.2514/1.C031956](https://doi.org/10.2514/1.C031956).
- [106] S. Andrew Ning and Ilan Kroo. “Multidisciplinary Considerations in the Design of Wings and Wing Tip Devices”. In: *Journal of Aircraft* 47.2 (2010), pp. 534–543. DOI: [10.2514/1.41833](https://doi.org/10.2514/1.41833).
- [107] Nicolas Bons et al. “High-Fidelity Aerodynamic Shape Optimization of a Full Configuration Regional Jet”. In: *2018 AIAA/ASCE/AHS/ASC Structures, Structural Dynamics, and Materials Conference*. 2018, p. 0106. DOI: [10.2514/6.2018-0106](https://doi.org/10.2514/6.2018-0106).
- [108] Boris Epstein and Sergey Peigin. “Constrained aerodynamic optimization of three-dimensional wings driven by Navier-Stokes computations”. In: *AIAA journal* 43.9 (2005), pp. 1946–1957.
- [109] Sergey Peigin and Boris Epstein. “Multipoint aerodynamic design of wing-body configurations for minimum drag”. In: *Journal of aircraft* 44.3 (2007), pp. 971–980.
- [110] Rhea P. Liem, Gaetan K. W. Kenway, and Joaquim R. R. A. Martins. “Multimission Aircraft Fuel Burn Minimization via Multipoint Aerostructural Optimization”. In: *AIAA Journal* 53.1 (2015), pp. 104–122. DOI: [10.2514/1.J052940](https://doi.org/10.2514/1.J052940).
- [111] Hugo Gagnon and David W Zingg. “High-fidelity aerodynamic shape optimization of unconventional aircraft through axial deformation”. In: *52nd Aerospace Sciences Meeting*. 2014, p. 0908. DOI: [10.2514/6.2014-0908](https://doi.org/10.2514/6.2014-0908).
- [112] Zhoujie Lyu and Joaquim R. R. A. Martins. “Aerodynamic Design Optimization Studies of a Blended-Wing-Body Aircraft”. In: *Journal of Aircraft* 51.5 (2014), pp. 1604–1617. DOI: [10.2514/1.C032491](https://doi.org/10.2514/1.C032491).
- [113] Ney R. Secco and Joaquim R. R. A. Martins. “RANS-based Aerodynamic Shape Optimization of a Strut-braced Wing with Overset Meshes”. In: *Journal of Aircraft* 56.1 (2019), pp. 217–227. DOI: [10.2514/1.C034934](https://doi.org/10.2514/1.C034934).
- [114] Howard P. Buckley, Beckett Y. Zhou, and David W. Zingg. “Airfoil Optimization Using Practical Aerodynamic Design Requirements”. In: *Journal of Aircraft* 47.5 (2010), pp. 1707–1719. DOI: [10.2514/1.C000256](https://doi.org/10.2514/1.C000256).
- [115] Howard P. Buckley and David W. Zingg. “Approach to Aerodynamic Design Through Numerical Optimization”. In: *AIAA Journal* 51.8 (2013), pp. 1972–1981. DOI: [10.2514/1.J052268](https://doi.org/10.2514/1.J052268).
- [116] Daniel J Poole, Christian B Allen, and T Rendall. “Objective Function and Constraints for Robust Transonic Aerofoil Optimization”. In: *58th AIAA/ASCE/AHS/ASC Structures, Structural Dynamics, and Materials Conference*. 2017, p. 0360.
- [117] DJ Poole, CB Allen, and TCS Rendall. “A Comparison of Single-Point, Multi-Point and Range-Based Objectives for Transonic Aerofoil Optimization”. In: *AIAA Journal* 56 (2018), p. 405.

- [118] Jichao Li, Mohamed Amine Bouhlef, and Joaquim R. R. A. Martins. “Data-based Approach for Fast Airfoil Analysis and Optimization”. In: *Journal of Aircraft* 57.2 (2019), pp. 581–596. DOI: [10.2514/1.J057129](https://doi.org/10.2514/1.J057129).
- [119] C Holden and W Wright. “Optimisation methods for wing section design”. In: *38th Aerospace Sciences Meeting and Exhibit*. 2000, p. 842.
- [120] Oleg Chernukhin and David W. Zingg. “Multimodality and Global Optimization in Aerodynamic Design”. In: *AIAA Journal* 51.6 (2013), pp. 1342–1354. DOI: [10.2514/1.j051835](https://doi.org/10.2514/1.j051835).
- [121] Max M Munk. “The reversal theorem of linearized supersonic airfoil theory”. In: *Journal of Applied Physics* 21.2 (1950), pp. 159–161. DOI: [10.1063/1.1699616](https://doi.org/10.1063/1.1699616).
- [122] Hsue-Shen Tsien and Judson R Baron. “Airfoils in slightly supersonic flow”. In: *Journal of the Aeronautical Sciences* 16.1 (1949), p. 55. DOI: [10.2514/8.11725](https://doi.org/10.2514/8.11725).
- [123] J Reuther et al. “Practical design optimization of wing/body configurations using the Euler equations”. In: *10th Applied Aerodynamics Conference*. 1992, p. 2633. DOI: [10.2514/6.1992-2633](https://doi.org/10.2514/6.1992-2633).
- [124] James Reuther et al. “Aerodynamic shape optimization of supersonic aircraft configurations via an adjoint formulation on distributed memory parallel computers”. In: *Computers & fluids* 28.4 (1999), pp. 675–700. DOI: [10.1016/S0045-7930\(98\)00050-4](https://doi.org/10.1016/S0045-7930(98)00050-4).
- [125] Hyoung-Jin Kim et al. “Aerodynamic optimization of supersonic transport wing using unstructured adjoint method”. In: *AIAA Journal*. Vol. 56. 2001, pp. 1011–1020. DOI: [10.2514/2.1441](https://doi.org/10.2514/2.1441).
- [126] Susan E. Cliff et al. “Single-Point and Multipoint Aerodynamic Shape Optimization of High-Speed Civil Transport”. In: *Journal of Aircraft* 38.6 (2001), pp. 997–1005.
- [127] U Herrmann and M Orlowski. “Numerical Aerodynamic Optimization Study for a Supersonic Aircraft”. In: *New Results in Numerical and Experimental Fluid Mechanics*. Springer, 1997, pp. 189–196. DOI: [10.1007/978-3-322-86573-1\\_24](https://doi.org/10.1007/978-3-322-86573-1_24).
- [128] Richard Grenon. “Numerical optimization in aerodynamic design with application to a supersonic transport aircraft”. In: *Proceedings of International Workshops on Numerical Simulation Technology for Design of Next Generation Supersonic Civil Transport (SST-CFD Workshop)*. 1998, p. 88.
- [129] Dirk von Reith. *Experience and Potential of Multidisciplinary Optimization Tools on Supersonic Aircraft*. Tech. rep. SAE Technical Paper, 1997.
- [130] Martin Laban. “Multi-disciplinary analysis and optimisation of supersonic transport aircraft wing planforms”. In: *10th AIAA/ISSMO Multidisciplinary Analysis and Optimization Conference*. 2004, p. 4542. DOI: [10.2514/6.2004-4542](https://doi.org/10.2514/6.2004-4542).
- [131] Martin Laban and Ulrich Herrmann. “Multi-Disciplinary Analysis and Optimisation Applied to Supersonic Aircraft Part 1: Analysis Tools”. In: *48th AIAA/ASME/ASCE/AH-S/ASC Structures, Structural Dynamics, and Materials Conference*. 2007, p. 1857. DOI: [10.2514/6.2007-1857](https://doi.org/10.2514/6.2007-1857).
- [132] Ulrich Herrmann and Martin Laban. “Multi-Disciplinary Analysis and Optimisation Applied to Supersonic Aircraft Part 2: Application & Results”. In: *48th AIAA/ASME/ASCE/AH-S/ASC Structures, Structural Dynamics, and Materials Conference*. 2007, p. 1858. DOI: [10.2514/6.2007-1858](https://doi.org/10.2514/6.2007-1858).

- [133] Daisuke Sasaki et al. “Aerodynamic Shape Optimization of Supersonic Wings by Adaptive Range Multiobjective Genetic Algorithms”. In: *Evolutionary Multi-Criterion Optimization*. 2001, pp. 639–652. DOI: [10.1007/3-540-44719-9\\_45](https://doi.org/10.1007/3-540-44719-9_45).
- [134] Daisuke Sasaki, Shigeru Obayashi, and Hyoung-Jin Kim. “Evolutionary algorithm vs. adjoint method applied to sst shape optimization”. In: *The Annual Conference of CFD Society of Canada, Waterloo*. 2001.
- [135] Yushin Kim, Yong-Hee Jeon, and Dong-Ho Lee. “Multi-objective and multidisciplinary design optimization of supersonic fighter wing”. In: *Journal of Aircraft* 43.3 (2006), pp. 817–824. DOI: [10.2514/1.13864](https://doi.org/10.2514/1.13864).
- [136] Naoto Seto. “Multi-Disciplinary Design Optimization of Supersonic Transport Wing Using Surrogate Model”. In: *27th International Congress of the Aeronautical Sciences, Nice, France, ICAS-Paper*. 369. 2010.
- [137] Antony Jameson et al. “Aerodynamic shape optimization of transonic and supersonic aircraft configurations”. In: *43rd AIAA Aerospace Sciences Meeting and Exhibit*. Reno, Nevada, 2005.
- [138] Siva K. Nadarajah, Antony Jameson, and Juan J. Alonso. *Sonic Boom Reduction using an Adjoint Method for Wing-Body Configurations in Supersonic Flow*. AIAA Paper 2002-5547. 2002.
- [139] Seongim Choi et al. “Multifidelity Design Optimization of Low-Boom Supersonic Jets”. In: *Journal of Aircraft* 45.1 (2008), pp. 106–118.
- [140] Juan J. Alonso and Michael R. Colonno. “Multidisciplinary Optimization with Applications to Sonic-Boom Minimization”. In: *Annual Review of Fluid Mechanics* 44.1 (2012), pp. 505–526. DOI: [10.1146/annurev-fluid-120710-101133](https://doi.org/10.1146/annurev-fluid-120710-101133). eprint: <http://www.annualreviews.org/doi/pdf/10.1146/annurev-fluid-120710-101133>. URL: <http://www.annualreviews.org/doi/abs/10.1146/annurev-fluid-120710-101133>.
- [141] Li Li et al. “Aerodynamic Design of the Supersonic Aircraft Wing-Shape and Wing-Twist Optimization”. In: *International Journal of Aeronautical and Space Sciences* 19.2 (2018), pp. 340–353.
- [142] James L Pittman. “Supersonic airfoil optimization”. In: *Journal of aircraft* 24.12 (1987), pp. 873–879. DOI: [10.2514/3.45532](https://doi.org/10.2514/3.45532).
- [143] Rui Hu, Antony Jameson, and Qiqi Wang. “Adjoint-based aerodynamic optimization of supersonic biplane airfoils”. In: *Journal of Aircraft* 49.3 (2012), pp. 802–814. DOI: [10.2514/1.C031417](https://doi.org/10.2514/1.C031417).
- [144] Yuki Suga and Wataru Yamazaki. “Aerodynamic Uncertainty Quantification of Supersonic Biplane Airfoil via Polynomial Chaos Approach”. In: *AIAA SciTech Forum, 17th AIAA Non-Deterministic Approaches Conference*. Kissimmee, Florida, 2015. DOI: [10.2514/6.2015-1815](https://doi.org/10.2514/6.2015-1815).
- [145] Heinz Adolf Gerhardt et al. *Laminar supersonic transport aircraft*. US Patent 5,842,666. 1998.
- [146] Richard R Tracy and James D Chase. *Lift and twist control using trailing edge control surfaces on supersonic laminar flow wings*. US Patent 7,004,428. 2006.
- [147] Hyoung-Jin Kim, Shigeru Obayashi, and Kazuhiro Nakahashi. “Flap-deflection optimization for transonic cruise performance improvement of supersonic transport wing”. In: *Journal of aircraft* 38.4 (2001), pp. 709–717.

- [148] Anna-Maria Rivas McGowan et al. “Recent results from NASA’s morphing project”. In: *Smart Structures and Materials 2002: Industrial and Commercial Applications of Smart Structures Technologies*. Vol. 4698. International Society for Optics and Photonics. 2002, pp. 97–112.
- [149] Jürgen Renken. “Mission-adaptive wing camber control systems for transport aircraft”. In: *3rd Applied Aerodynamics Conference*. 1985, p. 5006.
- [150] Edmund W. Pendleton et al. “Active Aeroelastic Wing Flight Research Program: Technical Program and Model Analytical Development”. In: *Journal of Aircraft* 37.4 (2000), pp. 554–561.
- [151] Ed Pendleton et al. “The X-53 A summary of the active aeroelastic wing flight research program”. In: *48th AIAA/ASME/ASCE/AHS/ASC Structures, Structural Dynamics, and Materials Conference*. 2007, p. 1855.
- [152] Howoong Namgoong. “Airfoil optimization for morphing aircraft”. PhD thesis. 2005.
- [153] JHS Fincham and MI Friswell. “Aerodynamic optimisation of a camber morphing aerofoil”. In: *Aerospace Science and technology* 43 (2015), pp. 245–255.
- [154] Zhoujie Lyu and Joaquim R. R. A. Martins. “Aerodynamic Shape Optimization of an Adaptive Morphing Trailing Edge Wing”. In: *Journal of Aircraft* 52.6 (2015), pp. 1951–1970. DOI: [10.2514/1.C033116](https://doi.org/10.2514/1.C033116).
- [155] Silvestro Barbarino et al. “A Review of Morphing Aircraft”. In: *Journal of Intelligent Material Systems and Structures* 22 (2011), pp. 823–877. DOI: [10.1177/1045389X11414084](https://doi.org/10.1177/1045389X11414084).
- [156] William M. Chan and Joseph L. Steger. “Enhancements of a three-dimensional hyperbolic grid generation scheme”. In: *Applied Mathematics and Computation* 51.2–3 (1992), pp. 181–205. ISSN: 0096-3003. DOI: [10.1016/0096-3003\(92\)90073-A](https://doi.org/10.1016/0096-3003(92)90073-A).
- [157] Edward Luke, Eric Collins, and Eric Blades. “A Fast Mesh Deformation Method Using Explicit Interpolation”. In: *Journal of Computational Physics* 231.2 (Jan. 2012), pp. 586–601. ISSN: 0021-9991. DOI: [10.1016/j.jcp.2011.09.021](https://doi.org/10.1016/j.jcp.2011.09.021).
- [158] Gaetan K.W. Kenway, Graeme J. Kennedy, and Joaquim R. R. A. Martins. “A CAD-Free Approach to High-Fidelity Aerostructural Optimization”. In: *Proceedings of the 13th AIAA/ISSMO Multidisciplinary Analysis Optimization Conference*. AIAA 2010-9231. Fort Worth, TX, Sept. 2010. DOI: [10.2514/6.2010-9231](https://doi.org/10.2514/6.2010-9231).
- [159] David Burdette et al. “Aerostructural Design Optimization of an Adaptive Morphing Trailing Edge Wing”. In: *Proceedings of the AIAA Science and Technology Forum and Exposition (SciTech)*. Kissimmee, FL, 2015. DOI: [10.2514/6.2016-1294](https://doi.org/10.2514/6.2016-1294).
- [160] Thomas W. Sederberg and Scott R. Parry. “Free-form Deformation of Solid Geometric Models”. In: *SIGGRAPH Comput. Graph.* 20.4 (Aug. 1986), pp. 151–160. ISSN: 0097-8930. DOI: [10.1145/15886.15903](https://doi.org/10.1145/15886.15903).
- [161] Michele Andreoli, Ales Janka, and Jean-Antoine Désidéri. *Free-form-deformation parameterization for multilevel 3D shape optimization in aerodynamics*. Tech. rep. 5019. Sophia Antipolis, France: INRIA, Nov. 2003.
- [162] Dominic A. Masters et al. “A Geometric Comparison of Aerofoil Shape Parameterisation Methods”. In: *54th AIAA Aerospace Sciences Meeting, AIAA SciTech Forum*. San Diego, California, 2016.
- [163] Dominic A Masters et al. “Impact of Shape Parameterisation on Aerodynamic Optimisation of Benchmark Problems”. In: *54rd AIAA Aerospace Sciences Meeting*. 2016.
- [164] Jean-Antoine Désidéri and Ales Janka. “Multilevel Shape Parameterization for Aerodynamic Optimization: Application to Drag and Noise Reduction of Transonic/Su-

- personic Business Jet”. In: *Proceedings of the European Congress on Computational Methods in Applied Sciences and Engineering, ECCOMAS 2004*. 2004.
- [165] CGNS Tools. [https://cgns.github.io/CGNS\\_docs\\_current/cgnstools/index.html](https://cgns.github.io/CGNS_docs_current/cgnstools/index.html). Accessed: 2018-08-29.
- [166] Mark J Lutton. *Comparison of C-and O-grid generation methods using a NACA 0012 airfoil*. Tech. rep. Air Force Institute of Technology, Wright-Patterson AFB OH, School of Engineering, 1989.
- [167] E. van der Weide et al. “Unsteady Turbomachinery Computations Using Massively Parallel Platforms”. In: *Proceedings of the 44th AIAA Aerospace Sciences Meeting and Exhibit*. AIAA 2006-0421. Reno, NV, 2006.
- [168] Gaetan K. W. Kenway et al. “Effective Adjoint Approaches for Computational Fluid Dynamics”. In: *Progress in Aerospace Sciences* (2019). (Submitted).
- [169] Gaetan K. W. Kenway et al. “An Efficient Parallel Overset Method for Aerodynamic Shape Optimization”. In: *Proceedings of the 58th AIAA/ASCE/AHS/ASC Structures, Structural Dynamics, and Materials Conference, AIAA SciTech Forum*. Grapevine, TX, 2017. DOI: [10.2514/6.2017-0357](https://doi.org/10.2514/6.2017-0357).
- [170] Goetz H Klopfer et al. “A diagonalized diagonal dominant alternating direction implicit (D3ADI) scheme and subiteration correction”. In: *AIAA paper* 2824 (1998), p. 1998.
- [171] Anil Yildirim et al. “A Jacobian-free approximate Newton–Krylov startup strategy for RANS simulations”. In: *Journal of Computational Physics* (2018). (Submitted).
- [172] Alberto Pueyo and David W Zingg. “Efficient Newton-Krylov solver for aerodynamic computations”. In: *AIAA journal* 36.11 (1998), pp. 1991–1997.
- [173] Marian Nemec and David W. Zingg. “Newton–Krylov Algorithm for Aerodynamic Design Using the Navier–Stokes Equations”. In: *AIAA Journal* 40.6 (June 2002), pp. 1146–1154.
- [174] Youcef Saad and Martin H. Schultz. “GMRES: A Generalized Minimal Residual Algorithm for Solving Nonsymmetric Linear Systems”. In: *SIAM Journal on Scientific and Statistical Computing* 7.3 (1986), pp. 856–869. DOI: [10.1137/0907058](https://doi.org/10.1137/0907058).
- [175] Graeme J. Kennedy and Joaquim R. R. A. Martins. “A parallel aerostructural optimization framework for aircraft design studies”. In: *Structural and Multidisciplinary Optimization* 50.6 (2014), pp. 1079–1101. DOI: [10.1007/s00158-014-1108-9](https://doi.org/10.1007/s00158-014-1108-9).
- [176] Ilse CF Ipsen and Carl D Meyer. “The idea behind Krylov methods”. In: *The American mathematical monthly* 105.10 (1998), pp. 889–899.
- [177] Andre C. Marta et al. “A methodology for the development of discrete adjoint solvers using automatic differentiation tools”. In: *International Journal of Computational Fluid Dynamics* 21.9 (2007), pp. 307–327. DOI: [10.1080/10618560701678647](https://doi.org/10.1080/10618560701678647).
- [178] P. Spalart and S. Allmaras. “A One-Equation Turbulence Model for Aerodynamic Flows”. In: *30th Aerospace Sciences Meeting and Exhibit*. 1992. DOI: [10.2514/6.1992-439](https://doi.org/10.2514/6.1992-439).
- [179] Ping He et al. “An Object-oriented Framework for Rapid Discrete Adjoint Development using OpenFOAM”. In: *AIAA Scitech 2019 Forum*. 2019, p. 1210.
- [180] David Rodriguez et al. “A Rapid, Robust, and Accurate Coupled Boundary-Layer Method for Cart3D”. In: *50th AIAA Aerospace Sciences Meeting including the New Horizons Forum and Aerospace Exposition*. 2012, p. 302. DOI: [10.2514/6.2012-302](https://doi.org/10.2514/6.2012-302).
- [181] Jacques E. V. Peter and Richard P. Dwight. “Numerical Sensitivity Analysis for Aerodynamic Optimization: A Survey of Approaches”. In: *Computers and Fluids* 39.3 (2010), pp. 373–391. DOI: [10.1016/j.compfluid.2009.09.013](https://doi.org/10.1016/j.compfluid.2009.09.013).

- [182] Joaquim R. R. A. Martins and John T. Hwang. “Review and Unification of Methods for Computing Derivatives of Multidisciplinary Computational Models”. In: *AIAA Journal* 51.11 (2013), pp. 2582–2599. DOI: [10.2514/1.J052184](https://doi.org/10.2514/1.J052184).
- [183] Joaquim R. R. A. Martins, Peter Sturdza, and Juan J. Alonso. “The Complex-Step Derivative Approximation”. In: *ACM Transactions on Mathematical Software* 29.3 (2003), pp. 245–262. DOI: [10.1145/838250.838251](https://doi.org/10.1145/838250.838251).
- [184] Philip E. Gill et al. *User’s Guide for SNOPT Version 7.6: Software for Large-Scale Non-linear Programming*. Tech. rep. 2017.
- [185] D. W. Zingg, M. Nemec, and T. H. Pulliam. “A Comparative Evaluation of Genetic and Gradient-Based Algorithms Applied to Aerodynamic Optimization”. In: *European Journal of Computational Mechanics* 17.1–2 (2008), pp. 103–126. DOI: [10.3166/remn.17.103-126](https://doi.org/10.3166/remn.17.103-126).
- [186] Zhoujie Lyu, Zelu Xu, and Joaquim R. R. A. Martins. “Benchmarking Optimization Algorithms for Wing Aerodynamic Design Optimization”. In: *Proceedings of the 8th International Conference on Computational Fluid Dynamics*. ICCFD8-2014-0203. Chengdu, Sichuan, China, 2014.
- [187] Yin Yu et al. “On the Influence of Optimization Algorithm and Starting Design on Wing Aerodynamic Shape Optimization”. In: *Aerospace Science and Technology* 75 (2018), pp. 183–199. DOI: [10.1016/j.ast.2018.01.016](https://doi.org/10.1016/j.ast.2018.01.016).
- [188] WF Lindsey, Bernard N Daley, and Milton D Humphreys. *The Flow and Force Characteristics of Supersonic Airfoils at High Subsonic Speeds, NASA Technical Note 1811*. Tech. rep. NASA, 1947.
- [189] Robert M Kulfan and Armand Sigalla. “Real Flow Limitations in Supersonic Airplane Design”. In: *Journal of Aircraft* 16.10 (1979), pp. 645–658.
- [190] Helmut Sobieczky. “Parametric airfoils and wings”. In: *Recent development of aerodynamic design methodologies*. Springer, 1999, pp. 71–87.
- [191] Feng Zhu and Ning Qin. “Intuitive class/shape function parameterization for airfoils”. In: *AIAA journal* 52.1 (2013), pp. 17–25.
- [192] Les Piegel and Wayne Tiller. *The NURBS book*. Springer Science & Business Media, 2012.
- [193] Brenda M. Kulfan. “A Universal Parametric Geometry Representation Method — “CST””. In: *Proceedings of the 45th AIAA Aerospace Sciences Meeting and Exhibit*. AIAA 2007-0062. Reno, NV, 2007.
- [194] Marco Ceze, Marcelo Hayashi, and Ernani Volpe. “A study of the CST parameterization characteristics”. In: *27th AIAA Applied Aerodynamics Conference*. 2009, pp. 1–12.
- [195] Michiel Hannes Straathof. “Shape parameterization in aircraft design: a novel method, based on b-splines”. PhD thesis. TU Delft, 2012.
- [196] Michiel H Straathof and Michel J L. Van Tooren. “Adjoint optimization of a wing using the class-shape-refinement-transformation method”. In: *Journal of Aircraft* 49.4 (2012), pp. 1091–1100.
- [197] John T Hwang, Gaetan K. W. Kenway, and Joaquim R. R. A. Martins. “Geometry and Structural Modeling for High-Fidelity Aircraft Conceptual Design Optimization”. In: *Proceedings of the 15th AIAA Multidisciplinary Analysis and Optimization Conference*. AIAA 2014-2041. Atlanta, GA, 2014. DOI: [10.2514/6.2014-2041](https://doi.org/10.2514/6.2014-2041).

- [198] Christian B Allen, Daniel J Poole, and Thomas CS Rendall. “Wing aerodynamic optimization using efficient mathematically-extracted modal design variables”. In: *Optimization and Engineering* (2018), pp. 1–25.
- [199] Daniel J Poole, Christian B Allen, and T Rendall. “Aerofoil design variable extraction for aerodynamic optimization”. In: *21st AIAA Computational Fluid Dynamics Conference*. 2013, p. 2705.
- [200] *NASA Uncertainty and Error in CFD Simulations tutorial*. <https://www.grc.nasa.gov/www/wind/valid/tutorial/errors.html>. Accessed: 2018-08-28.
- [201] Patrick J Roache. “Perspective: a method for uniform reporting of grid refinement studies”. In: *Journal of Fluids Engineering* 116.3 (1994), pp. 405–413. DOI: [10.1115/1.2910291](https://doi.org/10.1115/1.2910291).
- [202] John C Vassberg and Antony Jameson. “In pursuit of grid convergence for two-dimensional Euler solutions”. In: *Journal of Aircraft* 47.4 (2010), pp. 1152–1166.
- [203] *NASA Spatial Grid Convergence analysis tutorial*. <https://www.grc.nasa.gov/WWW/wind/valid/tutorial/spatconv.html>. Accessed: 2018-08-28.
- [204] Prabhat Hajela. “Genetic search-an approach to the nonconvex optimization problem”. In: *AIAA journal* 28.7 (1990), pp. 1205–1210.
- [205] John Henry Holland. *Adaptation in natural and artificial systems: an introductory analysis with applications to biology, control, and artificial intelligence*. MIT press, 1992.
- [206] R. C. Eberhart and J. A. Kennedy. “A New Optimizer Using Particle Swarm Theory”. In: *Sixth International Symposium on Micro Machine and Human Science*. Nagoya, Japan, 1995, pp. 39–43.
- [207] Mohamed A. Bouhlel and Joaquim R. R. A. Martins. “Gradient-enhanced kriging for high-dimensional problems”. In: *Engineering with Computers* 1.35 (2019), pp. 157–173. DOI: [10.1007/s00366-018-0590-x](https://doi.org/10.1007/s00366-018-0590-x).
- [208] O. Pironneau. “On optimum design in fluid mechanics”. In: *Journal of Fluid Mechanics* 64.01 (1974), pp. 97–110. ISSN: 0022-1120. DOI: [10.1017/S0022112074002023](https://doi.org/10.1017/S0022112074002023).
- [209] Joaquim R. R. A. Martins. “A Coupled-Adjoint Method for High-Fidelity Aero-Structural Optimization”. PhD thesis. Stanford University, 2002.